Structural and geochronological investigation of the southern Alexander terrane in the vicinity of Porcher Island, northwestern British Columbia

by

Joel Angen

A thesis
presented to the University of Waterloo
in fulfillment of the
thesis requirement for the degree of
Master of Science
in
Earth Sciences

Waterloo, Ontario, Canada, 2013

AUTHOR'S DECLARATION

I hereby declare that I am the sole author of this thesis. This is a true copy of the thesis, including any required final revisions, as accepted by my examiners.

I understand that my thesis may be made electronically available to the public.

Abstract

Abstract:

The Alexander terrane is an allochthonous terrane within the North American Cordillera. New structural mapping and geochronology within the southern Alexander terrane in the vicinity of Porcher Island provides evidence for two major tectonic events. The oldest is Late Silurian to Early Devonian magmatism and deformation assigned to the Klakas orogeny. The area has subsequently been affected by mid-Cretaceous conjugate shear zones potentially associated with tectonic escape.

Northwest-striking sinistral shear zones characterize mid-Cretaceous deformation in the western Coast Belt south of Prince Rupert in north coastal British Columbia. Structurally focused mapping and geochronology has revealed a component of lateral extension to this deformation. General flow characteristics of the shear zones are identified by comparison of fabric patterns to published models for fabric development in shear zones. U-Pb ages from synkinematic dykes constrain motion on northwest-striking sinistral transpressional shear zones, including the Useless, Barrett and Salt Lagoon shear zones, to ca. 104 – 96 Ma, and dextral transpression on the north-striking Telegraph Passage shear zone to ca. 97.6 ± 0.2 Ma. The geometry, kinematics, and coeval nature of these shear zones suggests that they formed in part as a ductile conjugate set. The presence of similarly-oriented conjugate shear bands in the apex zone between sinistral and dextral shear zones further reinforces this interpretation. The orientation of these conjugate sets indicates a component of north-northwest east-southeast extension. The conjugate shear zones merge together into the Grenville Channel shear zone, a sinistral transpressional shear zone with high strike-parallel stretch. A U-Pb age of 103 ± 32 Ma from a synkinematic dyke in the Grenville Channel shear zone coincides with a previously published Lu-Hf age of 102.6 ± 3.7 Ma on synkinematic garnet.

Overall, structural and geochronological data from Porcher Island and surrounding area in north coastal British Columbia indicate that mid-Cretaceous deformation was characterized by ENE-WSW (orogen normal) shortening and NNW-SSE (orogen parallel) extension. This local strain regime is consistent with large-scale mid-Cretaceous tectonic escape as proposed for the northern Cordillera at that time, expressed in coeval sinistral faulting in the Coast Belt and dextral faulting in the northern Omineca belt.

The Late Silurian to Early Devonian Ogden Channel complex is a mafic to intermediate metaplutonic-metamorphic complex within the southern Alexander terrane on southern Porcher Island and adjacent Pitt Island in north coastal British Columbia. Lithological characteristics of the

complex suggest that it represents the mid-crustal roots of a volcanic arc. An age of 413.3 ± 2.5 Ma from a comparatively weakly deformed quartz diorite dyke indicates that the synkinematic Ogden Channel complex is at least in part Early Devonian in age, corresponding to the Klakas orogeny that affected the Alexander terrane in southeast Alaska. Crosscutting relationships indicate that individual intrusions within the Ogden Channel complex were emplaced syn- to post-kinematically with respect to southwest-vergent sinistral reverse deformation (present coordinates). The structural and lithological characteristics of the Ogden Channel complex are consistent with the interpretation that this part of the Alexander terrane was located in the upper plate of a northeast-dipping subduction zone, which culminated in the Klakas orogeny.

Acknowledgements

I would like to thank the residents of Oona River, all of whom were eager to hear what I was doing and help out in any way including providing priceless local knowledge on campsite locations and navigating the local waters. Thanks for making me feel like part of the community for the 12 weeks I spent there. I look forward to joining you for another bonfire on the beach some day. I am forever indebted to Jan Lemon for her tireless efforts as an expediter. Thanks to Don Willson for the use of his boat, the 'Salmon Princess'. I thank my supervisors Dr. Cees van Staal and Dr. Shoufa Lin for their scientific guidance. I would also like to thank Dr. Mario Coniglio and Dr. Brian Kendall for taking the time out of their busy schedules to be part of my committee. I thank both Dr. Don Davis and Dr. Bill McClelland for carrying out geochronological analyses and taking the time to discuss results and interpretations. Thanks to Dr. Brian Mahoney for allowing me to discuss preliminary results which provide much more weight to the interpretations made herein. Thanks to Jean-Luc Pilote and Todd Lau who were both excellent field assistants and didn't let the soggy weather of British Columbia's north coast dampen their spirits. An extra special thanks goes out to JoAnne Nelson; without whom I never would have made it this far.

This research was funded by the Geological Survey of Canada through the North Coast subproject of the Edges Multiple Metals Northwest Canadian Cordillera (BC and Yukon) Project; a component of the Geo-mapping for Energy and Minerals (GEM) program. Thanks to Steve Irwin and Nicola Butt at the Geological Survey of Canada for all of their help with logistics and paperwork, and for providing me with a place to work while in Vancouver.

Finally, I would also like to thank my friends and family who have provided me with so much love and support. Thank you all.

Table of Contents

List of Figures

List of Tables

Chapter 1
Introduction

1.1 Introduction

The North American Cordillera is the type example of a complex accretionary orogen (Condie, 2007). It has been active as a convergent margin since the Devonian, undergoing periods of compression, extension and terrane accretion. Some of these terranes, including the Alexander terrane (Figure 1.1), record a Paleozoic tectonic history distinct from the rest of the Cordillera (Colpron and Nelson, 2009, 2011a; Beranek *et al*., 2012a). Post-accretion structures in the western and eastern portions of the northern Cordillera suggest that the orogen underwent tectonic escape during the mid-Cretaceous (Figure 1.1 inset).

1.2 This Study

The study area for this thesis is located within the Coast Belt where the southern Alexander terrane is intruded by the Coast Plutonic Complex (Figure 1.1). It records a complex polyphase structural history, and new geochronology presented herein indicates that these structures record both Early Devonian and mid-Cretaceous tectonic events.

The Grenville Channel shear zone has long been interpreted as part of a system of mid-Cretaceous sinistral shear zones within the Coast Belt (Woodsworth *et al*., 1991; Chardon *et al*., 1999; Gehrels *et al*., 2009). Excellent coastal exposure at the northern end of Grenville Channel makes it an area of particular interest to study sinistral transpression within the Coast Belt.

Fieldwork was carried out during the summers of 2010 and 2011. Due to the rugged terrain of British Columbia's North Coast, mapping was dominantly conducted along shorelines accessible only by boat. Supplementary traverses were carried out along available logging roads. Geospatial analysis of structural data as well as observations made in the field led to the characterization of both previously reported and newly identified shear zones. Uranium-lead geochronology of synkinematic dykes provides temporal context for identified structures, allowing for correlation of new observations to the developing tectonic framework of the northern Cordillera.

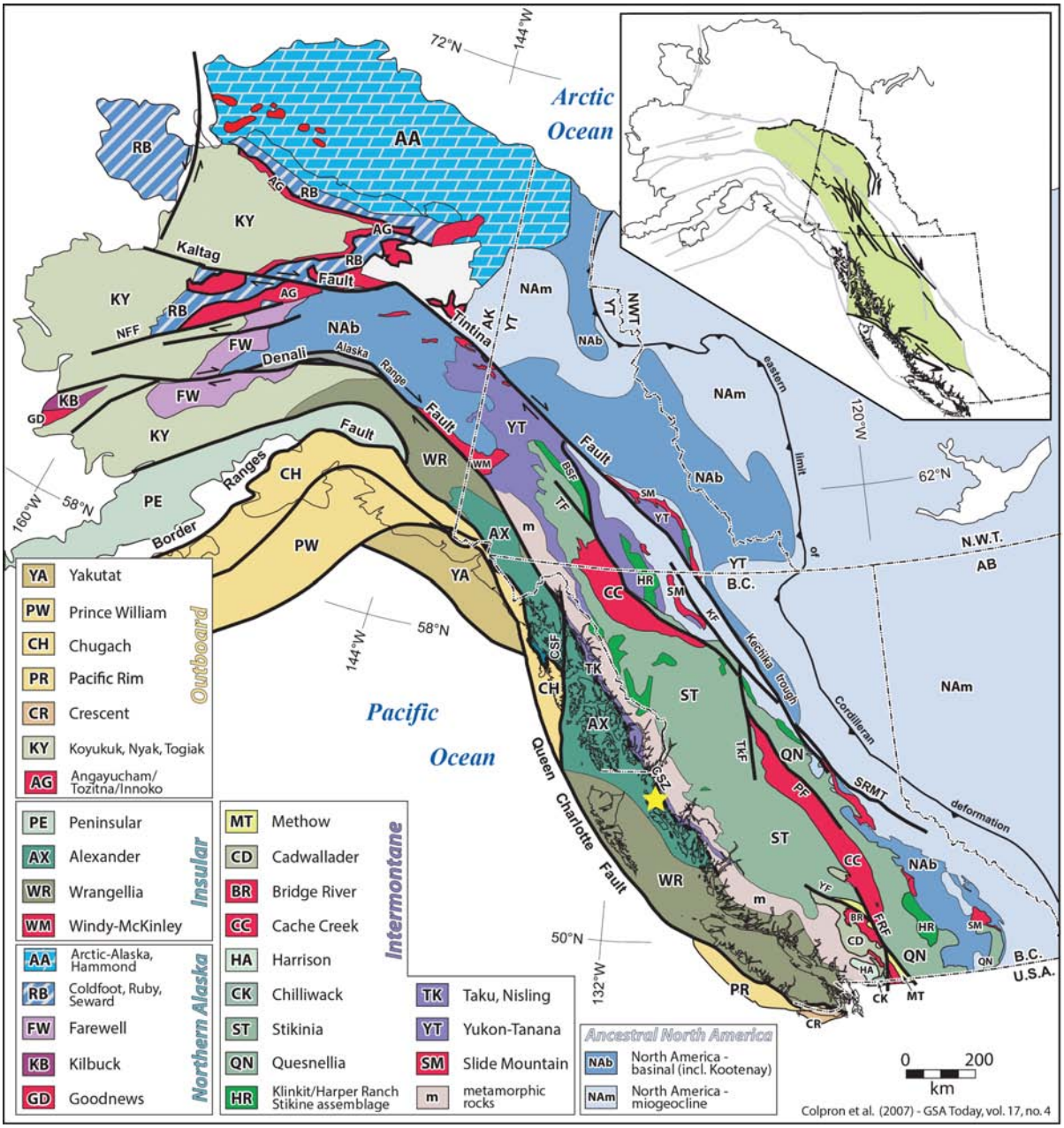

Figure 1.1: Terrane map of the northern Cordillera showing the location of the study area for this thesis (yellow star). Inset shows the relationship between major structures across the northern Cordillera, with sinistral shear zones in the west and dextral shear zones in the east. Note that 450 km of younger dextral displacement across the Tintina fault has been removed in inset map (modified after Colpron *et al.*, 2007; Colpron and Nelson, 2011b; Colpron *et al.*, 2011a).

1.3 Objectives of thesis

The main objectives of this research were: 1) to document the structures of the southern Alexander terrane in the vicinity of Porcher Island with particular focus on suspected mid-Cretaceous shear zones; 2) determine the geometry and kinematics of these structures; 3) establish age constraints on structural events; 4) relate this structural history to the overall tectonic history of the Alexander terrane and the northern Cordillera.

1.4 Organization of thesis

This thesis has been divided into 4 chapters. The first chapter is this introduction. Chapter 2 presents a review of pertinent theories of fabric development within shear zones used in the interpretation of structural data in subsequent chapters. Chapter 3 was written as a stand-alone manuscript entitled 'Timing and kinematics of shear zone deformation in the western Coast Belt: evidence for mid-Cretaceous orogen-parallel extension' intended for publication. It includes geospatial structural analysis and geochronology constraining orogen parallel extension within the western Coast Belt suggestive of mid-Cretaceous tectonic escape. Chapter 4 is a manuscript entitled 'The Ogden Channel complex: lower crustal root of the Klakas orogeny', which presents new data pertinent to the Late Silurian to Early Devonian history of the Alexander terrane. A discussion of controls on tectonic escape as well as concluding remarks and proposed future work are presented in Chapter 5.

Chapter 2
Models for fabric development in shear zones

2.1 Introduction

Shear zones are localized planar zones of high strain originally referred to as 'shear belts' (Ramsay and Graham, 1970). Lineations have historically been used as a tool to determine shear direction within shear zones (Berthe *et al*., 1979; Simpson and Schmid, 1983). With the advent of transpressional shear zone models, first outlined by Sanderson and Marchini (1984), it became clear that the relationship between lineation orientation and shear direction was much more complex. Most of the fabric data presented in this thesis is interpreted to have formed in shear zone settings, thus an investigation of shear zone models and how they relate to fabric development is warranted.

In the first four models described herein it is assumed that fabrics within shear zones can be correlated to the overall finite strain ellipsoids. The S foliation is represented by the XY plane and stretching lineation (Ls) orientation is represented by the X axis where X, Y, and Z are the long, intermediate, and short axes of the finite strain ellipsoid, respectively. The final model presented takes into account flow partitioning and the fabric elements are correlated to deformed preexisting ellipsoids.

2.2 General velocity gradient tensor and reference frame

All shear zone models described herein are developed on the basis of a velocity gradient tensor that defines the instantaneous velocity field. The coordinate system used is that of Lin *et al*., (1998) in which the x_1 direction is parallel to the strike of the shear zone boundary, x_2 is normal to the boundary, and x_3 is vertical (or down dip) (Figure 2.1a). The velocity gradient tensor is calculated from the vector representing the velocity ($\mathbf{v}$) of one boundary with respect to the other. It can be resolved into a boundary parallel component ($\mathbf{v}_{\|}$) and a boundary perpendicular component ($\mathbf{v}_{\perp}$).

If $\mathbf{v}_{\|}$ is not horizontal, the angle of inclination is denoted ϕ (inset in Figure 2.1d). The boundary parallel component results in simple shear; the simple shear strain rate is defined as $\dot{\gamma}=v_{\|}/h$, where $v_{\|}$ is the magnitude of $\mathbf{v}_{\|}$, and h is the instantaneous width of the zone. The boundary perpendicular component results in pure shear; the pure shear strain rate is defined as $\dot{\varepsilon}$ which is comprised of three orthogonal components: $\dot{\varepsilon}_a$, $\dot{\varepsilon}_b$, and $\dot{\varepsilon}_c$ which are parallel to x_1, x_2, and x_3, respectively. Therefore,

$\dot{\varepsilon}_b = \nu_\perp / h$, where $\nu_\perp$ is the magnitude of $\boldsymbol{\nu}_\perp$. The angle between $\boldsymbol{\nu}$ and $\boldsymbol{\nu}_\parallel$ is denoted α (inset in Figure 2.1c), such that:

$$\tan(\alpha) = \frac{\dot{\varepsilon}_b}{\dot{\gamma}} \qquad \text{Eq.1}$$

The general velocity gradient tensor for shear zone deformation can be written as (Ramberg, 1975; Lin *et al*., 1998; Jiang and Williams, 1998):

$$L = \begin{matrix} \dot{\varepsilon}_a & \dot{\gamma}\cos\phi & 0 \\ 0 & \dot{\varepsilon}_b & 0 \\ 0 & \dot{\gamma}\sin\phi & \dot{\varepsilon}_c \end{matrix} \qquad \text{Eq.2}$$

Figure 2.1 (following page): Flow geometries of the four homogeneous high strain zone models discussed herein: (a) An undeformed high strain zone; (b) Homogeneous domain in the undeformed state, x_1, x_2, and x_3 are the three axes of an external coordinate system; (c) The unit cube in its final state resulting from simple shear; $\dot{\gamma}$ is shear strain rate and ω represents vorticity; (d) The unit cube in its final state resulting from monoclinic transpression. The velocity $\boldsymbol{\nu}$ is at an angle α with respect to the shear zone boundary and is partitioned into $\boldsymbol{\nu}_\parallel$ and $\boldsymbol{\nu}_\perp$. $\dot{\varepsilon}_a$, $\dot{\varepsilon}_b$, and $\dot{\varepsilon}_c$ are the three principal stretches of the pure shear component, $\dot{\varepsilon}_a$ is set to 0 and $\dot{\varepsilon}_b$=-$\dot{\varepsilon}_c$; (e) The unit cube in its final state resulting from triclinic transpression with pure shear stretches that are the same as above, $\boldsymbol{\nu}_\parallel$ is at an angle ϕ with respect to horizontal and defines the vorticity normal section (VNS); (f) The unit cube in its final state resulting from triclinic transpression with $\dot{\varepsilon}_c$ set to 0 and $\dot{\varepsilon}_b$=-$\dot{\varepsilon}_a$. (g)-(j) Equal-area lower-hemisphere projections of S-foliations and stretching lineations (Ls) for the four corresponding high strain zone models. Arrows indicate evolution of elements with time. HSZB – high strain zone boundary. (g) Simple shear; (h) Monoclinic transpression; (i) Triclinic transpression with ϕ=20^o and $\dot{\varepsilon}_b$=-$\dot{\varepsilon}_c$; (j) Triclinic transpression with ϕ=20^o and $\dot{\varepsilon}_b$=-$\dot{\varepsilon}_a$. The dashed arrow in (g) indicates lineation 'switch'. Dark blue circles indicate the orientation of the minimum axis of the finite strain ellipsoid, a proxy for poles to foliation. Triangles indicate the orientation of the long axis of the finite strain ellipsoid, a proxy for lineations. Colours indicate the $\dot{\gamma}/\dot{\varepsilon}_b$ ratio as follows: red – 20, orange – 6, yellow – 4, green – 2, light blue – 1. See text for further discussion (modified after Lin *et al*., 1998; 2007, and Jiang and Williams, 1998).

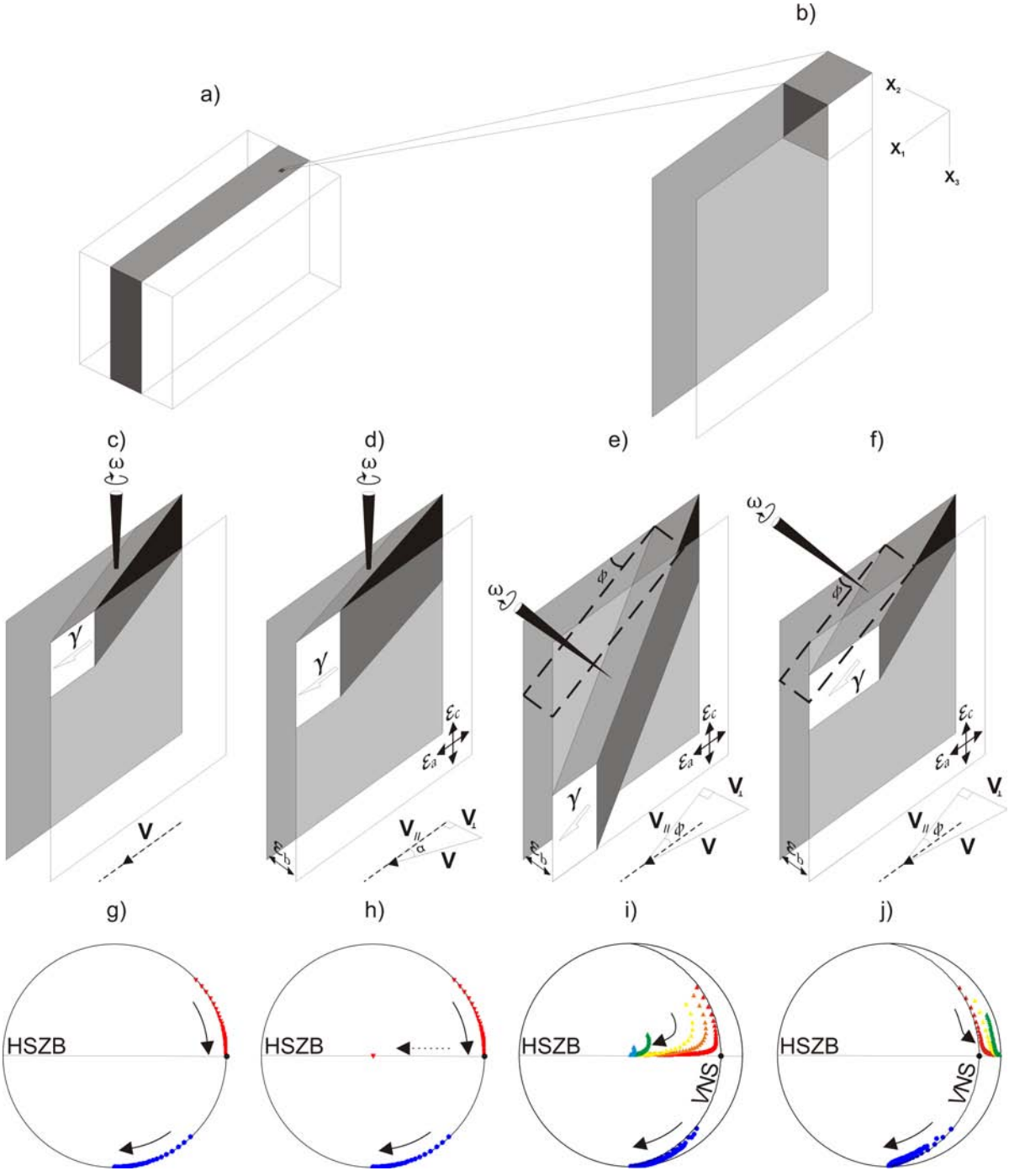
a)
b)
x_2
x_1
x_3
c)
d)
e)
f)
ω
γ
V
ε_c
ε_a
$V_{||}$
$V_\perp$
α
Φ
g)
h)
i)
j)
HSZB
VNS

2.3 Shear zone flow models

2.3.1 Simple Shear

The original shear zone models are the plane strain simple shear models of Ramsay and Graham (1970) and Ramsay (1980). They account for only simple shear so $\dot{\varepsilon}_a$, $\dot{\varepsilon}_b$, and $\dot{\varepsilon}_c$ are all equal to zero. The example in Figure 2.1c assumes horizontal shear. Plane strain exhibits twofold rotational symmetry about the vorticity vector (ω) and is therefore referred to as a monoclinic deformation.

Simple shear involves no boundary perpendicular component of velocity so α=0. If the velocity is horizontal, as presented in Figure 2.1c, ϕ=0 as well and the velocity gradient tensor reduces to:

$$L = \begin{matrix} 0 & \dot{\gamma} & 0 \\ 0 & 0 & 0 \\ 0 & 0 & 0 \end{matrix} \qquad \text{Eq.3}$$

The maximum instantaneous stretching axis (ISA) is horizontal and oriented at an angle of 45 degrees to the shear direction throughout deformation for simple shear. Because simple shear is non-coaxial, the material line aligned with the maximum ISA rotates progressively away from that orientation and towards the shear direction. The cumulative effect is that the long axis of the finite strain ellipsoid approaches the shear direction.

The arrows in Figure 2.1g indicate the change in orientation with increasing finite strain for both poles to S foliation (blue circles) and lineations (red triangles) as represented by the finite strain ellipsoid. In this example, the foliation is always vertical and rotates towards parallelism with the shear zone boundary while the lineation is always horizontal and rotates towards the shear direction; as such, the shear direction is the 'fabric attractor' in simple shear (Passchier, 1997).

2.3.2 Monoclinic Transpression

Many large scale shear zones exhibit near vertical stretching lineations but shear sense indicators which consistently indicate subhorizontal shear (Hudleston *et al*., 1988; Robin and Cruden, 1994; Greene and Schweickert, 1995). Sanderson and Marchini (1984) adapted the terms transpression and transtension, originally coined by Harland (1971) for oblique plate convergence, to represent oblique convergence (or divergence) between shear zone boundaries. Only transpression will be considered herein. Sanderson and Marchini (1984) assume no strike parallel stretch ($\dot{\varepsilon}_a$) so the stretch perpendicular to the shear zone boundary ($\dot{\varepsilon}_b$) is accommodated by a vertical stretch ($\dot{\varepsilon}_c$) to maintain constant volume. The shear strain (γ) is restricted to the horizontal plane, meaning that the

irrotational principal axis (vorticity vector, ω) of the simple shear component is vertical and coincides with one of the principal axes of the pure shear component. As such, Sanderson and Marchini type transpression is also monoclinic (Figure 2.1d). Given that the simple shear component is horizontal, ϕ is equal to zero and therefore the velocity gradient tensor reduces to:

$$L = \begin{matrix} 0 & \dot{\gamma} & 0 \\ 0 & \dot{\varepsilon}_b & 0 \\ 0 & 0 & \dot{\varepsilon}_c \end{matrix} \qquad \text{Eq.4}$$

A major criticism of the Sanderson and Marchini model is that it assumes homogeneous deformation across the zone which requires the shear zone boundaries to be free slipping in the vertical direction but able to apply a shear stress in the horizontal direction (Sanderson and Marchini, 1984; Schwerdtener, 1989; Robin and Cruden, 1994).

Fossen and Tikoff (1998) expanded on this model to include both vertical ($\dot{\varepsilon}_c$) and strike parallel ($\dot{\varepsilon}_a$) stretches, describing a spectrum of deformation types ranging from vertical to strike parallel stretch dominated. Strike parallel stretch is considered to be a rare scenario as shear zones generally pinch out laterally so the material would have nowhere to extrude into, whereas the Earth's surface is always an unconstrained boundary. For the sake of simplicity, this section will focus on the scenario of no strike parallel stretch and stick to the two end members of Sanderson and Marchini style transpression: simple shear dominated and pure shear dominated. The case of strike parallel stretch is discussed further below as it relates to triclinic transpression. Pure shear dominated transpression is, as the name suggests, dominated by the pure shear component so the maximum ISA is vertical and therefore the long axis of the finite strain ellipsoid will be vertical throughout deformation. In simple shear dominated transpression, the long axis of the finite strain ellipsoid is initially controlled by the simple shear component and therefore rotates in the horizontal plane similar to plane strain models. However, because coaxial deformation accumulates much more efficiently than non-coaxial deformation, the long axis 'switches' from horizontal to vertical at higher strain (Figure 2.1h). As with simple shear, the maximum ISA in simple shear dominated transpression is always in the horizontal plane at an angle of 45° to the shear direction. The intermediate ISA, which represents the ε_c pure shear stretch, is always vertical and the minimum ISA is perpendicular to both. Each instantaneous step is controlled by this regime. Since simple shear is non-coaxial, the maximum ISA is acting on a different material line at each step of deformation while the intermediate one, the pure shear stretch, is always acting on the same material line so it accumulates faster. The cutoff value between simple and pure shear dominated transpression is at α = 20 (Tikoff and Greene, 1995). It

should be noted that these models assume continuous strain and therefore do not account for the effects of pure shear being a strain hardening process and simple shear being a strain softening process (Williams and Price, 1990).

In terms of stretching lineations, monoclinic transpression predicts vertical lineations only for pure shear dominated transpression. For simple shear dominated transpression it predicts horizontal lineations at low strain which rotate towards the shear direction with increasing strain, followed by a 'flip' to vertical lineations at high strain (Figure 2.1h). While this makes it sound like a dramatic change it is not. It is a gradual process, with the 'flip' represented by oblate ellipsoids marking the transition from horizontally prolate to vertically prolate ellipsoids.

2.3.3 Triclinic Transpression

Lin *et al*. (1998) and Jiang and Williams (1998) considered transpressional (and transtensional) shear zones in which the zone boundary parallel component of deformation is not horizontal. Transtension is not considered herein as it predicts subhorizontal foliation not observed in the field. Jiang and Williams (1998) included an investigation of all types of pure shear stretch as well as volume change. Only the isochoric endmember cases are considered herein: those being strictly vertical pure shear stretch as above, and strictly horizontal pure shear stretch. In both cases, $\mathbf{v}_{\|}$ is at an angle Φ with respect to horizontal and defines the vorticity normal section (VNS), (Figure 2.1e,f) (Jiang and Williams, 1998; Lin *et al*., 1998). Since ω is inclined with respect to the axes of the pure shear component, the deformation exhibits no symmetry and is referred to as triclinic (Robin and Cruden, 1994; Lin *et al*., 1998; Jiang and Williams, 1998).

2.3.3.1 Vertical Stretch

As with the monoclinic model described above, orogen perpendicular shortening is generally interpreted to be accommodated by vertical extension alone ($\varepsilon_c=-\varepsilon_b$). The $\mathbf{v}_{\|}$ component is comprised of a vertical component ($\mathbf{v}_{\|}\sin\phi$) and a horizontal component ($\mathbf{v}_{\|}\cos\phi$). The resulting velocity gradient tensor is the general form in equation 1. In Figure 2.1e, the greatest asymmetry of the deformed unit cube is not aligned with the vorticity normal section (VNS). This is a result of an apparent rotation due to the pure shear deformation that effectively rotates the material plane corresponding to the VNS at each step of deformation while the VNS itself does not change orientation. A vertical pure shear stretch will move two points at different heights away from one another, steepening all previously inclined material lines as shown in Figure 2.2.

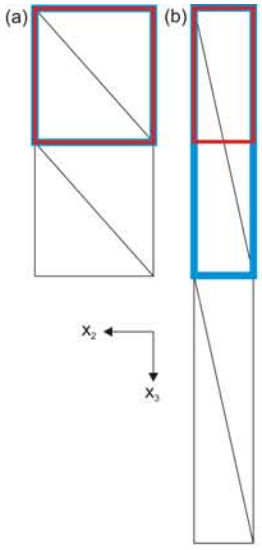

Figure 2.2: Two dimensional representation of the relationship between the VNS and the material plane corresponding to it (a) before and (b) after a pure shear stretch. The x_2 and x_3 orientations correspond to those in Figure 2.1.

As with the monoclinic model described above, the pure shear component of deformation dominates at high strain. However, triclinic transpression does not induce a 'switch' in the long axis of its finite strain ellipsoid. The long axis is initially oriented somewhere between a pitch of 45° on the VNS and vertical; it then rotates towards the shear direction at low strain and curves towards vertical (or down-dip) at higher strain (Figure 2.1i). The specific path it follows is dependent on the simple shear to pure shear ratio ($\dot{\gamma}:\dot{\varepsilon}$) and ϕ. It follows from equation 1 that $\dot{\gamma}:\dot{\varepsilon}$ is equal to the inverse of $\tan\alpha$. Figure 2.1i includes $\dot{\gamma}:\dot{\varepsilon}$ ratios of 20, 6, 4, 2, and 1 all at a ϕ of 20°. The orientation of the short axis falls close to the VNS in all cases and rotates towards horizontal, representing a foliation approaching parallelism with shear zone boundary at high strain. For a shear zone with a vertical pure shear stretch, lineations should fall somewhere between the VNS and vertical.

2.3.3.2 Strike Parallel Stretch

Most transpression models assume that the pure shear shortening is accommodated by vertical, or up-dip stretch, as horizontal stretch leads to space problems as discussed above. Kuiper *et al*. (2011) present evidence from the Aiken river shear zone in northern Manitoba which suggests transpression

with significant strike parallel stretch. One tectonic setting in which shear zones with strike parallel stretch can occur is tectonic escape.

To model triclinic transpression with strike-parallel stretch, $\dot{\varepsilon}_c$ is reduced to zero and $\dot{\varepsilon}_a$=-$\dot{\varepsilon}_b$. The corresponding velocity gradient tensor is:

$$L = \begin{matrix} \dot{\varepsilon}_a & \dot{\gamma}\cos\phi & 0 \\ 0 & \dot{\varepsilon}_b & 0 \\ 0 & \gamma\sin\phi & 0 \end{matrix} \qquad \text{Eq.5}$$

It is worth noting that the **ν** for Figures 2.1 e and f are the same, the only difference is that in the latter the pure shear component is accommodated by strike parallel stretch. The affect on lineations is that the orientation of the fabric attractor changes from vertical to horizontal. The long axis of the finite strain ellipsoid initiates somewhere between the VNS at 45^o to the shear direction and horizontal and rotates initially towards the shear direction then towards the horizontal component of the shear direction along a curved path. Figure 2.1j includes $\dot{\gamma}$:$\dot{\varepsilon}$ ratios of 20, 4, and 2 all once again for a ϕ of 20^o. Lineations are predicted to fall somewhere between the VNS and horizontal.

2.4 MOPLA

All of the shear zone models described above assume homogeneous deformation and that the orientation of lineations observed in the field can be appropriately estimated by the finite strain ellipsoid of that homogeneous flow. These models predict a tightly constrained distribution of lineations. Systematic variation in stretching lineations across a shear zone has been effectively explained by a localization of simple shear, which is a strain softening process, while pure shear is more evenly distributed as it is a strain hardening process (Lin *et al*., 1998; Kuiper *et al*., 2011). Other field studies of high strain zones report great circle girdle distributions of lineations without a systematic trend: these include the Wabigoon-Quetico Subprovince boundary (Czeck and Hudleston, 2003), the Jiaoluotage zone (Xu *et al*., 2003), the Cascade Lake shear zone (Bentley, 2004; Jiang and Bentley, 2012), and several of the shear zones outlined in this study. The majority of large-scale shear zones observed in the field affect a variety of rock types with differing rheology (Jiang and Bentley, 2012). This leads to flow partitioning between rock units as described by Lister and Williams (1983). As such, the fabric elements within each rock unit will evolve according to the partitioned flow field within that unit, not the overall flow field (Jiang and Bentley, 2012). Furthermore, elements defining stretching lineations are generally compositionally distinct (ie. clasts within matrix) and therefore another order of flow partitioning must be considered. The Multi-Order

Power Law Approach (MOPLA) is an application of micromechanics to investigate fabric development in lithologically heterogeneous shear zones (Jiang, 2012; Jiang and Bentley, 2012). It accounts for strain partitioning at two scales by treating each lithological unit as a deformable ellipsoid within a homogeneous matrix, and each stretching lineation as a deformable ellipsoid within a homogeneous lithological unit.

In order to understand MOPLA, we must first define all of the relevant orders, or scales, that it encompasses (Figure 2.3). The largest scale is the overall medium of the shear zone; this will be called the 0^{th} order. It deforms according to the overall velocity gradient tensor (L) defined by the shear zone boundary velocity (**v**). All of the lithological units within a large-scale shear zone are 1^{st} order elements. Each 1^{st} order element has a relatively homogeneous composition (e.g. granite or basalt); deformation within a given 1^{st} order element is defined by its partitioned velocity gradient tensor (L_{p1}). Within each 1^{st} order element there are 2^{nd} order elements with distinct composition (eg. a single mineral grain within a granite or a quartzite clast within a conglomerate); the velocity gradient tensor is partitioned once again for each 2^{nd} order element (L_{p2}). During shear zone formation, 1^{st} order elements are transposed to align with the shear zone boundary. This alignment is referred to as a transposition foliation as defined by Williams and Jiang (2005). Fabric elements that can be measured in the field, such as mineral elongation lineations, are represented by 2^{nd} order elements.

The method follows from Eshelby (1957), which allows for the calculation of stress and strain within an ellipsoid embedded within a homogeneous medium with a given stress and strain state when the ellipsoid and homogeneous medium are isotropic and linearly elastic. Jiang and Bentley (2012; and references therein) have further developed the theory to apply it to power law materials and Jiang (2012) implemented the theory numerically. In reality, the 0^{th} and 1^{st} order media are comprised of numerous heterogeneous 1^{st} and 2^{nd} order elements, respectively. As a result, the homogeneous media as they are presented in Figure 2.3 should actually be homogeneous equivalent media (HEM) that correspond to the average of all their constituent elements (Molinari *et al*., 1983; Mura, 1987; Jiang and Bentley, 2012).

The 1^{st} order elements are treated as Eshelby inhomogeneities within the 0^{th} order flow field. As previously mentioned, the 1^{st} order elements define the transposition foliation. The short axis of a 1^{st} order strain ellipsoid is used to simulate the pole to foliation. One 2^{nd} order element is embedded within each 1^{st} order element such that it deforms as an Eshelby inhomogeneity within the given 1^{st}

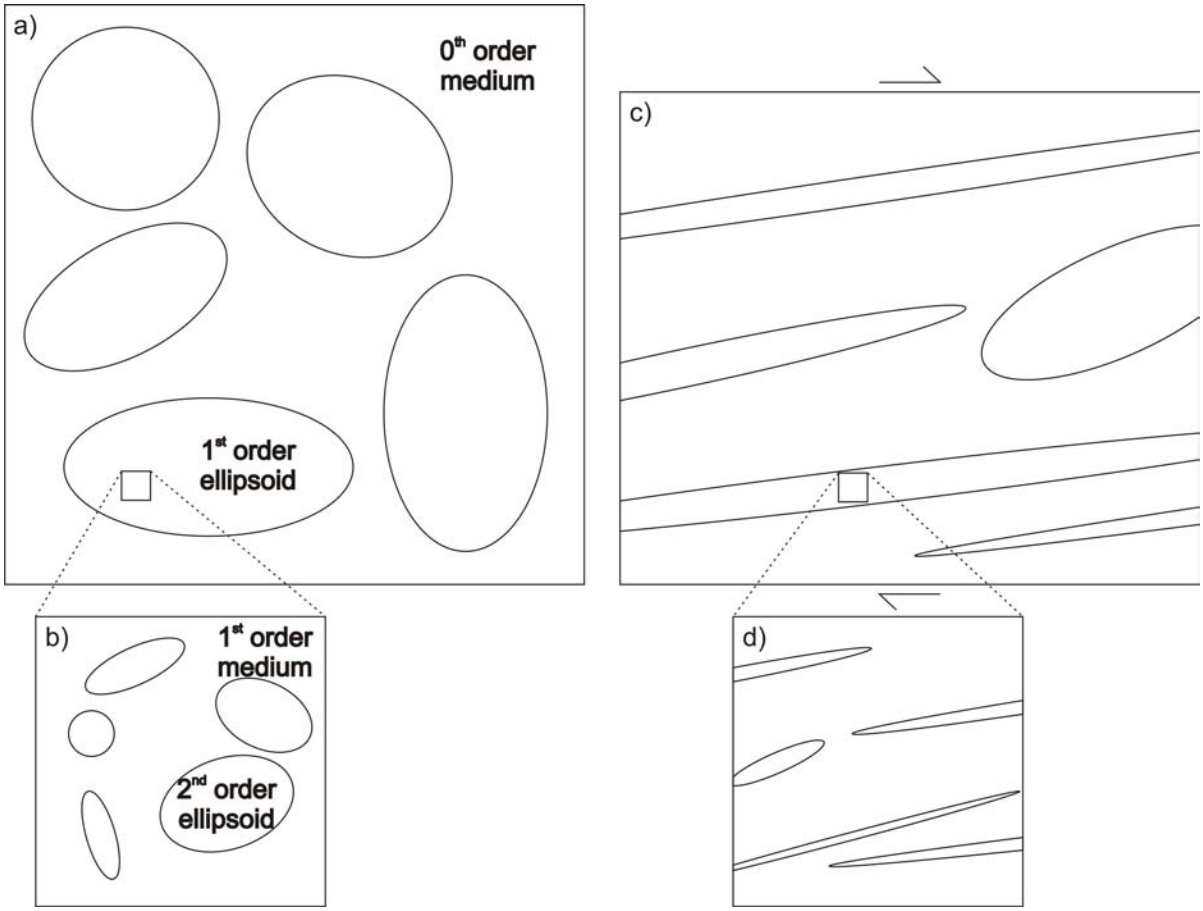

Figure 2.3: Schematic representation of the orders of elements considered in MOPLA modeling: (a) A series of 1st order ellipsoids within the homogeneous 0th order medium; (b) A series of 2nd order ellipsoids within a 1st order element; (c) The same 1st order ellipsoids from (a) in the deformed state; (d) The same 2nd order ellipsoids from (b) in the deformed state. Note that 1st and 2nd order ellipsoids do not all deform equivalently, some are more strained than others. This is a result of strain partitioning due to rheological contrasts between elements (modified after Jiang and Bentley, 2012).

order flow field. The long axis of each 2nd order strain ellipsoid simulates a stretching lineation. Jiang and Bentley (2012) developed a set of predicted stretching lineation patterns (Figure 2.4) by tracking the orientation of the long axis of an originally randomly oriented set of 2nd order ellipsoids, each within its own 1st order ellipsoid, for a range of boundary conditions and finite strain states. Comparing observed lineation patterns from field data to the patterns produced using MOPLA provides a semi-quantitative measure of the boundary conditions of the overall flow field and an

estimate of the accumulated strain. The strain intensity (N) reported for the lineation patterns in Figure 2.4 is calculated following Ramsay and Huber (1983):

$$N = \sqrt{\left(R_{xy} - 1\right)^2 + \left(R_{yz} - 1\right)^2} \qquad \text{Eq.6}$$

where R_{xy} and R_{yz} are the two principal plane strain ratios. It is important to keep in mind that $x \geq y \geq z$. In general, lineation patterns become more restricted at higher strain for a given value of α (left to right), and the distribution along the girdle correlates to α, with greater distribution for smaller values of α (top). The poles to foliation are not presented as they cluster at relatively low strain regardless of convergence angle and therefore provide little information (Jiang and Bentley, 2012).

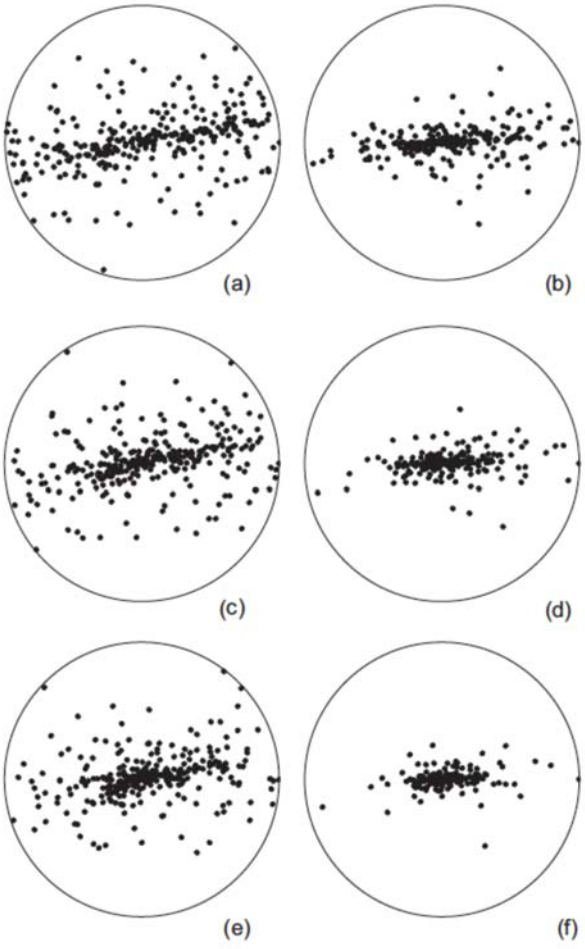

Figure 2.4: Stretching lineation patterns predicted by MOPLA model: (a) α =20°, 0th order strain field N=10; (b) α =20°, N=48; (c) α =25°, N=9.45; (d) α =25°, N=48); (e) α =30°, N=8.8; (f) α =30°, N= 48 (from Jiang and Bentley, 2012).

2.5 Accessory Fabric Elements Pertinent to Movement Picture

2.5.1 Ductile Slickenside Striae

Both monoclinic and triclinic transpression models lead to the important conclusion that stretching lineations do not always indicate shear direction. A different type of lineation only present on C foliation surfaces of S-C mylonites have been defined by Lin and Williams (1992) and Lin *et al*. (1998, 2007). These surfaces are planes of high shear strain (very high simple shear to pure shear ratio) and the ductile slickenside striae on them (Lc) therefore do approximate the shear direction. Figure 2.5 contains examples of S-C fabric as well as Ls and Lc lineations.

2.5.2 Drag Folds

Drag folds are minor, noncylindrical folds which form within shear zones with their hinge lines roughly perpendicular to the overall shear direction. The formation and evolution of drag folds was discussed in detail by Jiang and Williams (1999). Once formed the hinge lines of drag folds, like any other linear element, rotate towards the fabric attractor discussed above. In the case of simple shear, two halves of the drag fold rotate in opposite directions until they become subparallel to the stretching lineation, forming a sheath fold. In shear zones where sheath folds are observed, both S and Z shaped folds will also be found, making drag folds a potentially ambiguous shear sense indicator. Their obliquity to the shear direction (if it can be deciphered) is the only way they can be used to identify sense of shear. During monoclinic Sanderson and Marchini type transpression the fabric attractor is parallel to the original orientation of the fold hinge line (vertical) so folds become more cylindrical with continued deformation. The sense of shear identified from drag folds in such zones is unambiguous since they will all indicate the same sense of shear. In triclinic transpression zones, drag folds may or may not evolve into sheath folds depending on their original orientation and how noncylindrical they were with respect to the fabric attractor.

2.6 Conjugate shear zones: Mohr-Coulomb vs maximum effective moment

The Mohr-Coulomb failure criterion states that failure will occur at an angle of 30^{o} to the maximum compressive stress (maximum shortening direction) and 60^{o} to the minimum compressive stress (maximum extension direction). This yields two orientations of faults for any given stress field: a

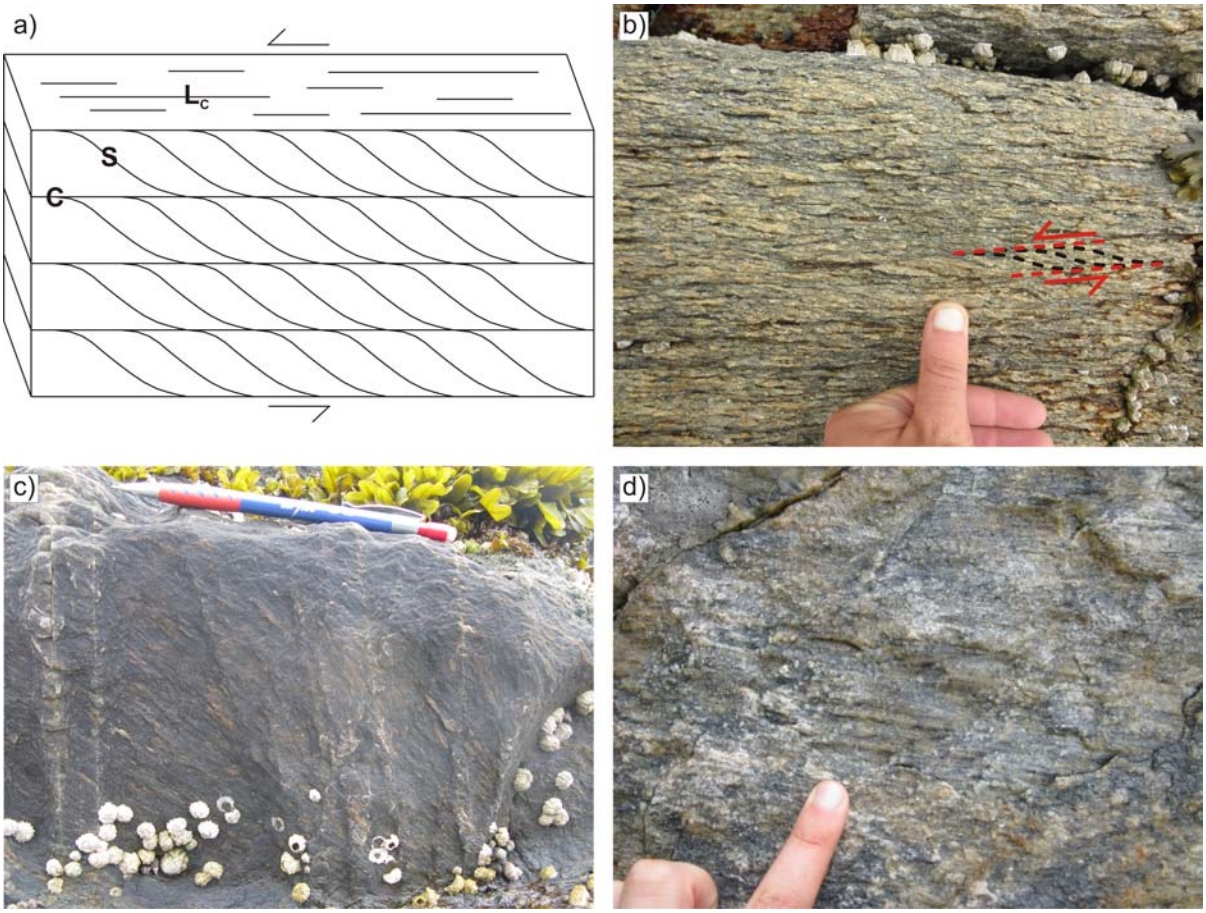

Figure 2.5: Examples of Ls and Lc lineations: (a) Schematic of S-C fabric. S-foliation represents the plane of flattening (XY plane), C-planes are planes of high shear strain and should parallel shear zone boundaries (modified after Lin *et al*., 2007); (b) S-C mylonite from the Swede Point Pluton; (c) Typical stretching lineation, Ls. Notice that even within this small area the stretching lineations vary; (d) Typical ductile slickenside striae, Lc. Note the continuity of Lc lineations regardless of composition.

conjugate set. However, this orientation only holds if the rocks are behaving according to the Mohr-Coulomb failure criterion. Under ductile conditions, shear deformation is accommodated by rotation rather than failure so the shear zones are expected to form at the orientation of the maximum moment, where moment is defined as the tendency of an applied force to rotate an object. Zheng *et al*. (2004; 2011) outlined this phenomenon and calculated the effective moment acting on a plane which makes an angle (θ) with respect to the maximum compressive stress. The maximum effective moment occurs at an angle of 54.7^{o} as represented in Figure 2.6. Furthermore, since the maximum value

occurs at the peak of a curve, there is no significant drop in the effective moment over the range 54.7° ± 10°. This can be compared to the Mohr-Coulomb failure criterion (also plotted in Figure 2.6) in which the material cannot sustain a shear stress greater than the value encountered at 30° so brittle failure should always occur at that angle. Zheng *et al*. (2004) outlined the Maximum Effective Moment (MEM) criterion focusing mainly on what they call extensional crenulation cleavage after Platt (1979), but are also commonly referred to as C'-surfaces (Berthe *et al*., 1979) or shear band cleavages (White, 1979). Zheng *et al*. (2011) provided numerous other real world examples including wide-angle V-shaped conjugate faults as outlined by Yin and Taylor (2011). According to MEM, ductile shear zones will form at an angle of 54.7° ± 10° to the maximum compressive stress yielding a conjugate angle of 109.4° ± 20°, which corresponds remarkably well with field and laboratory observations of ductile conjugate sets (Zheng *et al*., 2011).

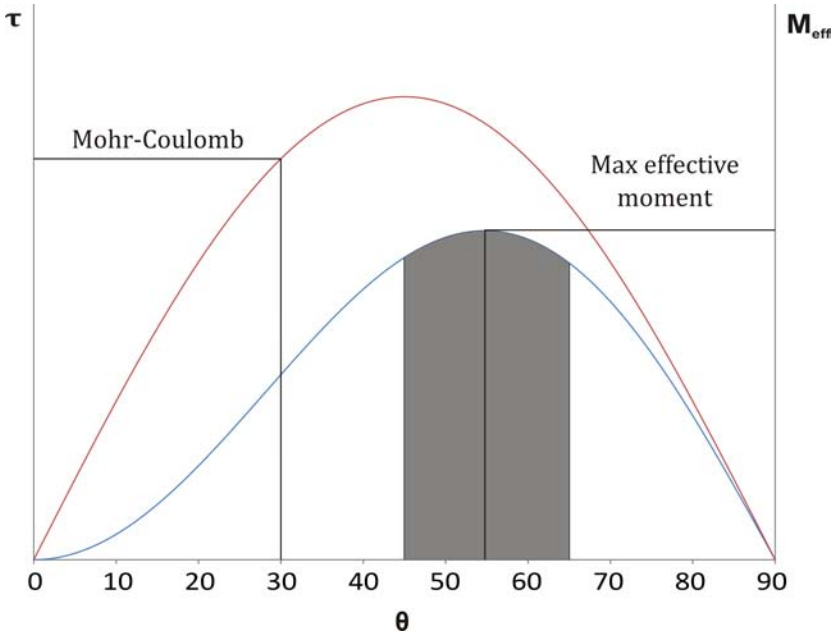

Figure 2.6: Comparison of the maximum effective moment and Mohr-Coulomb failure criteria. The red line shows a plot of the shear stress (τ) on a plane at an angle (θ) with respect to the maximum compressive stress. The blue line shows a plot of the effective moment (M_{eff}) on the same plane (modified after Zheng *et al*., 2004; 2011).

2.7 Conclusion

The structural concepts and models presented above are fundamental to understanding the subsequent descriptions and interpretations related to the tectonic history of the Porcher Island area. In general, the relationship between stretching lineations and shear zone deformation is complex and interpretations based on stretching lineation data should be made cautiously and supported by other lines of evidence including ductile slickenside striae and drag folds.

Chapter 3

Timing and kinematics of shear zone deformation in the western Coast Belt: evidence for mid-Cretaceous orogen-parallel extension

3.1 Introduction

The North American Cordillera is the type example of a complex accretionary orogen (Condie, 2007). It has been active as a convergent margin since the Devonian, undergoing periods of compression, extension, terrane accretion, and strike-slip shearing. The terranes of the northern Cordillera have been grouped into five lithotectonic entities on the basis of stratigraphic, intrusive, isotopic, and faunal connections (Colpron *et al*., 2007; Figure 3.1). The easternmost of these is ancestral North America, which includes the Laurentian craton, marginal sedimentary rocks, and associated parautochthonous terranes. The core of the northern Cordillera is occupied by the Intermontane terranes which evolved as a series of island arcs built on pericratonic fragments that rifted away from western North America during the Devonian (Colpron *et al*., 2006; Nelson *et al*., 2006). Outboard of the Intermontane terranes are the Insular and Northern Alaskan terranes which appear to have evolved in close proximity to Baltica and Siberia during the Neoproterozoic to mid Paleozoic (Colpron and Nelson, 2009; 2011a; Beranek *et al*., 2012a). Mesozoic and younger arc and accretionary complexes fringe the western margin of the northern Cordillera. Oceanic and accretionary complexes (in red on Figure 3.1) provide a record of ocean basins that have closed during evolution of the northern Cordillera. Two metaplutonic 'welts' overprint the terranes outlined above (Monger *et al*., 1982). They include the Omineca Belt, which roughly corresponds to the Intermontane-ancestral North America boundary, and the Coast Belt along the Insular-Intermontane boundary (Figure 3.1). They have historically been attributed to arc magmatism, terrane accretion, or a combination of the two (Monger, 1972; Monger *et al*., 1982; van der Heyden, 1992; McClelland *et al*., 1992).

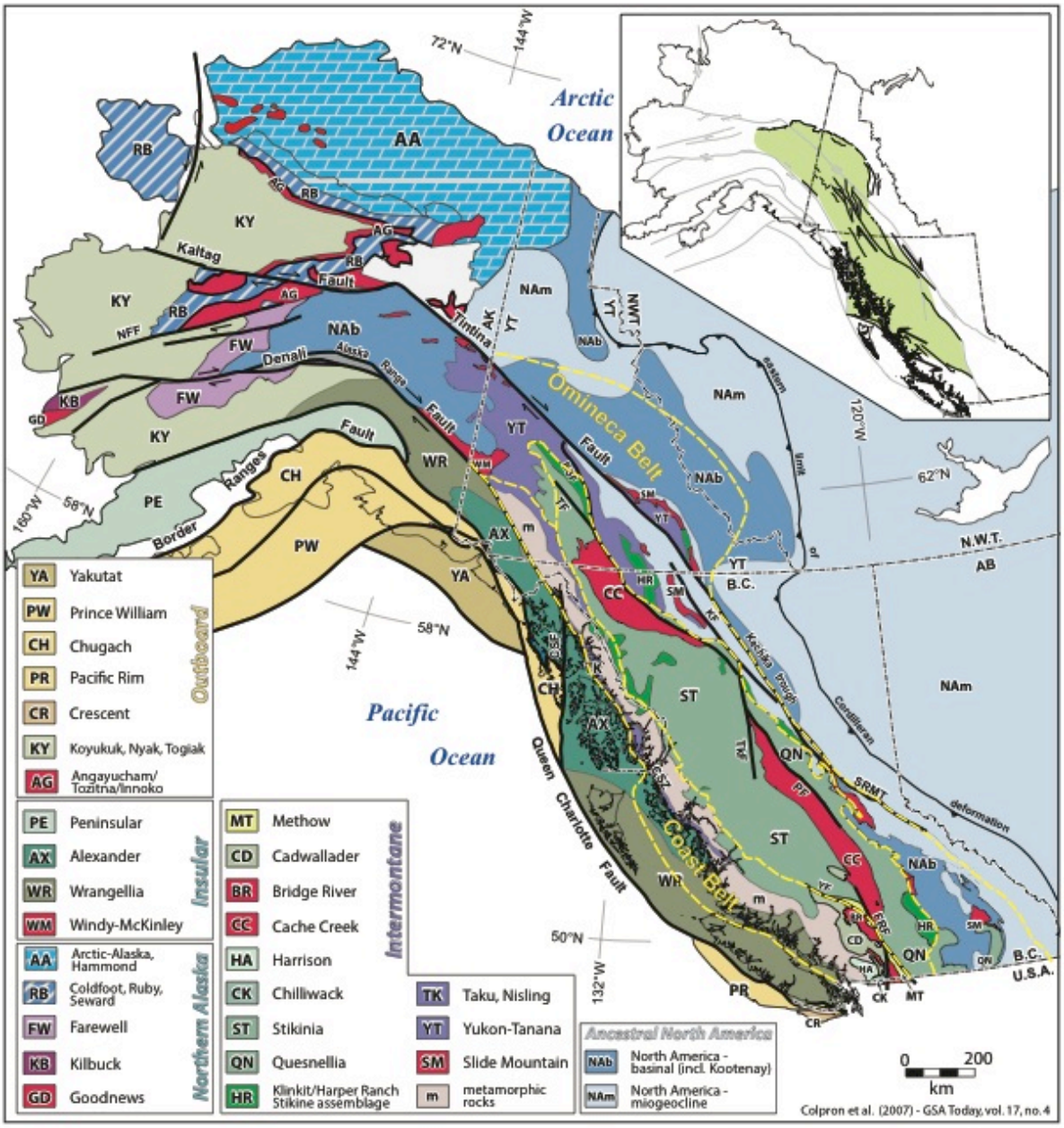

Figure 3.1: Terrane map of the northern Cordillera and location of the metaplutonic 'welts' outlined in yellow (modified after Colpron *et al*., 2007; Colpron and Nelson, 2011b; Wheeler and McFeeley, 1991). Inset map includes major mid-Cretaceous structures through the northern Cordillera which are dominantly sinistral in the Coast Belt and dextral in the Omineca belt, outlining an escape block comprised of the Intermontane terranes (modified

after Colpron *et al*., 2011a). Note that 450 km of younger dextral displacement across the Tintina fault has been removed in inset map.

The mid-Cretaceous was a time of active deformation, magmatism, and metamorphism in the northern Cordillera in British Columbia, Yukon, and Alaska, as well as northern Washington state. Observations along the Coast Belt indicate sinistral transpression (Roddick, 1970; Lawrence, 1978; Rusmore, 1985; Miller, 1988; Leitch, 1989; Schiarizza *et al*., 1990, 1997; Woodsworth *et al*., 1991; Greig, 1992; Greig *et al*., 1992; Hurlow, 1993; Chardon *et al*., 1999; Israel, 2001, 2008; Israel *et al*., 2006; Demerse, 2008; Mahoney *et al*., 2009; Nelson *et al*., 2010a, 2011a, 2012), whereas observations within the Omineca Belt indicate dextral transpression (Gabrielse, 1969; Gabrielse *et al*., 1985, 2006; Abbot and Turner 1991; Mortensen and Hansen 1992; Murphy, 1997; Gabrielse, 1998; Mortensen *et al*., 2006; Colpron, 2006). These observations led to the proposal that the northern Cordillera was undergoing tectonic escape, with the Intermontane terranes escaping towards the north (Nelson *et al*., 2011b; Colpron *et al*., 2011b; Figure 3.1 inset). Tectonic escape within the northern Cordillera had previously been proposed by Wernicke and Klepacki (1988) to explain the lack of Stikinia within the Columbia embayment. In their model, Wrangellia acted as an indentor, effectively splitting Stikinia in two and causing the northern portion of it to escape to the north during the Middle to Late Jurassic. It is based on a correlation of the Seven Devils (Wallowa) terrane to Wrangellia and the apparent lack of Stikinia within the Columbia embayment. However, several other studies have suggested that Seven Devils may be better correlated to Stikinia eliminating both the need for tectonic escape and the driving mechanism (Mortimer, 1986; McGroder and Umhoefer, 1989). The proposed mid-Cretaceous tectonic escape is considered more robust as it is based on observed structures and not dependent on terrane correlations.

The Grenville Channel shear zone in north coastal British Columbia is part of the sinistral transpressive system described above, the structural geology of the area had only previously been investigated as part of broader structural studies (Chardon *et al*., 1999; Chardon, 2003). Structurally focused mapping on Porcher Island and the surrounding area at the northern end of Grenville Channel has documented several northwest-striking sinistral shear zones and one north-striking dextral shear zone. The observations outlined herein, combined with new U-Pb geochronology, indicate that the dextral shear zone formed as a conjugate to the sinistral system during the mid-Cretaceous. Overall, the mid-Cretaceous structures on and near Porcher Island indicate ENE-WSW (orogen perpendicular) shortening and NNW-SSE (orogen parallel or lateral) extension. Lateral motion of material out of a

compressive orogen is the definition of tectonic escape (Burke and Sengor, 1986), so the structures described herein are consistent with the proposed mid-Cretaceous tectonic escape within the northern Cordillera.

The interpretation of conjugate sets is similar to tectonic escape in that they both require not only identification of the appropriate geometry and kinematics, but also an indication that the separate components were active at the same time (Burke and Sengor, 1986). With that in mind, this paper is subdivided into two sections; the first presents data and interpretations related to shear zone kinematics and geometry, while the second presents new geochronological data and discusses its relationship to previous interpretations.

3.2 Geological Setting

3.2.1 Regional Tectonic Setting

3.2.1.1 Coast Belt

The Coast Belt is the region of high topography that covers most of southeast Alaska, coastal British Columbia and northwestern Washington state (Figure 3.1). It is comprised of Jurassic to Tertiary plutons of the Coast Plutonic Complex, as well as metamorphosed rocks belonging to the Insular terranes (Alexander, Wrangellia), Intermontane terranes (Yukon-Tanana, Stikinia), and Jurassic to Cenozoic overlap assemblages (Gravina, Taku). Initial interaction between the Insular and Intermontane terranes is inferred to have occurred during the Middle Jurassic on the basis of overlapping strata, detrital zircon studies, and coincident deformation and metamorphism (van der Heyden, 1992; McClelland and Gehrels, 1990; Kapp and Gehrels, 1998; Gehrels, 2001; Israel *et al*., 2006); however, major crustal thickening associated with high grade metamorphism and plutonism is constrained to mid-Cretaceous to Eocene (Monger *et al*., 1982; Crawford *et al*., 1987; 2000; Crawford and Crawford, 1991; Rubin and Saleeby, 1992; Rusmore *et al*., 2005). The gap between initial interaction and formation of the metaplutonic welt suggests a greater role for Andean-style upper plate contraction and arc magmatism as opposed to terrane accretion for formation of the Coast Belt (van der Heyden, 1992; McClelland *et al*., 1992; Israel *et al*., 2006). An overall eastward younging of plutons of the Coast Plutonic Complex has been identified, with Late Jurassic plutons present only along the western margin of the Coast Belt (van der Heyden, 1992; Butler *et al*., 2006; Gehrels *et al*., 2009). The remainder of the Coast Belt would have been located in the hot back arc region at that time. Enhanced heat flow in the back-arc region would have weakened the lithosphere,

setting the stage for deformation as well as high grade metamorphism during subsequent Cretaceous shortening (Hyndman *et al*., 2005; Hyndman and Currie, 2011; Evenchick *et al*., 2007).

The metamorphic rocks of the Coast Belt in the vicinity of Prince Rupert (Figure 3.1) have been subdivided into three belts separated by major tectonic breaks (Crawford *et al*., 1987; 2000). From west to east, they include greenschist to amphibolite grade schists and gneisses of the western metamorphic belt, high grade gneisses and migmatites of the Central Gneiss Complex, and the low grade to unmetamorphosed sedimentary and volcanic rocks of the eastern belt (Crawford *et al*., 1987). The study area is located within the western metamorphic belt (Figure 3.2). The western and central belts are separated by the Coast shear zone (Stowell and Hooper, 1990; McClelland *et al*., 1992; Klepeis *et al*., 1998; Hollister and Andronicos, 2006; Figure 3.2), which follows the Coast Ranges megalineament in southeast Alaska (Brew and Ford, 1978) and the Work Channel lineament in British Columbia (Hutchison, 1982; Crawford *et al*., 1987). The Coast shear zone is an up to 10 km wide zone of ductile deformation with consistently steep foliations and lineations (Crawford *et al*., 1987; Chardon *et al*., 1999; McClelland *et al*., 2000). It has had a complex polyphase history including mainly east-side-up reverse motion from 65 Ma to 57 Ma, followed by mainly east-side-down normal motion ending by 50 Ma (Klepeis *et al*., 1998; Klepeis and Crawford, 1999; Rusmore *et al*., 2001, 2005; Andronicos *et al*., 1999, 2003; Hollister and Andronicos, 1997, 2000, 2006; Gehrels *et al*., 2009). Dextral shear sense indicators suggest the Coast shear zone also accommodated an important dextral strike-slip component as early as 85 Ma (Stowell and Hooper, 1990; Klepeis *et al*., 1998; Andronicos *et al*., 1999, 2003; Hollister and Andronicos, 1997, 2000, 2006). Early thickening associated with kyanite grade metamorphism within the Central Gneiss Complex is constrained to pre-90 Ma, based on ages for monazite inclusions within garnets that also contain kyanite inclusions (Rusmore *et al*., 2005). The initial thickening of the central belt is inferred to be the result of mid-Cretaceous orogen perpendicular shortening which affected the entire Coast Belt (Crawford *et al*., 1987; 2000; Rusmore *et al*., 2005). It is conceivable that the Coast shear zone had a pre-85 Ma movement history that has been completely erased and overprinted by the younger events. McClelland *et al*. (2000) suggest that the consistent down-dip lineations within the Coast shear zone may even partially be the result of transpression (see Chapter 2).

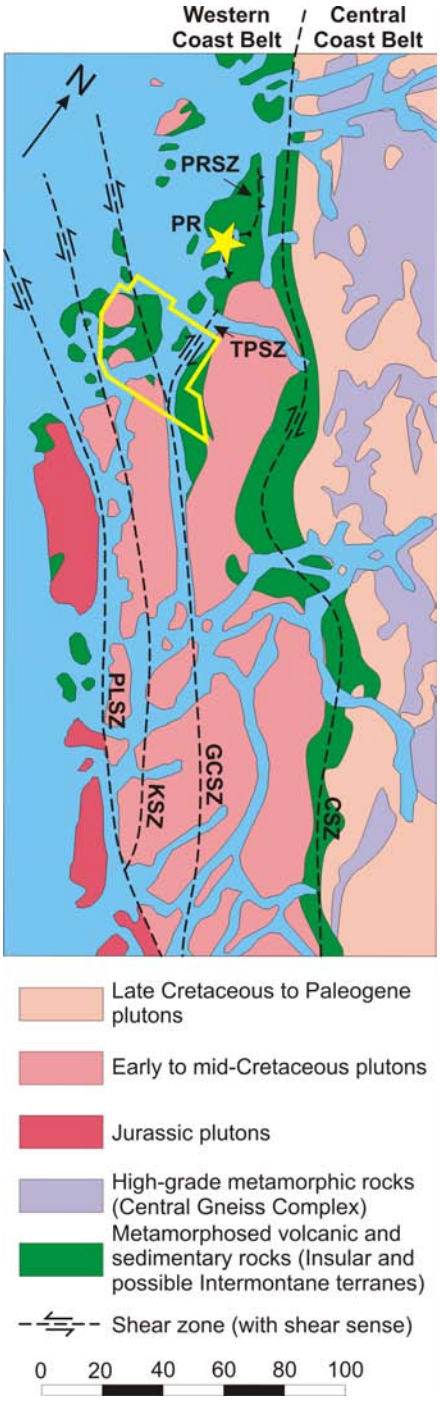

Figure 3.2: Map of the north coastal region of British Columbia. The location of Figure 3.3 is represented by the yellow line. CSZ – Coast shear zone, GCSZ – Grenville Channel shear zone, KSZ – Kitkatla shear zone, PLSZ – Principe-Laredo shear zone, PR – Prince Rupert, PRSZ – Prince Rupert shear zone. Geology is modified after Chardon *et al.* (1999).

3.2.1.2 Western metamorphic belt

The western metamorphic belt consists of greenschist to amphibolite grade schists and gneisses with an increase in metamorphic grade from west to east; Ar-Ar cooling ages are in the 100 to 80 Ma range, indicating that peak metamorphism occurred prior to that time (Crawford *et al*., 1987; van der Heyden, 1989; Chardon *et al*., 1999). Prograde metamorphic garnet growth in the western metamorphic belt has been constrained by 102-108 Ma Lu-Hf ages of garnet (Wolf *et al*., 2010). Protoliths of the western metamorphic belt have been correlated with the Alexander, Yukon-Tanana, Taku and possibly Wrangellia terranes, as well as the Jurassic-Early Cretaceous Gravina Belt overlap assemblage (Brew and Ford, 1978; Stowell and Hooper, 1990; Crawford *et al*., 2000; Nelson *et al*., 2012). The latter locally provides an older limit for deformation and metamorphism. The Coast Plutonic Complex intrusions in the western belt include Late Jurassic (160-140 Ma) plutons in the west, Early Cretaceous (140-100 Ma) plutons in the centre and early Late Cretaceous (100-80 Ma) plutons in the east (van der Heyden, 1989, 1992; Butler *et al*., 2006; Gehrels *et al*., 2009). Gehrels *et al*. (2009) report an eastward younging of Coast Plutonic Complex crystallization ages between 120 and 80 Ma indicating a migration of the magmatic front at a rate of 2.0 to 2.7 km/My.

In the area around Prince Rupert and north through southeast Alaska, dominant structures in the western belt are west-and southwest-vergent thrusts (Crawford and Hollister, 1982; Crawford *et al*., 1987; 2000; Rubin *et al*., 1990; Gehrels *et al*., 1992; Rubin and Saleeby, 1992; Haeussler, 1992; McClelland *et al*., 1992; McClelland and Mattinson, 2000); the southernmost of these is the Prince Rupert shear zone (Figure 3.2). Seismic refraction data has imaged some of these faults down to lower crustal depths where they appear to be truncated by the Coast shear zone (Morozov *et al*., 1998; Hollister and Andronicos, 2006). South of Prince Rupert, the western belt is dominated by northwest-striking, sinistral shear zones (Roddick, 1970; Woodsworth *et al*., 1991; Chardon *et al*., 1999; Chardon, 2003; Wolf *et al*., 2010; Nelson *et al*., 2010a,b, 2011a, 2012; Figure 3.2). In southeast Alaska, both northwest-striking sinistral faults (Brew, 1995; Gehrels and Saleeby, 1987a) and sinistral reverse faults (Rubin and Saleeby, 1992) were simultaneously active during the mid-Cretaceous. Northwest-vergent thrusting in the Gravina Belt reported by Haeussler (1992) may represent a constricting bend during orogen parallel shear. When combined, these relationships suggest strain partitioning during sinistral transpression (Chardon *et al*., 1999; Chardon, 2003).

3.2.2 Geology of the Porcher Island area

The study area is underlain by highly deformed metaplutonic and metamorphosed supracrustal rocks and late synkinematic plutons (Figure 3.3). Reconnaissance 1:250000 scale mapping was carried out by Roddick (1970) and Hutchison (1982). More recent 1:50000 scale mapping was carried out during the summers of 2009 and 2011, leading to detailed lithological descriptions and correlation to known stratigraphy further north (Nelson *et al*., 2010a,b, 2012).

Both fabrics and the overall geology of Porcher Island are largely controlled by northwest striking sinistral shear zones. From southwest to northeast these include the Useless shear zone, the Barrett shear zone, the Salt Lagoon shear zone and the Lamppost shear zone. They are all interpreted to feed into the Grenville Channel shear zone to the southeast, with the Salt Lagoon shear zone representing the main strand, as it records a significant lithological break. In contrast, fabric and lithologies along Telegraph Passage are controlled by the north striking Telegraph Passage shear zone that also merges with the Grenville Channel shear zone to the south. The Salt Lagoon, Telegraph Passage, and Grenville Channel shear zones separate three lithologically distinct regions. The area southwest of the Salt Lagoon and Grenville Channel shear zones is underlain by a mafic to felsic metaplutonic complex of Late Silurian to Early Devonian age with metavolcanic and metasedimentary pendants, all metamorphosed to amphibolite grade (Silurian to Early Devonian metaplutonic complex of Figure 3.3). A late synkinematic to post kinematic granodiorite, part of the Porcher Creek pluton of Nelson *et al*., (2010a), south of the Useless shear zone yielded an age of 410 ± 19 Ma (U-Pb zircon LA-ICP-MS; J.B. Mahoney, unpublished data), constraining the deformation in that region to pre Early Devonian (see Chapter 4; Nelson *et al*., 2012). North of the Useless shear zone, the metaplutonic complex is completely transposed[1] such that primary relationships are obscured. The Swede Point pluton is a distinct, sheet-like, planar intrusion that crosscuts the Silurian to Early Devonian metaplutonic complex. It is comprised of granodiorite, granite, tonalite, and diorite, all ubiquitously deformed into an SC mylonite (Figure 2.5b). It is reported as Devonian (382 Ma ± 14 Ma; U-Pb zircon ID-TIMS; van der Heyden, 1989), although complex systematics were reported which bring into question the reliability of this age.

The area between the Salt Lagoon and Telegraph Passage shear zones is underlain by supracrustal

[1] Transposition is used following the definition of Jiang and Williams (2005) to describe parallel layering due to shearing except where explicitly indicated.

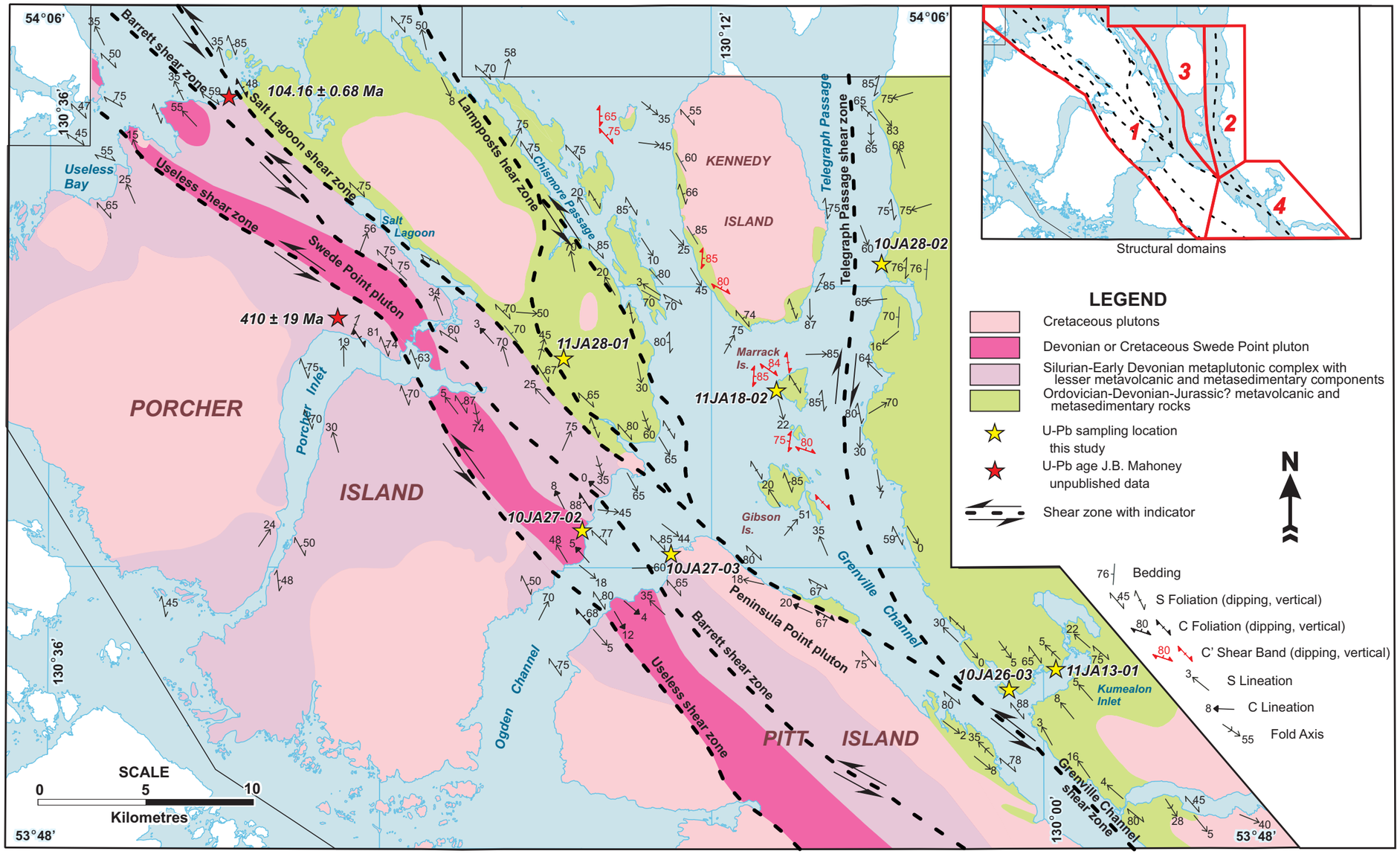

Figure 3.3: Simplified geology of the Porcher Island area. Geochronology sampling locations are identified with yellow stars. Locations of unpublished ages discussed within the text are presented as well. Inset map indicates domains referred to in text (modified after Nelson *et al.*, 2010b; 2012; Angen *et al.*, 2012).

rocks of greenschist to amphibolite grade that are assigned largely to the Descon and Mathieson Channel Formations of the Alexander terrane. Throughout most of this region, layering has been transposed during shear zone deformation; however, on the western shore of Kennedy Island trough cross stratification is preserved.

The area east of the Telegraph Passage shear zone and north of the Grenville Channel shear zone includes rocks of the Descon and Mathieson Channel Formations as well as possible correlatives of the Yukon Tanana terrane and the Gravina belt overlap assemblage. These are ubiquitously transposed and metamorphosed to amphibolite facies. The highest grade rocks in the study area, near the head of Kumealon Inlet, contain sillimanite (as fibrolite) in elongate, diamond shaped masses suggesting it is pseudomorphed after kyanite (Figure 3.4), similar to observations within the Central Gneiss Complex to the east (Rusmore *et al*., 2005). Wolf *et al*. (2010) estimated P-T conditions of 640 – 720 ^{o}C and 360 – 810 MPa for a sample within Kumealon Inlet; they also dated garnet growth for the same sample at 102.6 ± 3.7 Ma by Lu-Hf isotopic methods.

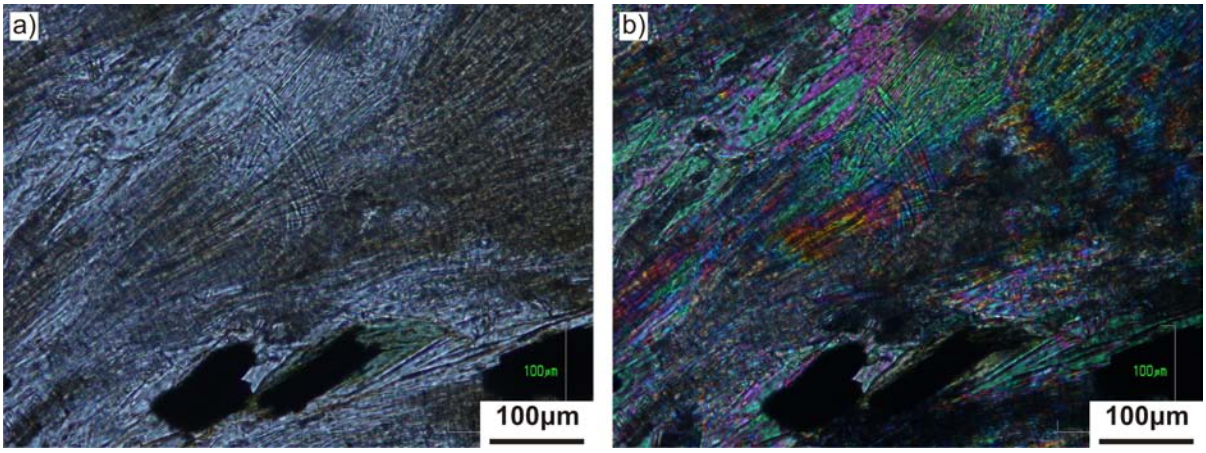

Figure 3.4: Photomicrographs of sillimanite muscovite schist. Sillimanite (fibrolite) masses resembled kyanite blades in outcrop: (a) Plane polarized light; (b) Crossed polarized light.

Both the metaplutonic complex and the supracrustal rocks are intruded by Cretaceous plutons of the Coast Plutonic Complex. These include the Captain Cove pluton (108.5 ± 1.0 Ma -107.5 ± 1.5 Ma, U-Pb zircon ID-TIMS; Butler *et al*., 2006), Peninsula Point pluton (97.1 ± 0.4 Ma, this study), as well as numerous undated plutons. All of these lithologically resemble the Captain Cove and

Peninsula Point plutons; hence they have been assigned to the 109-96 Ma Captain Cove plutonic suite (Nelson and Diakow, 2013.)

3.3 Shear Zones, Structures and Kinematics

The map area has been divided into four domains that are defined on the basis of their characteristic structural elements and kinematic evolution of these structures. The breakdown of domains is as follows: (1) Porcher Island sinistral domain, (2) Telegraph Passage dextral domain, (3) Marrack Island conjugate domain, and (4) Grenville Channel sinistral domain (Figure 3.3). The Porcher Island sinistral domain is characterized by a moderately to steeply northeast dipping foliation, highly variable stretching lineations, and sinistral shear sense indicators. The Telegraph Passage dextral domain is characterized by a steeply east (and west) dipping foliation, variable stretching lineations, and dextral shear sense indicators. The Marrack Island conjugate domain, located between the Porcher Island and the Telegraph Passage domains, is defined on the presence of conjugate shear bands that affect a steep, northwest-striking foliation. The Grenville Channel sinistral domain contains ubiquitous subhorizontal stretching lineations, a steep, northwest-striking foliation, and sinistral shear sense indicators. Where possible, data is presented for subdomains to aid discussion (ie. within identifiable shear zones).

The study area includes evidence for at least four distinct generations of structures (D_1, D_2, D_{3a}, and D_{3b}). The oldest fabrics have been observed within the Silurian to Early Devonian metaplutonic complex, south of the domains discussed herein (Figure 3.3). They are Early Devonian and/or older, as they predate a mildly deformed to undeformed 410 ± 19 Ma pluton (U-Pb zircon, LA-ICP-MS; J.B. Mahoney, unpublished data; Figure 3.3). A 356.1 ± 4.3 Ma (U-Pb zircon, SHRIMP-RG) dyke that crosscuts foliation north of the Salt Lagoon shear zone indicates that this area underwent Paleozoic deformation as well, but has dominantly been overprinted by younger deformation (see Chapter 4). The Late Silurian - Early Devonian deformation (D_1) is discussed in Chapter 4. It is not considered further in the present discussion of Cretaceous structures. The next oldest deformation event, D_2, is recorded as a layer parallel foliation (S_2) observed only in a few localities within Kumealon Inlet of domain 4 (Figure 3.3). The dominant structures in the study area are assigned to a progressive D_{3ab} event related to overall sinistral transpression but accommodated differently in different domains.

3.3.1 Domain 1: Porcher Island sinistral domain

Domain 1 includes northern Porcher Island and adjacent Pitt Island as well as several smaller islands north of Chismore Passage (Figure 3.3). It contains the Useless, Barrett, Salt Lagoon and Lamppost shear zones. Structural data are presented for the areas outside specific shear zones, separately for each shear zone, and for the entire domain including shear zones. The Salt Lagoon shear zone represents a significant lithological break, with the area to the south defined by well developed transposition foliation (S_3) recorded within the northeastern part of the Silurian to Early Devonian metaplutonic complex and the Devonian(?) Swede Point pluton; and the area to the north defined by more heterogeneous fabric development in mainly greenschist-grade metavolcanic and metasedimentary rocks of the Ordovician Descon Formation. Given the major lithological contrast across the Salt Lagoon shear zone, it is interpreted as the main strand of the Grenville Channel shear zone. A distinction is made for lineation and fold hinge line measurements collected north (filled) and south (hollow) of the Salt Lagoon shear zone, only to highlight that they yield the same pattern (Figure 3.5a,b). As discussed below, the high strain deformation in this domain is interpreted as a Cretaceous feature. The southern extent of this domain is limited by the undeformed to weakly deformed 410 ± 19 Ma pluton (J.B. Mahoney, unpublished data) which outcrops immediately south of the Useless shear zone (Figure 3.3). A lack of solid-state fabrics in this pluton indicates that it did not undergo significant Cretaceous deformation. Sinistral shear is indicated throughout domain 1 by porphyroclasts, folded and boudinaged veins and dykes, and drag folds. The transposition foliation (S_3) in domain 1 is consistently subvertical to steeply northeast-dipping (Figure 3.5a). The two northwest-dipping measurements were collected on the short limbs of S-shaped drag folds. Stretching and mineral lineations (L_s) within domain 1 outside of shear zones exhibit a great circle girdle spread of lineations along the average foliation plane (Figure 3.5c), a pattern reflected by the domain as a whole (Figure 3.5a). Ridge-and-groove lineations (L_c; c.f. Lin *et al*., 2007) are constrained to shallowly southeast and northwest plunging (Figure 3.5a). Fold hinge lines (L_f) also exhibit a great circle girdle distribution; distinction of hinges by S- vs Z-folds indicates a major predominance of S-folds but no consistent trend for either type (Figure 3.5b).

3.3.1.1 Useless shear zone

The Useless shear zone is characterised by mylonite and is spatially associated with the tabular, elongated Swede Point pluton (Figure 3.3). The mylonite contains rare long-limbed isoclinal folds (Figure 3.6a). Refolded folds were observed at several localities along the Useless shear zone (Figure

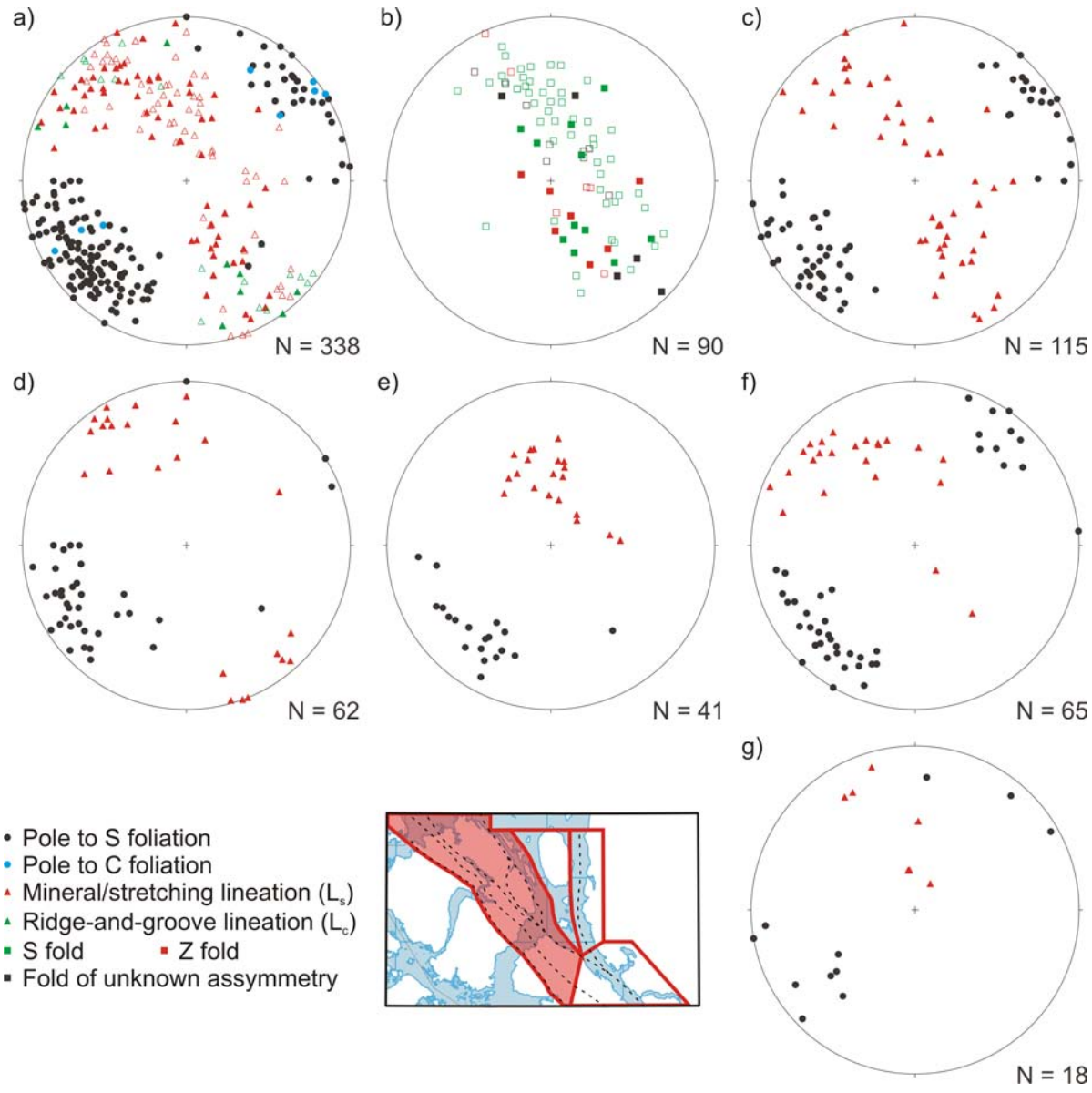

Figure 3.5: Equal-area lower-hemisphere projections of structural data from domain 1: (a) Foliation and lineation data from all of domain 1, filled and hollow triangles indicate measurements within and north of the Salt Lagoon shear zone, respectively, with the shear zone itself included with the northern data as it is dominantly observed within Descon Formation volcanics; (b) Fold hinge line data from all of domain 1; (c) Foliation and lineation data not assigned to specific shear zones, note that it exhibits the same great circle girdle distribution as the domain as a whole; (d) Useless shear zone; (e) Barrett shear zone; (f) Salt Lagoon shear zone; (g) Lamppost shear zone.

3.6b). The Swede Point pluton has been overprinted, at least in part, by the shear zone, as it contains a well developed foliation and locally contains S-C fabrics indicating sinistral shear (Figure 2.5b). However, the planar geometry of the pluton suggests that it was emplaced along a pre-existing structure (Nelson *et al*., 2010a). The foliation within the shear zone is essentially identical to that of domain 2 overall (Figure 3.5d). Stretching and mineral lineations for the Useless shear zone are somewhat variable but are generally shallow relative to the data for the domain as a whole, with a point maximum plunging shallowly to the northwest (Figure 3.5d).

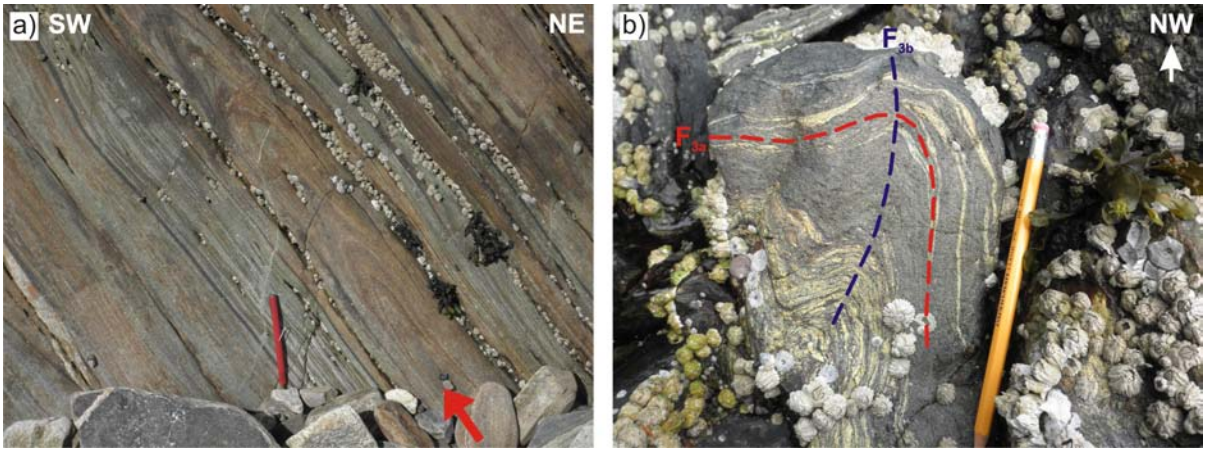

Figure 3.6. Structural observations within Domain 2: (a) Straight gneiss of the Ogden Channel complex including a long limbed isoclinal fold, Useless shear zone north of Bareside Point on southeastern Porcher Island; (b) Ogden Channel orthogneiss with F_{3a} isoclinal folds refolded around F_{3b} folds. Dotted lines represent axial traces, photograph was taken looking down toward the northwest. Both phases of folding are consistent with sinistral reverse sense of shear, Useless shear zone south of Bareside Point on southeastern Porcher Island

3.3.1.2 Barrett shear zone

The Barrett shear zone is located immediately north of the Useless shear zone, localised in a discontinuous belt of metasedimentary screens within the metaplutonic complex (Figure 3.3). Foliations cluster tightly, dipping moderately to the north-northeast (Figure 3.5e). In contrast to the Useless shear zone, lineation orientations within the Barrett shear zone are relatively uniform, plunging moderately to the north (Figure 3.5e). Similar to the Useless shear zone, isoclinal F_{3a} folds are refolded by asymmetrical sinistral F_{3b} folds (Figure 3.7a). Locally sheath folds have been observed (Figure 3.7b), but elsewhere folds appear cylindrical without formation of sheath-like

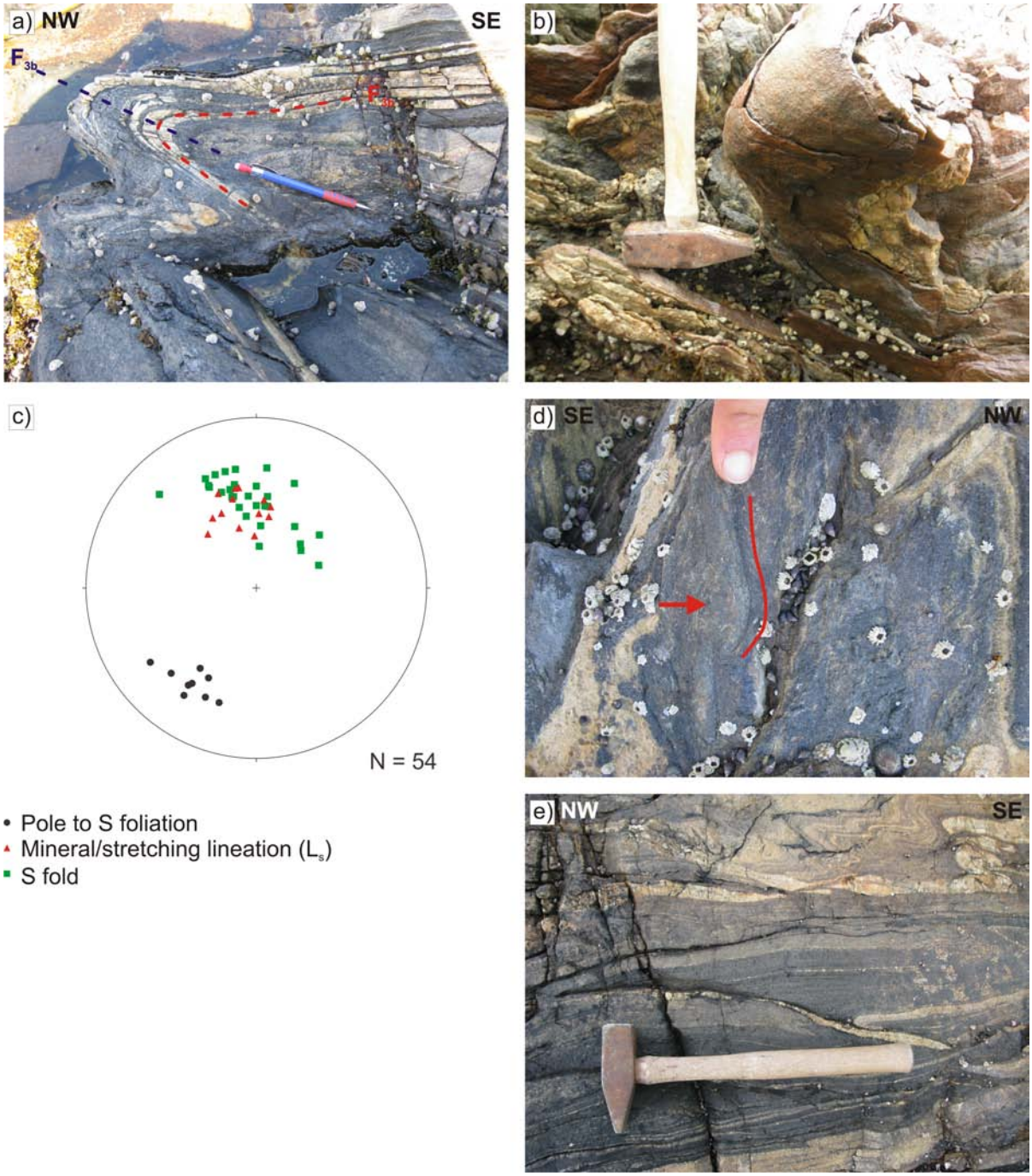

Figure 3.7: Structures associated with the Barrett shear zone, from both northwestern and southeastern Porcher Island: (a) F_{3a} isoclinal folds refolded around F_{3b} folds, northwestern Porcher Island; (b) Highly curvilinear hinge of a sheath fold along the Barrett shear zone, southeastern Porcher Island; (c) Lower hemisphere, equal area stereonet plot of lineations and

foliations from the Barrett shear zone along northwestern Porcher Island. Fold hinge lines and crenulation lineations are plotted as blue circles, and stretching lineations are plotted as red triangles. Poles to transposition foliation are plotted as black squares; (d) Minor, initiated fold with demonstrably non-cylindrical hinge traced by red line, red arrow indicates proposed shear direction; (e) Mylonitized pegmatite dykes both cutting F_2 folds parallel to their axial planes, and being incorporated in folding, northwestern Porcher Island.

geometries (cf. Jiang and Williams, 1998). As previously reported by Nelson *et al*. (2010a) and Angen *et al*. (2012), fold hinge lines along the Barrett shear zone exposure on northwestern Porcher Island are parallel to lineations and are all S-folds (3.7c). Furthermore, tight to isoclinal folds appear highly cylindrical while small, more open folds appear distinctly non-cylindrical (Figure 3.7d).

A swarm of mylonitized pegmatite dykes are observed both crosscutting the F_3 folds parallel to their axial planes and locally folded (Figure 3.7e). Lineations within the mylonitized dykes vary from shallowly northwest to steeply north plunging, and δ-porphyroclasts associated with these lineations indicate sinistral oblique normal motion. One of these dykes yielded a U-Pb zircon LA-ICP-MS age of 104.5 Ma ± 0.9 Ma (U-Pb zircon, LA-ICP-MS; J.B. Mahoney, unpublished data), indicating that at least some of the sinistral shearing took place during the mid-Cretaceous.

3.3.1.3 Salt Lagoon shear zone

The Salt Lagoon shear zone is topographically defined by a linear valley bisecting Porcher Island (Figure 3.3). This shear zone is interpreted as a major structure because it separates the Silurian to Early Devonian metaplutonic complex to the southwest from supracrustal metavolcanic rocks to the northeast, and is therefore interpreted as the northwestern continuation of the main strand of the Grenville Channel fault. Foliation dips moderately to steeply to the northeast (Figure 3.5f). Stretching lineations fall along a great circle girdle with a point maximum plunging shallowly to the northwest (Figure 3.5f). Shear sense indicators include folded and boudinaged veins and dykes, porphyroclasts, and drag folds. They indicate dominantly sinistral shear with minor superimposed dextral shear.

3.3.1.4 Lamppost shear zone

The Lamppost shear zone is a 50-100 metre- wide, heterogeneous deformation zone, comprising numerous smaller-scale, anastomosing greenschist-grade shear zones. This structure occurs along the northeastern shore of Porcher Island (Figure 3.3). Shear sense indicators such as S-C fabrics and

boudinaged veins record sinistral-normal shear. The limited data from the Lamppost shear zone are plotted in Figure 3.5g.

3.3.1.5 Interpretation

The great circle girdle distribution of lineation data from domain 1 is similar to that reported for other lithologically heterogeneous high strain zones (Jiang and Bentley, 2012; Jiang, 2012, and references therein). The overall flow field is accommodated differently within each rheologically distinct unit due to strain partitioning (Lister and Williams, 1983). Jiang (2012) and Jiang and Bentley (2012) have applied micromechanics to model the development of lineations within lithologically heterogeneous high strain zones under idealized Sanderson and Marchini (1984) type monoclinic transpression, with horizontal simple shear and vertical pure shear extension, and produced girdles very similar to those observed in Figure 3.5a.

The separate shear zones within these domains represent specific zones of partitioned strain, and as a result have relatively internally consistent lineation patterns. The Useless and Salt Lagoon shear zones have similar lineation patterns with a shallowly northwest plunging concentration (Figure 3.5d,f). This pattern is consistent with a high simple shear/pure shear ratio at moderate strain in a triclinic transpression zone (Lin *et al*., 1998; Jiang and Williams, 1998); particularly well developed shear sense indicators along these zones also suggest high simple shear/pure shear ratio. The strong, nearly down-dip concentration of lineations within the Barrett shear zone (Figure 3.5e) indicates extremely high strain regardless of simple shear/pure shear ratio (Lin *et al*., 1998; Jiang and Williams, 1998). This is corroborated by the intense grain size reduction and characteristic straight gneiss development of the Barrett shear zone rocks.

The L_c lineations observed are the most reliable indicator of shear direction (Lin *et al*., 2007), suggesting that the simple shear component of deformation was close to subhorizontal. Overall, the distribution of fabric elements within this domain is interpreted to indicate a broad zone of sinistral transpression, with the Useless, Barrett, and Salt Lagoon shear zones representing zones of enhanced strain localization.

Folds with hinge lines parallel to the stretching lineations observed along the northwestern Porcher Island exposure of the Barrett shear zone consistently have S-shapes looking down plunge. These structures are best explained by fold initiation in a flow field dominated by horizontal simple shear followed by pure shear dominated stretching toward the down dip fabric attractor (c.f. Passchier,

1997). This process has previously been discussed by Jiang and Williams (1999) and Kuiper *et al*. (2007). The presence and distribution of Z-folds within these domains is likely the result of a combination of processes. Some of these Z-folds in dykes or veins, which initially formed at an angle to the foliation, started out as S- or M-folds, but progressively changed asymmetry as they rotated from the shortening quadrant into the extensional quadrant of the shear zone as described by Ramsay (1980). We refer herein to such structures as over-rotated folds, because when the dykes and veins rotate into the extensional quadrant they will be stretched and possibly boudinaged into apparent Z-folds but still indicate sinistral motion (Figure 3.8). Other Z-folds demonstrably formed as parasitic structures on the short-limbs of larger scale S-folds. There is also strong evidence for at least one phase of earlier deformation (see Chapter 4). Pre-existing folds will rotate passively towards the fabric attractor and, depending on their original shape and orientation, may be either S- or Z-shaped, or evolve into sheath like geometries (Jiang and Williams, 1999).

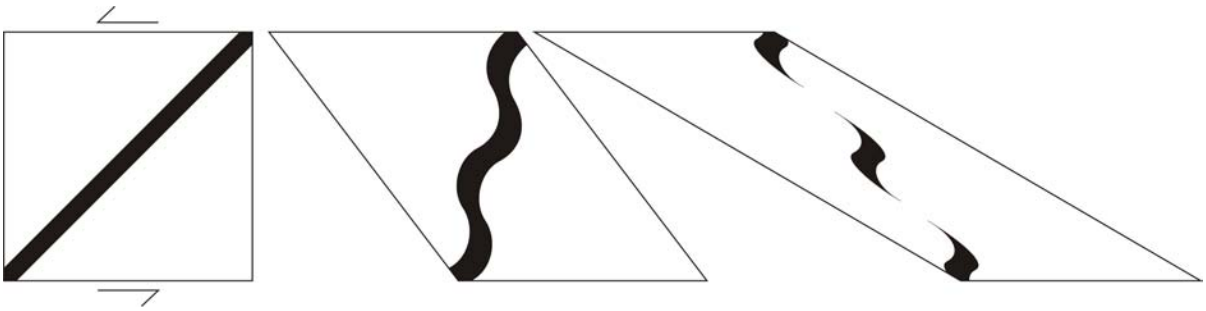

Figure 3.8: Schematic of how over-rotated folds form, showing how sinistral simple shear can result in apparent Z-folds.

3.3.2 Domain 2: Telegraph Passage dextral domain

Domain 5 includes both shores of Telegraph Passage (Figure 3.3). It is characterized by north-striking foliation associated with the Telegraph Passage shear zone. The transposition foliation is steeply dipping, with poles to foliation constrained to an east-west point maximum (Figure 3.9a). Stretching lineations are moderately to steeply plunging, forming a widely distributed subvertical point maximum (Figure 3.9a). Dextral shear with a west side up component is indicated by asymmetric folds, boudinaged veins and dykes, porphyroclasts, and the sense of refraction of foliation at the outcrop scale (Figure 3.10a,b). The map pattern also shows a clockwise rotation of foliation as Telegraph Passage is approached, suggesting dextral deflection of a pre-existing northwest striking foliation (S_{3a}). Shear sense indicators are generally best observed on near-subhorizontal planes, not

parallel to the stretching lineations. The large degree of separation of boudins in pulled-apart veins and dykes indicates significant strike parallel stretch (Angen *et al*., 2012). The distribution of fold hinge lines roughly follows that of stretching lineations (Figure 3.9b). There is a strong predominance of S- over Z-type folds, and several sheath folds have been observed (Figure 3.10c). The distribution of fold hinges in Figure 3.9b exhibits a typical pattern of drag fold evolution into sheath folds where hinge lines of fully developed sheath folds with indistinguishable asymmetry are oriented parallel to the stretching direction and mark a boundary between S- and Z-type folds. Drag folds that do not appear to have rotated since formation indicate dextral motion with a minor west side up component (Figure 3.10a). The dashed circle and lines in Figure 3.9b represent an assumed approximation of the initial orientation and evolution of drag fold hinge lines. The hinge below (or above) an initial perturbation would rotate directly towards the fabric attractor, while the hinge on the opposite side of the perturbation would rotate in the opposite direction through horizontal, becoming Z-shaped, and continue to rotate towards the fabric attractor.

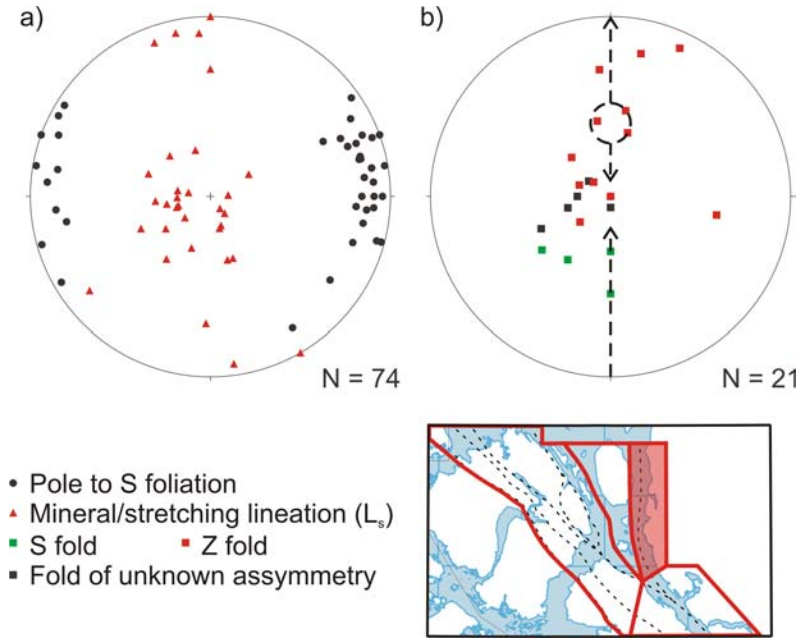

Figure 3.9: Equal-area lower-hemisphere projections of structural data from domain 2: (a) Foliation and lineation data; (b) Fold hinge lines, dashed lines indicate presumed initial orientation of hinge lines and subsequent rotation towards the fabric attractor.

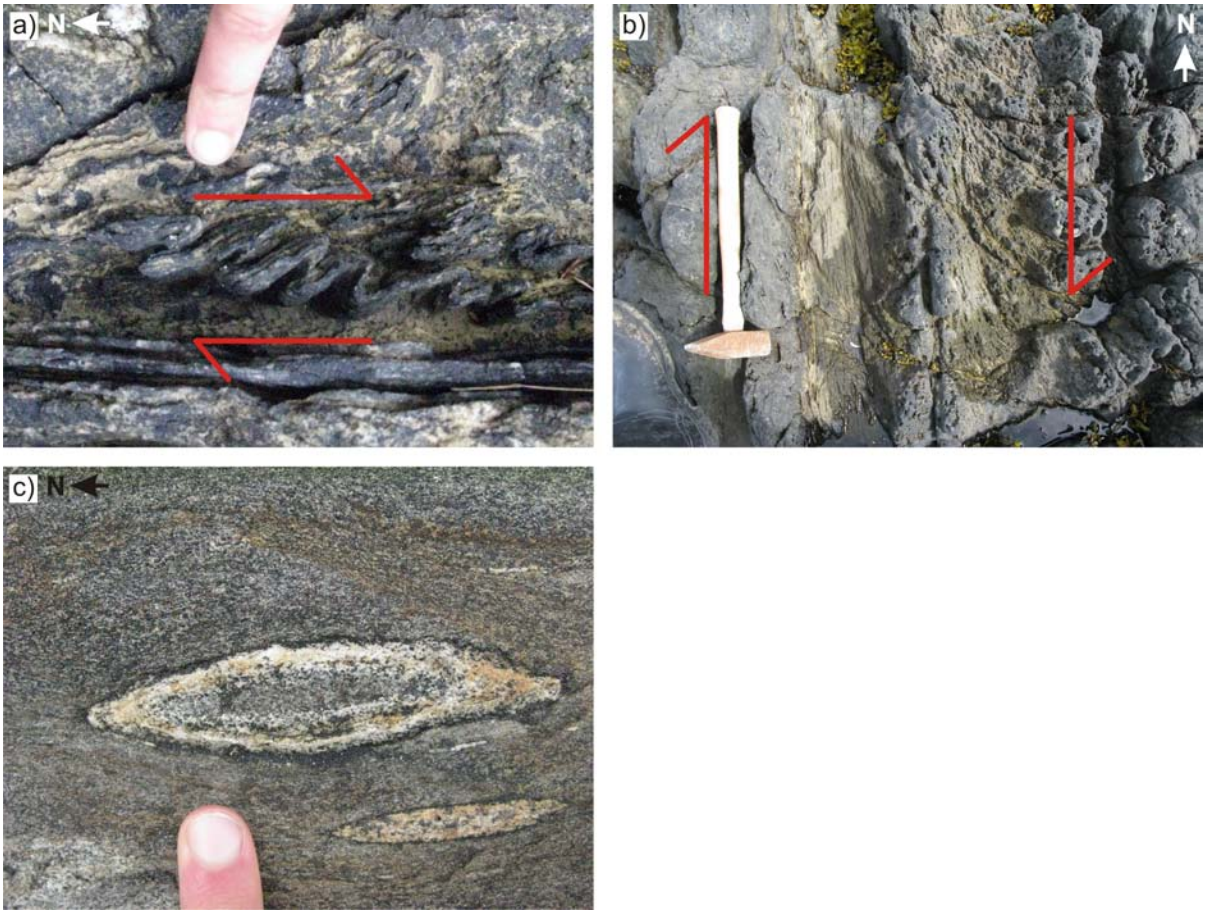

Figure 3.10: Kinematic indicators associated with Telegraph Passage shear zone along the eastern shore of Telegraph Passage: (a) Strongly asymmetric folds which do not appear to have rotated since formation, photo taken looking down towards the north; (b) Dextral deflection of foliation into a local high strain zone, photo taken looking straight down; (c) Oval trace of sheath fold, photo taken looking straight down. Red arrows indicate shear sense.

3.3.2.1 Interpretation

The great circle girdle spread of lineations with a weak down dip concentration in domain 2 corresponding to the Telegraph Passage shear zone is consistent with a transpressional model with significant shear zone perpendicular shortening (Jiang and Bentley, 2012). Unfortunately, no L_c lineations were observed in this zone to provide a reliable indicator of shear direction. The best indicators available are immature drag folds that suggest dextral deformation with a minor west side up component (Figure 3.10a). This is corroborated by other shear sense indicators which are best observed on near horizontal planes. The typical drag fold/sheath fold pattern in Figure 3.9b also

supports a triclinic transpression model since sheath folds are not predicted to form in monoclinic transpression zones (Jiang and Williams, 1999). During triclinic transpression, sheath folds may or may not develop, depending on the initial perturbation of the hinge line (Jiang and Williams, 1999). Overall, the observed structures and distribution of fabric elements are interpreted to indicate dextral transpression with a minor west side up component.

3.3.3 Domain 3: Marrack Island conjugate domain

Domain 3 occupies the zone between the northwest-striking shear zones of domain 1 and the north-striking Telegraph Passage shear zone of domain 2 (Figure 3.3). It contains a steeply northeast-dipping foliation, interpreted to be S_{3a}, that is variably developed as a result of heterogeneous strain (Figure 3.11a). On the western shore of Kennedy Island strain is weak enough that bedding and primary trough cross stratification can be observed. In other areas where strain is high, bedding is parallel to S_{3a} and can only be recognized by marked compositional contrasts. Stretching and mineral lineations exhibit a great circle girdle distribution (Figure 3.11a). The S_{3a} foliation is affected by open

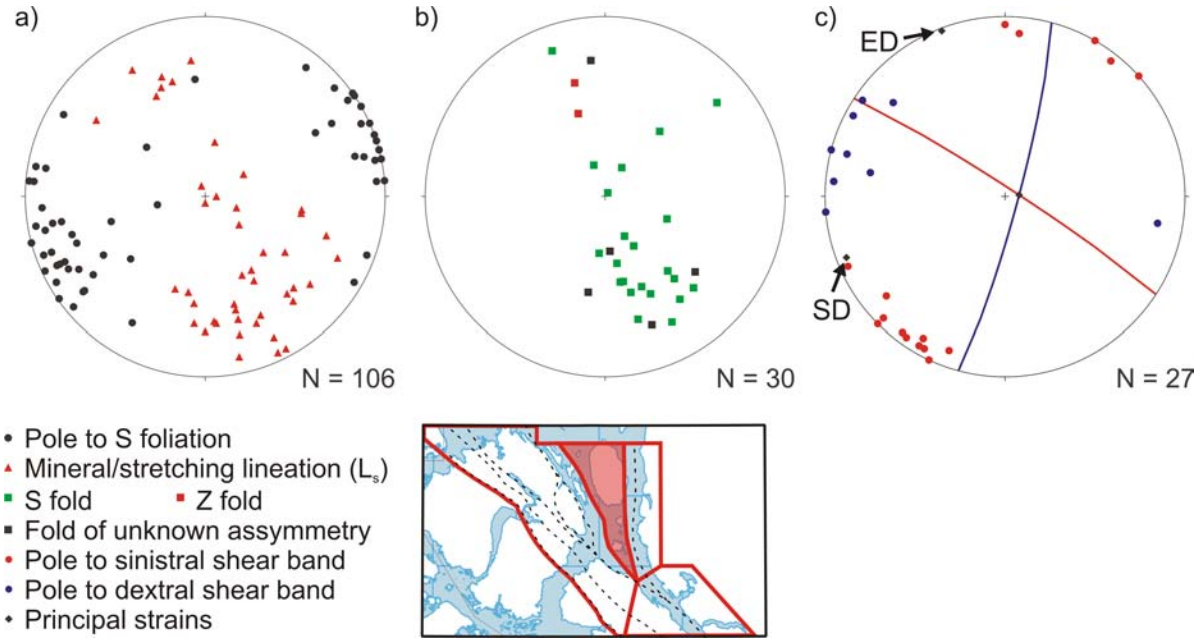

Figure 3.11: Equal-area lower-hemisphere projections of structural data from domain 3. (a) Foliation and lineation data; (b) Fold hinge lines; (c) Conjugate shear bands, measurements are plotted as poles, average values are plotted as the corresponding great circles, SD – shortening direction, ED – extension direction.

to isoclinal F_3 drag folds; these are dominantly S-folds with variable plunges, similar to the widely distributed lineations (Figure 3.11b).

The distinctive feature of domain 3 is the presence of conjugate C' shear bands, considered S_{3b} as they are observed affecting the S_{3a} foliation (Figure 3.11c, 3.12). Sinistral shear bands strike west-northwest and dextral shear bands strike north. One mesoscale sinistral shear band parallel with the local C' shear bands crosscuts a dyke which in turn crosscuts an S-shaped F_3 drag fold; the C' shear bands therefore postdate sinistral folding.

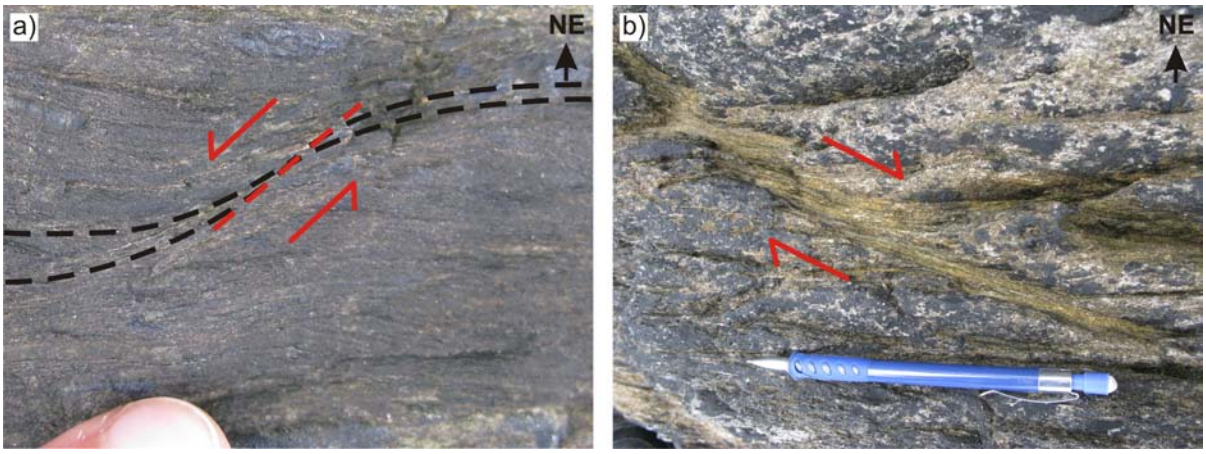

Figure 3.12: Shear bands in domain 3: (a) Sinistral shear band, foliation traces (black dashed lines) curve into shear band (red dashed line) indicating sinistral shear; (b) Dextral shear band. Red arrows indicate shear sense.

3.3.3.1 Interpretation:

The dominant foliation present in this domain associated with variably oriented lineations is interpreted to have formed due to sinistral transpression associated with early deformation in domain 1 and is therefore referred to as S_{3a}. The average orientations of S_{3b} shear bands define a conjugate angle of 108.3° (Figure 3.11c). This is in agreement with the observed and predicted range of 110° ± 20° for ductile conjugate sets (Zheng *et al*., 2004; 2011, and references therein). If the shortening direction is assumed to bisect the conjugate angle following Zheng *et al*. (2004; 2011), then it would be oriented at 6.2° → 248.9° (Figure 3.11c). The corresponding extension direction would be 1.7°→339.1° (Figure 3.11c). The shortening direction corresponds to the average S_{3a} pole orientation (Figure 3.11a). Domain 3 records a transition from sinistral transpression to shortening orthogonal to the dominant foliation, which was accommodated by near horizontal extension.

3.3.4 Domain 4: Grenville Channel Sinistral Domain

Domain 4 comprises the northeast shore of Pitt Island as well as the mainland on the opposite shore of Grenville Channel, including Kumealon Inlet (Figure 3.3). It encompasses the Grenville Channel shear zone proper, the core of which underlies the channel of the same name. The characteristic structure of this domain is consistently subhorizontal stretching and mineral lineations, L_s (Figure 3.13a). At several localities within Kumealon Inlet two generations of foliation are observed. The older, S_2, is a layer parallel foliation. It is folded around open to isoclinal, upright to northeast-vergent folds with subhorizontal hinge lines (Figure 3.13b). These folds, referred to herein as F_{3h} to distinguish them from drag folds, are accompanied by a sub-vertical axial planar cleavage, S_3 (Figure 3.14a). Folds progressively become tighter towards the Grenville Channel shear zone such that S_2 has

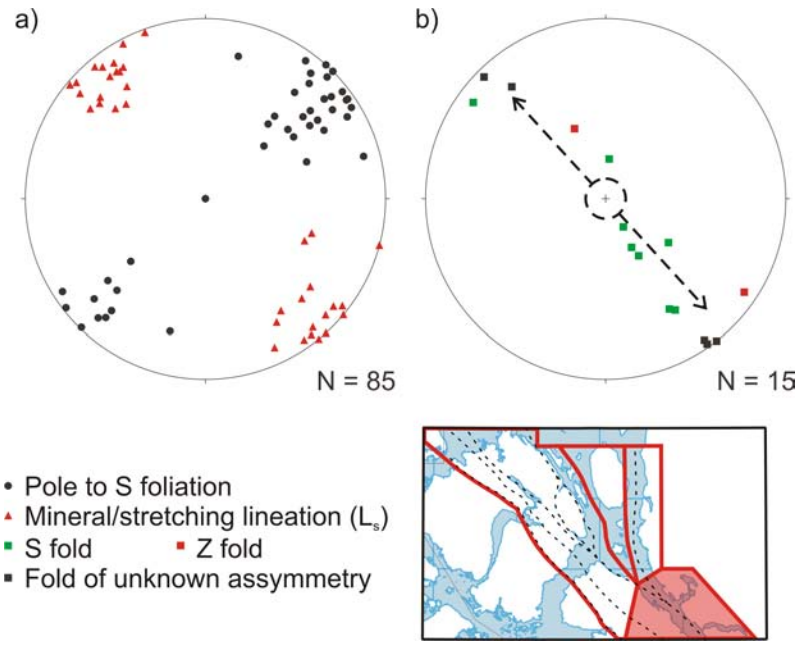

Figure 3.13: Equal-area lower-hemisphere projections of structural data for domain 4: (a) Foliation and lineation data; (b) Fold hinge lines, the dashed circle indicates the interpreted original orientation of hinge lines of drag folds. The upper and lower portions of a drag fold hinge line would evolve along the dashed lines towards horizontal, remaining S-shaped throughout.

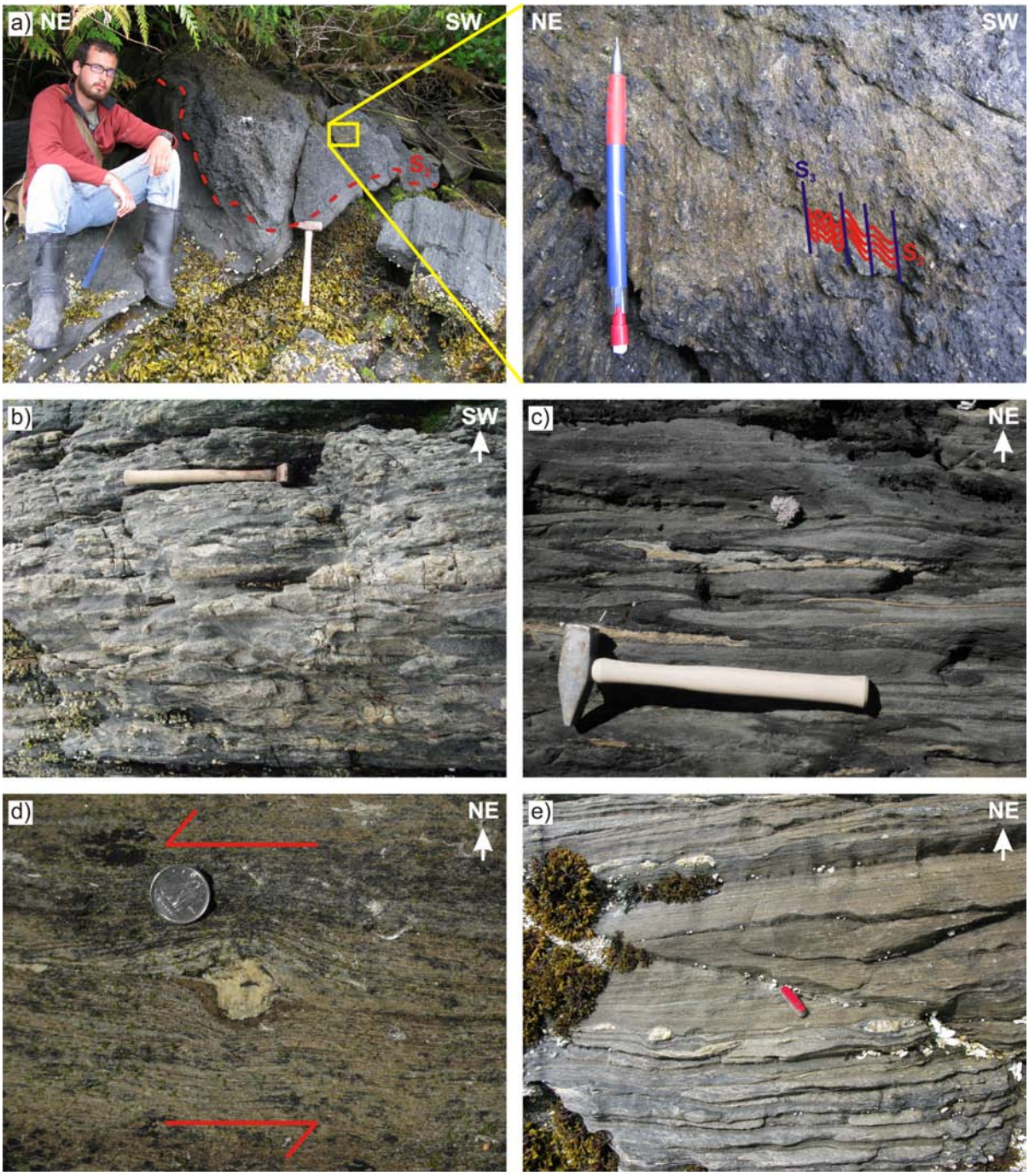
a) NE
SW
S_3
NE
SW
S_3
S_2
b)
SW
c)
NE
d)
NE
e)
NE

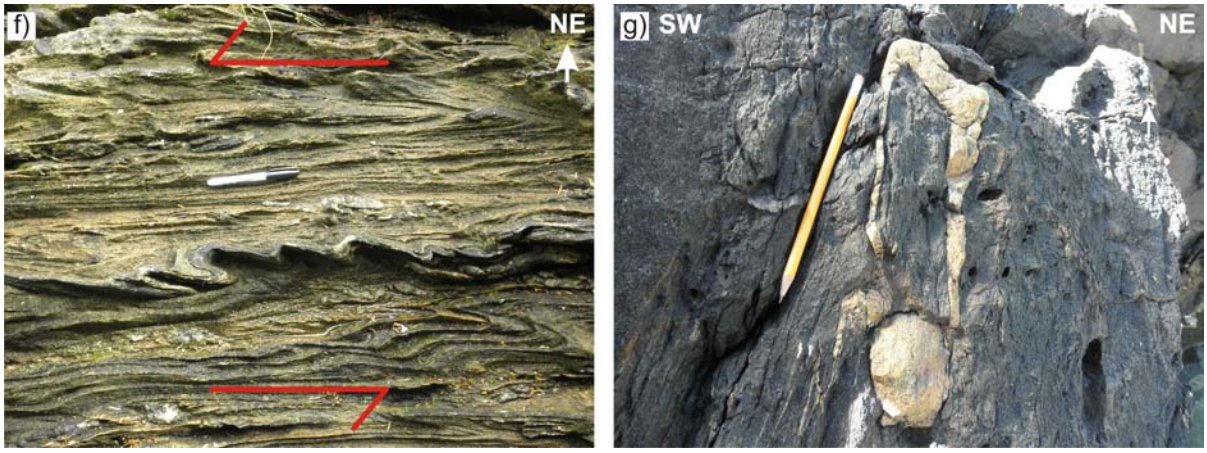

Figure 3.14: Structural features of the Grenville Channel domain: (a) Upright, open F_{3h} fold, S_2 trace follows lithological contact, yellow box outlines detail represented in b; (b) Cobble conglomerate of the Mathieson Channel Formation with 6:1 aspect ratios; (c) Pillow basalt of the Descon Formation with 20:1 aspect ratios; (d) Sigma porphyroclast indicating sinistral shear. Red arrows indicate shear sense; (e) Boudinaged dykes with large spaces between boudins indicating large horizontal stretch; (f) F_{3d} drag folds with highly variable hinge line orientations, ranging from subvertical to subhorizontal within one outcrop. Red arrows indicate shear sense; (g) Oval shaped trace of an F_{3d} sheath fold, photo taken looking towards the northwest.

been completely transposed[2] into S_3 and generally can no longer be recognised. Hence, S_2 and S_3 were plotted together as a composite $S_{2/3}$ foliation (Figure 3.13a). The weak girdle defined by poles to $S_{2/3}$ corresponds to folding of S_2 around subhorizontal hinge lines. The subhorizontal point maximum within the girdle corresponds to the consistent near vertical orientation of the S_3 foliation. The strain gradient is also associated with an increase in sinistral shear sense indicators and increasing horizontal aspect ratios; a cobble conglomerate approximately 500 metres from the mouth of Kumealon Inlet records aspect ratios of 6:1 whereas pillow basalt at the mouth of the inlet records aspect ratios of 20:1 (Figures 3.14b,c). Sinistral shear sense indicators include porphyroclasts as well as folded and boudinaged veins and dykes (Figure 3.14d,e). Foliation boudinage with vertically plunging boudin necks and large horizontal separation of some boudinaged veins indicate a large horizontal stretch within the shear zone (Figure 3.14e).

[2] Note here transposition is used in the traditional sense to refer to foliation which is realigned due to isoclinal folding (Hobbs *et al*.,1976).

In addition to the horizontal F_{3h} folds, this domain also contains drag folds (F_{3d}), the hinge lines of which spread along a sub-vertical great circle girdle (Figure 3.13b). The F_{3d} folds are nearly always S-folds, and their plunges vary significantly within a single outcrop (Figure 3.14f). The only Z-fold observed plunges very shallowly to the southeast. Several sheath folds were observed on vertical planes with fold noses pointing northwest or southeast (Figure 3.14g).

3.3.4.1 Interpretation

The upright to northeast-vergent folds indicate a component of shortening perpendicular to the shear zone boundaries, suggesting that the shear zone was transpressional. The subhorizontal stretching lineations observed along the Grenville Channel shear zone, and throughout domain 4, are anomalous for transpressional shear zones. In most cases, shear zone perpendicular shortening is accommodated by vertical extrusion, causing a steepening of lineations as observed in domain 1. Most transpressional models assume vertical extrusion since the principal unconstrained boundary is the Earth's surface and shear zones pinch out laterally (Sanderson and Marchini, 1984; Tikoff and Greene, 1997; Lin *et al*., 1998; Czeck and Huddleston, 2003; Vitale and Mazzoli, 2008; see Chapter 2). Jiang and Williams (1998) present transpression with horizontal pure shear stretch as an endmember scenario in their unified model. If the maximum pure shear stretch is horizontal, lineations become shallower with continued deformation (see Chapter 2). Therefore, the subhorizontal stretching lineations characteristic of domain 4 are interpreted to indicate that it underwent sinistral transpression with horizontal extension oriented NW-SE.

The hinge lines of both types of folds observed in domain 4 also support sinistral transpression with strike parallel extension. Assuming the shear direction was similar to the horizontal extension direction, slightly non-cylindrical drag folds would evolve from subvertical S-type folds into sheath folds due to opposing sense of rotation of the hinge lines across a perturbation as described above (following the dashed lines on Figure 3.13b). It should be noted that the sense of asymmetry would not change in this case since the hinge lines do not cross the origin. The hinge lines of originally shallowly plunging F_{3h} folds are close to the fabric attractor and as such any rotation towards the fabric attractor would serve to make the folds more cylindrical (Jiang and Williams, 1999).

Subhorizontal lineations in a transpressional shear zone could also be caused by extremely high simple shear/pure shear ratio. Simple shear appears to be concentrated along Grenville Channel, whereas pure shear is distributed more evenly, similar to observations made along the Roper Lake shear zone in Nova Scotia and the Aiken River shear zone in Manitoba (Lin *et al*., 1998; Kuiper *et al*.,

2011). If the simple shear to pure shear ratio was responsible for lineation orientations, one would expect lineations to become steeper (or more variable) away from the core of the shear zone. All lineations observed in domain 4 are shallowly plunging regardless of distance from the Grenville Channel shear zone; therefore, a high simple shear/pure shear ratio is considered an unlikely cause of the subhorizontal lineations in this domain.

3.3.5 Structural Discussion

3.3.5.1 D_{3a} vs D_{3b}

The distinction between D_{3a} and D_{3b} is made on the basis of observations in domains 2 and 3 where there is evidence for a pre-existing northwest-striking foliation (S_{3a}). In domain 2 it is in the form of a clockwise deflection of foliation as the shear zone is approached, suggesting foliation was initially northwest-striking and has been deflected to north-striking (S_{3b}) by dextral shear. In domain 3, the main S_{3a} foliation is attributed to sinistral shear and has been subsequently affected by conjugate shear bands S_{3b}. S_{3a} and S_{3b} are not explicitly distinguishable in domains 1 and 4 which only record sinistral transpression. Therefore D_{3a} is interpreted as northwest striking sinistral transpression which affected all four domains (Figure 3.15a). D_{3b} was accommodated by further sinistral transpression in domains 1 and 4, by dextral transpression in domain 2, and by conjugate shear bands in domain 3 (Figure 3.15b).

3.3.5.2 Relationship between sinistral and dextral D_{3b} structures

The geometry of the sinistral shear zones of domain 1 and dextral shear zone of domain 2 corresponds to that of a ductile conjugate set. The average orientation of foliation within the high strain zones of domain 1(where it should be closest to parallel with the shear zone boundary) are averaged in Figure 3.16. Because the core of the Telegraph Passage is under water, all of the foliations from the Telegraph Passage domain are averaged. The conjugate angle defined by these average orientations is 120.6^{o} (Figure 3.16), at the high end but well within the range (110^{o} ± 20^{o}) of observed and predicted values for ductile conjugate sets (Zheng *et al*., 2004, 2011; references therein). The dextral shear zone is partially identified by the curvature of a pre existing northwest striking fabric, therefore the effect of averaging all values within the domain is that the average value represented in Figure 3.16 is clockwise rotated with respect to the true value. In other words, the reported conjugate angle of 120.6^{o} is an overestimate; the true conjugate angle for these shear zones would be closer to the

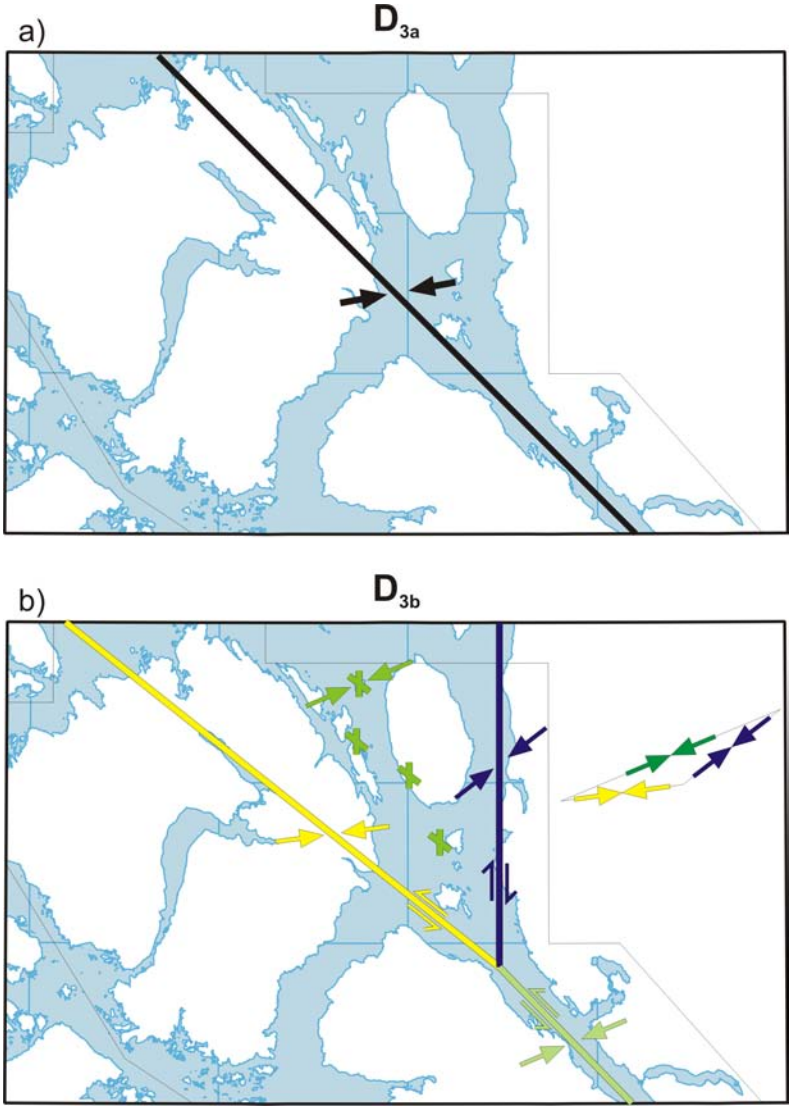

Figure 3.15: Schematic representation of how D3a and D3b deformation events were accommodated in the study area: (a) D3a was a sinistral transpressional event which affected the entire region with an inferred convergence direction represented by the black arrows; (b) D3b was accommodated by sinistral transpression in domain 1 (yellow), dextral transpression in domain 2 (blue), conjugate shear bands in domain 3 (intermediate green), and sinistral transpression with a high convergence angle (pale green). Since domain 1 and 2 structures are inferred to represent a conjugate set, the overall shortening direction would be the combination of their separate shortening directions (dark green in inset). Inferred shortening directions for conjugate shear zones (dark green), conjugate shear bands (intermediate green), and the Grenville Channel shear zone (light green) are all the same.

idealized value of 110°. If the overall shortening direction is assumed to bisect the conjugate angle following Zheng *et al*. (2004; 2011), it would be oriented at 15.4° → 244.7° or roughly ENE-WSW (Figure 3.16). The corresponding extensional direction would be oriented 16.9° →149.9° (Figure 3.16). It is important to note that this differs from the shortening direction inferred for the sinistral and dextral shear zones if they are considered independently. If domain 1 is considered on its own it indicates sinistral transpression with an inferred shortening direction oriented nearly E-W; whereas the domain 1 indicates dextral transpression and an inferred shortening direction oriented nearly NE-SW. The shortening directions for domains 1 and 2 are represented by the yellow and blue arrows in Figure 3.15b, respectively. The overall shortening direction across both would be a combination of the two as represented by the green arrows in the inset in Figure 3.15b; this works out to be roughly ENE-WSW, the same as predicted by bisecting the conjugate angle (Figure 3.16).

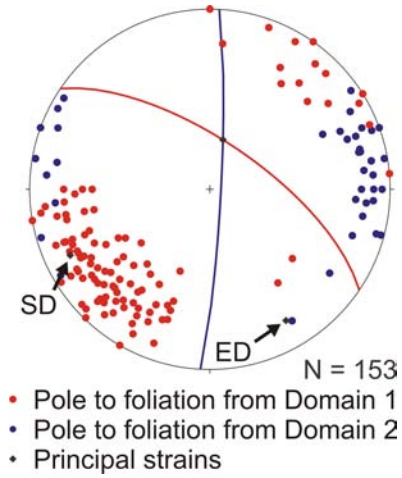

Figure 3.16: Average foliations from the shear zones of domain 1 and all of domain 2. Corresponding principal strain orientations are plotted as black diamonds SD – stretching direction, ED – extension direction, the unlabeled one at the intersection of the two average foliation orientations represents the intermediate strain.

The conjugate shear bands present in domain 3 of roughly the same orientation as the larger shear zones provide direct support for the conjugate set hypothesis. They also may represent a more reliable record of the conjugate angle as the orientation of shear bands is not affected by the orientation of a pre-existing foliation. As presented above, they record a conjugate angle of 108.3° (Figure 3.11c). The corresponding shortening direction of 6.2° → 248.9° is once again ENE-WSW

(Figure 3.15). The geometry of both the map scale and outcrop scale conjugate sets indicates subhorizontal ENE-WSW shortening and NNW-SSE extension.

The Telegraph Passage shear zone does not appear to offset the sinistral shear zone system, nor does it have a known offset counterpart south of it; rather, the sinistral and dextral shear zones appear to merge together towards the Grenville Channel shear zone proper in domain 4. This is similar to observations of ductile conjugate shear zones in Asia, particularly the central Tibet conjugate system (Yin and Taylor, 2011). Therefore, the Grenville Channel shear zone domain should retain the same convergence direction since it represents deformation between the same two external blocks (Figure 3.15b). The high degree of shear zone perpendicular shortening indicated by upright to northeast-vergent folds in this domain, some of which are isoclinal, supports such a high convergence angle. The horizontal, strike parallel extension reported for the Grenville Channel domain corroborates the horizontal extension implied by the conjugate set hypothesis. Extension in this domain is oriented NW-SE, probably the result of the Grenville Channel shear zone being partially controlled by a pre-existing anisotropy.

Dextral, north-striking shear zones, albeit minor ones, are reported at other locations within the western metamorphic belt as far south as Klemtu (Chardon *et al*., 1999; Nelson *et al*., 2011a) and as far north as southern Prince of Wales Island (Gehrels and Saleeby, 1987b), a distance of approximately 250 km. They were previously interpreted to predate the sinistral shear zones due to the lack of offset of the latter. However considering the structural evidence related to the Telegraph Passage shear zone presented herein it is possible that these also represent conjugates to the sinistral shear zone system. Radiometric age dating of the deformation in these dextral shear zones could test whether they are coeval with the adjacent sinistral shears, as presented below for the Porcher Island area.

3.4 Geochronology

Geometry and kinematics alone are not sufficient to conclude that these shear zones formed as a conjugate set. As is the case for tectonic escape, interpretation of a conjugate set requires not only identification of the correct geometry, but also evidence that these shear zones were active at the same time. To test this hypothesis, a series of geochronology samples from dykes which displayed informative relationships to constrain deformation were collected and analyzed via U-Pb zircon geochronology to provide absolute ages for the events outlined above. Samples are presented as they

relate to structural domains described above. Two samples were collected which relate to sinistral transpression in domain 1: the Swede Point (10JA27-02) and Peninsula Point (10JA27-03) samples. Dextral transpression in domain 2 is constrained by the Telegraph Passage sample (10JA28-02). Conjugate shear bands are constrained by the Marrack Island sample (11JA18-02). The sinistral transpression in domain 4 is constrained by the Grenville Channel (10JA26-03) and Kumealon Inlet (11JA13-01) samples. Sampling localities are plotted on Figure 3.3.

3.4.1 Analytical methods:

The data presented herein represent three methods of analysis from two labs: LA-ICP-MS (Laser Ablation Inductively Coupled Plasma Mass Spectrometry) and ID-TIMS (Ion Dilution Thermal Ionization Mass Spectrometry) carried out at the Jack Satterly Geochronology Laboratory and SHRIMP-RG (Sensitive High Resolution Ion Microprobe – Reverse Geometry) carried out at the Stanford USGS Micro Analysis Centre. Samples collected during the summer of 2010 were analyzed by LA-ICP-MS and ID-TIMS while samples collected during the summer of 2011 were analyzed by SHRIMP-RG. For all methods, zircon was separated from up to 20 kg samples following standard methods including disc milling, Wilfley™ table concentration, magnetic separation using a Frantz™ Isodynamic Magnetic separator, and heavy liquids separation. Zircons were then hand picked under alcohol. All graphical plots and age calculations were produced using Isoplot 3.7 (Ludwig, 2009).

3.4.1.1 LA-ICP-MS AND ID-TIMS METHODS

Picked zircons were imaged under reflected light. Samples 10JA26-03 (Grenville Channel), 10JA27-03 (Peninsula Point), and 10JA28-02 (Telegraph Passage) contained zircons greater than 200 μm, a representative subset of which were mounted in 2.54 cm epoxy resin rounds and polished to expose cross sections. The zircons in the polished mount were imaged using a JEOL JSM-6610 scanning electron microscope (SEM) in backscattered electron (BSE) and cathodoluminescence (CL) modes in order to identify potential core and rim structures. Whole zircons from sample 10JA27-02 (Swede Point), as well as extra grains from samples 10JA26-03 and 10JA28-02 were mounted on a glass slide using double-sided tape and imaged under reflected light. All LA-ICP-MS analyses were carried out using a Nu-Wave UP-213 laser ablation microprobe attached to a Thermo Elemental (VG) PlasmaQuad PQ ExCell quadrupole mass spectrometer. U-Pb isotopic composition was calibrated to standards BR266 (559.0 ± 0.3 Ma; Stern *et al*., 2001) and DD 91-1 (2682.4 ± 1.0 Ma; Davis, 2002). Samples 10JA27-02, 10JA27-03, and 10JA28-02 produced concordant ages, and grains without

evidence for inherited cores were reanalyzed by ID-TIMS following the standard methods of Krogh (1973) in order to achieve higher precision. All zircons were abraded prior to ID-TIMS analysis to remove domains affected by lead loss (Krogh, 1982). Data reduction for LA-ICP-MS and ID-TIMS analyses was completed using the program of Davis (1982).

3.4.1.2 SHRIMP-RG METHODS

Samples 11JA13-01 (Kumealon Inlet) and 11JA18-02 (Marrack Island) were analyzed via SHRIMP-RG. Zircons were mounted in 2.54 cm epoxy resin rounds and polished to expose cross sections. The grains were imaged via transmitted light, reflected light, and cathodoluminesence once again to identify potential core and rim structures. The procedure for SHRIMP-RG analyses followed that of Williams (1998), with data reduction completed using the SQUID program (Ludwig, 2005). U-Pb isotopic composition was calibrated to zircon standard R33 (419 Ma; Black *et al*., 2004).

3.4.2 U-Pb Results:

Isotopic analyses are presented in appendix A. Graphical representation of all LA-ICP-MS, ID-TIMS, and SHRIMP-RG data are presented in Figures 3.17, 3.18, and 3.19, respectively. Uncertainty ellipses are plotted at 2 sigma and all age uncertainties are reported at 95% confidence levels. Decay constants used are from Jaffey *et al*. (1971), and common Pb isotope compositions were estimated from Stacey and Kramers (1975).

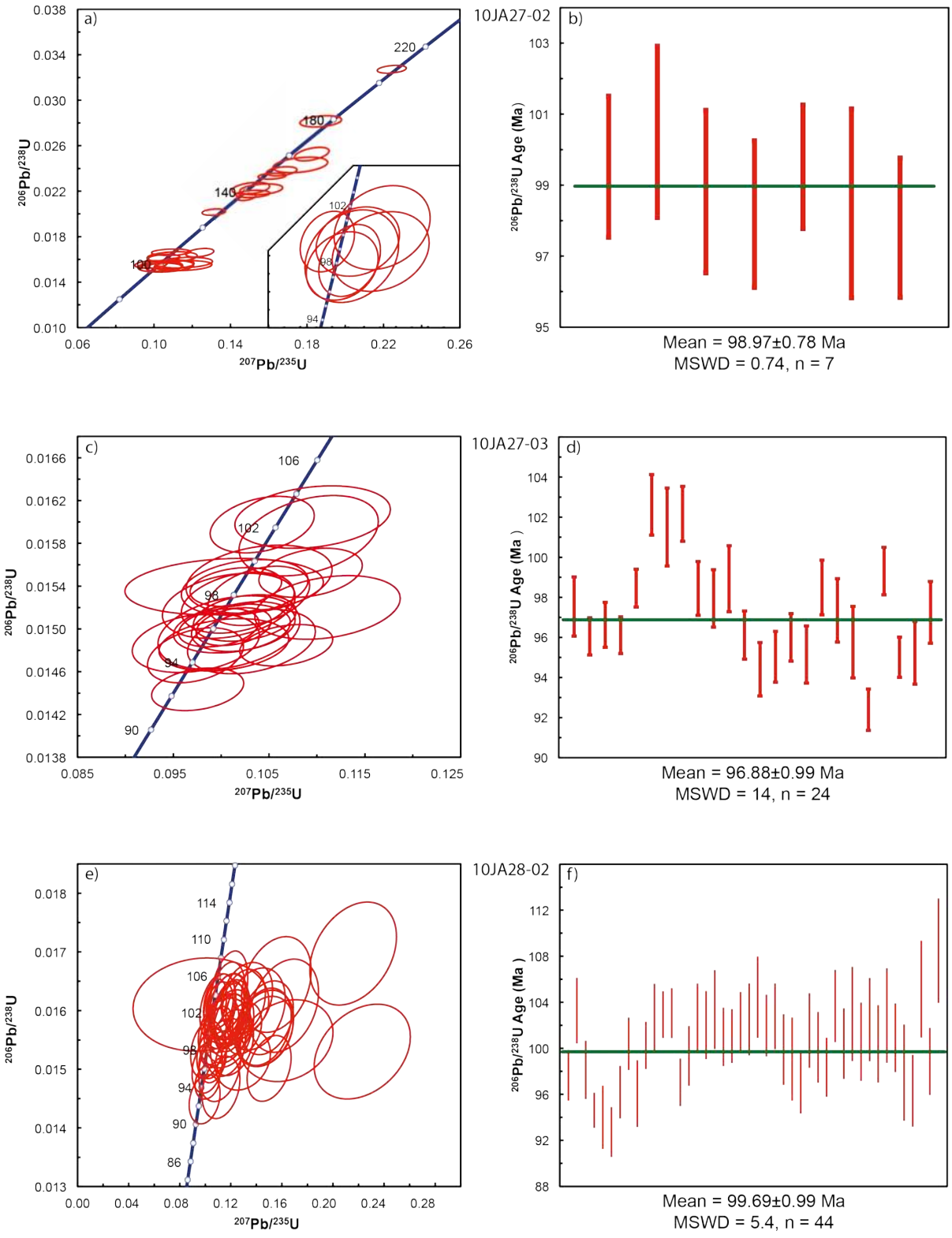
a)
b)
10JA27-02
c)
d)
10JA27-03
e)
f)
10JA28-02
$^{206}Pb/^{238}U$
$^{207}Pb/^{235}U$
$^{206}Pb/^{238}U$ Age (Ma)
Mean = 98.97±0.78 Ma
MSWD = 0.74, n = 7
Mean = 96.88±0.99 Ma
MSWD = 14, n = 24
Mean = 99.69±0.99 Ma
MSWD = 5.4, n = 44

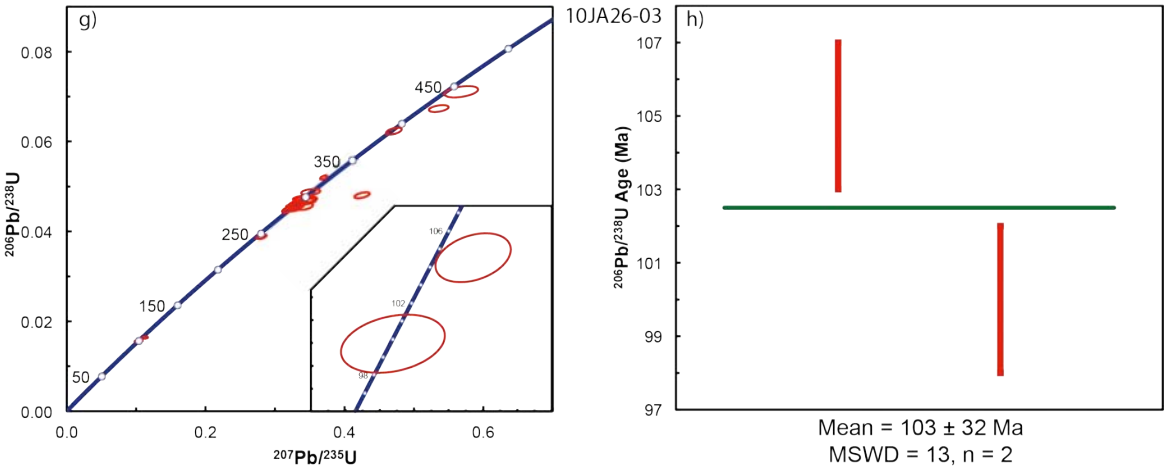

Figure 3.17: Concordia and $^{206}Pb/^{238}U$ weighted average plots for all LA-ICP-MS analyses. Where samples contain a significant range of ages, the youngest data are presented in an inset. Data point uncertainties are 2σ. Reported ages are all weighted average $^{206}Pb/^{238}U$ ages at 95% confidence, with uncertainties calculated from data point uncertainties only. One concordant analysis was removed from (g) to allow the rest of the data to be displayed in more detail. Analytical data are presented in table A.1.

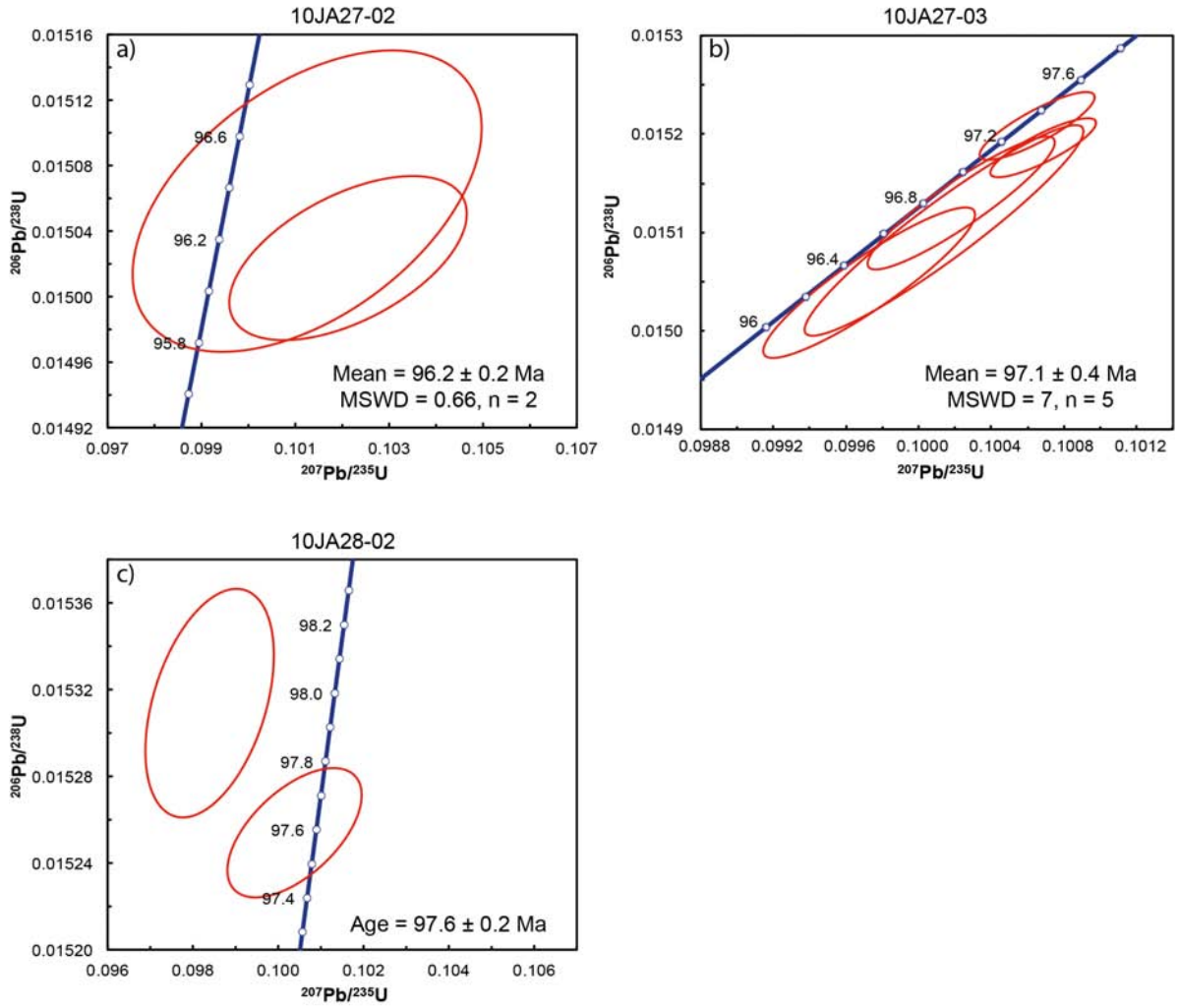

Figure 3.18: Concordia plots for all ID-TIMS analyses. Data point uncertainties are 2σ. Reported ages are all weighted average $^{206}Pb/^{238}U$ ages at 95% confidence, with uncertainties calculated from data point uncertainties only. Reported age for (c) is calculated from the younger of the two analyses only, see text for more details. Analytical data are presented in table A.2.

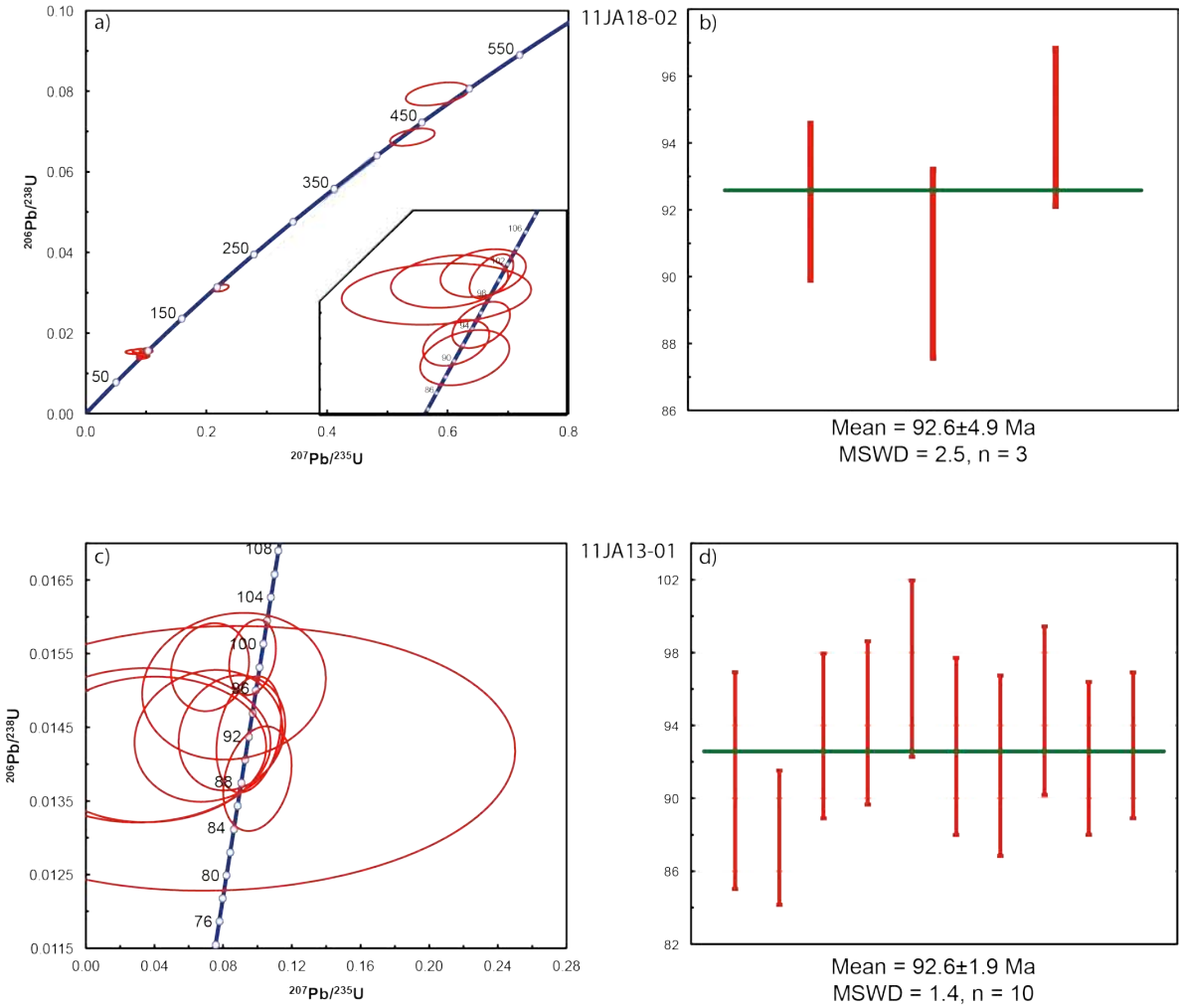

Figure 3.19: Concordia and $^{206}Pb/^{238}U$ weighted average plots for all SHRIMP-RG analyses. Where samples contain a significant range of ages, the youngest data are presented in an inset. Data point uncertainties are 2σ. Reported ages are all weighted average $^{206}Pb/^{238}U$ ages at 95% confidence, with uncertainties calculated from data point uncertainties only. Analytical data are presented in table A.3.

3.4.2.1 10JA27-02 Swede Point

Sample 10JA27-02 was collected from one of a series of weakly foliated tonalite dykes spatially associated with the Swede Point pluton, and interpreted as late synkinematic with respect to sinistral shear. The sampling location was along the western shore of Ogden Channel (Figure 3.3) but similar dykes were observed throughout the extent of the Swede Point pluton. These dykes range from medium to very coarse grained, even pegmatitic in places; they are light grey in colour with a weak

foliation defined by biotite. The north-northwest-striking foliation within the dykes is consistently oblique to the much stronger northwest-striking foliation that dominates the Swede Point pluton (Figure 3.20). The higher angle of S-foliation with respect to shear zone boundaries suggests that these dykes have experienced less sinistral shear strain than the Swede Point pluton (Ramsay and Graham, 1970). It is thus inferred that the dykes were emplaced late during sinistral shear.

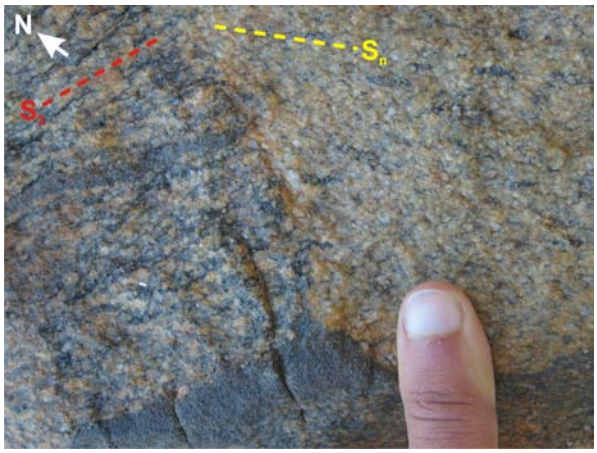

Figure 3.20: Oblique foliation relationship between Swede Point pluton and one of the crosscutting tonalite dykes. The northwest striking foliation in the swede point pluton (red) is referred to as S_3 as it is parallel with the overall foliation within domain 1, while the NNW-striking foliation in the tonalite dyke (yellow) is referred to as S_n to distinguish it even though it is interpreted to have formed late during the same deformation event. Dyke sampled as 10JA27-02 is not shown.

The Swede Point sample (10JA27-02) contains pale honey coloured zircons with few to no inclusions. They are dominantly elongate prismatic crystals between 25-75 µm wide and 100-200 µm long, with a subordinate amount of more equant crystals. They are dominated by {110} prismatic forms and {101} pyramidal forms (cf. Pupin, 1980). Such forms are assigned to fluid rich granites and pegmatites, consistent with field observations of the dykes as pegmatites. The 22 concordant LA-ICP-MS analyses are plotted in Figure 3.17a. There is a cluster of analyses near 100 Ma and a scatter between approximately 130 Ma and 210 Ma (Figure 3.17a). The time resolved data for zircons of this sample typically indicate the presence of an inherited core, so the scattered older ages are interpreted as inherited. The inset in Figure 3.17a as well as Figure 3.17b contain only the seven overlapping mid-Cretaceous data which yielded a weighted average $^{206}Pb/^{238}U$ age of 98.97 ± 0.78 Ma. Two grains which did not show any evidence for inherited cores were selected for ID-TIMS analysis. One

of these lies slightly right of Concordia (Figure 3.18a). This emphasizes the imprecise nature of $^{207}Pb/^{235}U$ ratios in young zircons due to the small amount of ^{207}Pb accumulated, and hence why reported ages are based on the $^{206}Pb/^{238}U$ ratio alone. The two ID-TIMS analyses yield a weighted average $^{206}Pb/^{238}U$ age of 96.2 ± 0.2 Ma (Figure 3.18a) which is reported as the age for this sample. Because this sample is interpreted as late-synkinematic, it suggests that sinistral shear deformation in domain 1 took place during the mid-Cretaceous, coming to an end shortly after 96 Ma.

3.4.2.2 10JA27-03 Peninsula Point pluton

Sample 10JA27-03 was collected from one of a series of tonalite dykes in between the Salt Lagoon and Barrett shear zones (Figure 3.3) which are inferred to be late synkinematic with respect to sinistral shear zones. The dykes are correlated with the Peninsula Point pluton based on proximity and strong petrographic similarity; of note is the presence of zoned plagioclase visible in hand specimen. The dykes crosscut foliation in the Ogden Channel complex orthogneiss and metasedimentary pendants within it. They record varying degrees of folding and stretching depending on orientation consistent with a small amount of sinistral motion (Figure 3.21). Those dykes oriented in the shortening quadrant are folded, whereas dykes oriented in the extensional quadrant are stretched. The dyke indicated by yellow arrows in Figure 3.21 is both folded and stretched indicating that it was originally oriented in the shortening quadrant where it became folded, then rotated into the extensional quadrant where it was subsequently stretched.

Transparent, euhedral, stubby zircons from the Peninsula Point sample (10JA27-03) range in size from 100-250 μm in width and 200-500 μm in length, and the larger grains have common inclusions. The SEM images of zircons from this sample consistently exhibit oscillatory zoning indicative of igneous zircon growth (Hoskin and Schaltegger, 2003) (Figure 3.22a). The 24 near concordant LA-ICP-MS analyses produced a weighted average $^{206}Pb/^{238}U$ age of 96.88 ± 0.99 Ma (Figure 3.17d). Five grains were selected for ID-TIMS analysis, all of which lie on, or nearly on Concordia and yield

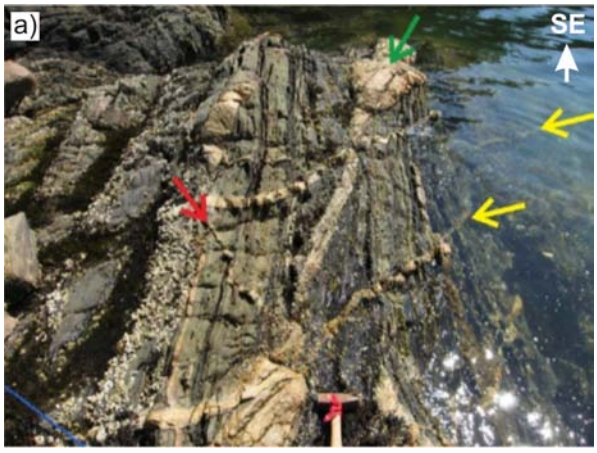

Figure 3.21: Sinistrally deformed dykes associated with the Peninsula Point pluton, collected as sample 10JA27-03. The red arrow points to a dyke in the shortening quadrant that is folded. The green arrow points to a dyke in the extensional quadrant that is stretched. The yellow arrows point to two portions of one dyke which exhibits evidence for folding and stretching consistent with rotation from the shortening quadrant to the extensional quadrant.

a weighted average $^{206}Pb/^{238}U$ age of 97.1 ± 0.4 Ma (Figure 3.18b). The Peninsula Point sample (10JA20-03) corroborates the result from the Swede Point sample that sinistral shear in domain 1 occurred through the mid-Cretaceous.

3.4.2.3 10JA28-02 Telegraph Passage

Sample 10JA28-02 was collected from a medium grained diorite dyke along the eastern shore of Telegraph Passage (Figure 3.3). It is interpreted as late synkinematic with respect to dextral shear along the Telegraph Passage shear zone. It intrudes a metasedimentary sequence assigned to the Descon Formation that locally displays asymmetric, isoclinal folds indicating dextral shear (Figure 3.10a). The dyke cuts across some of these folds and exhibits pinch and swell structures consistent with dextral shear, suggesting late-synkinematic emplacement. In thin section plagioclase commonly exhibits deformation twins indicating it accommodated a small amount of strain (Figure 3.23).

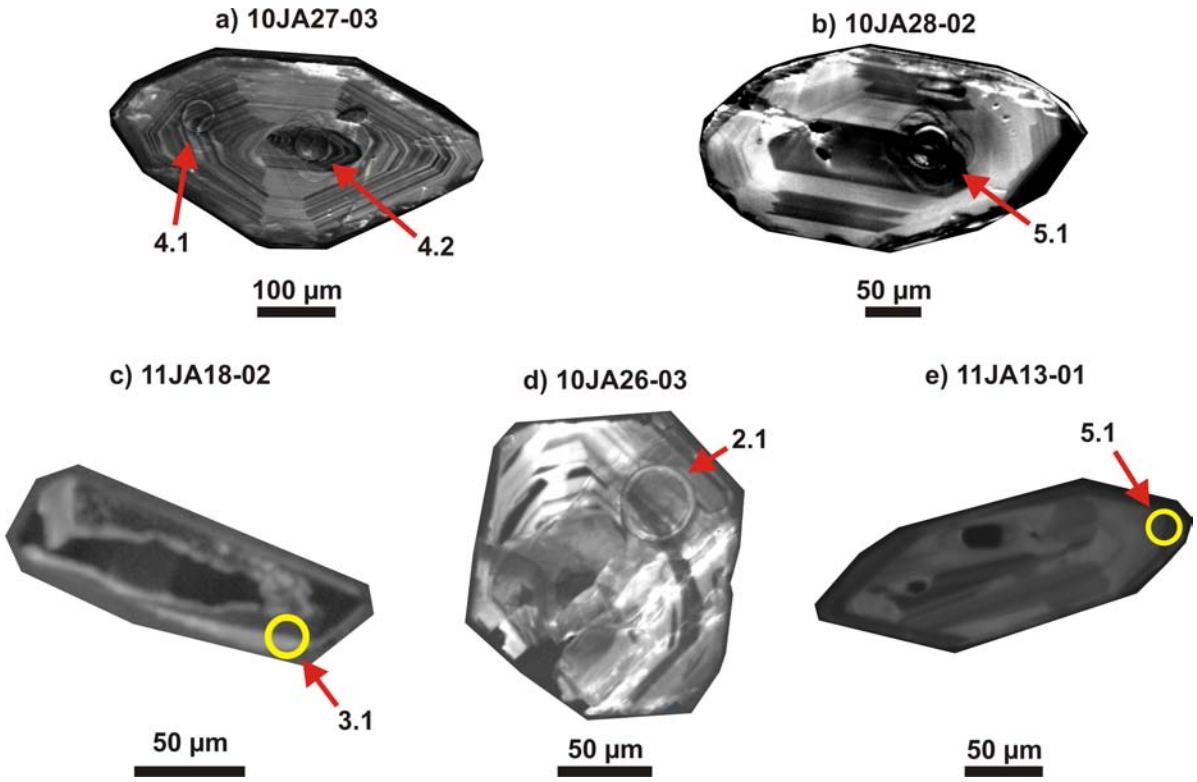

Figure 3.22: Representative cathodoluminesence images: (a) Sample 10JA27-03 grain 4 taken after ablation showing two ablation pits, corresponding to analyses 4.1 and 4.2 in Table A.1. The two analyses were carried out in what were thought to be a core and rim, respectively, due to partially truncated oscillatory zoning; (b) Sample 10JA28-02 grain 5 taken after ablation showing continuous oscillatory zoning pattern and ablation pit corresponding to analysis 5.1; (c) Sample 11JA18-02 grain 3 showing homogeneous dark domain with irregular boundaries and location of ablation pit corresponding to analysis 3.1 within concentrically zoned section; (d) Sample 10JA26-03 grain 2 taken after ablation, note the deviation from simple oscillatory zoning suggesting presence of a xenocrystic core, the ablation pit corresponding to analysis 2.1 is located entirely outside the potential core; (e) Sample 11JA13-01 grain 5 exhibiting oscillatory zoning combined with a change in luminescence near the edge and location of ablation pit corresponding to analysis 5.1.

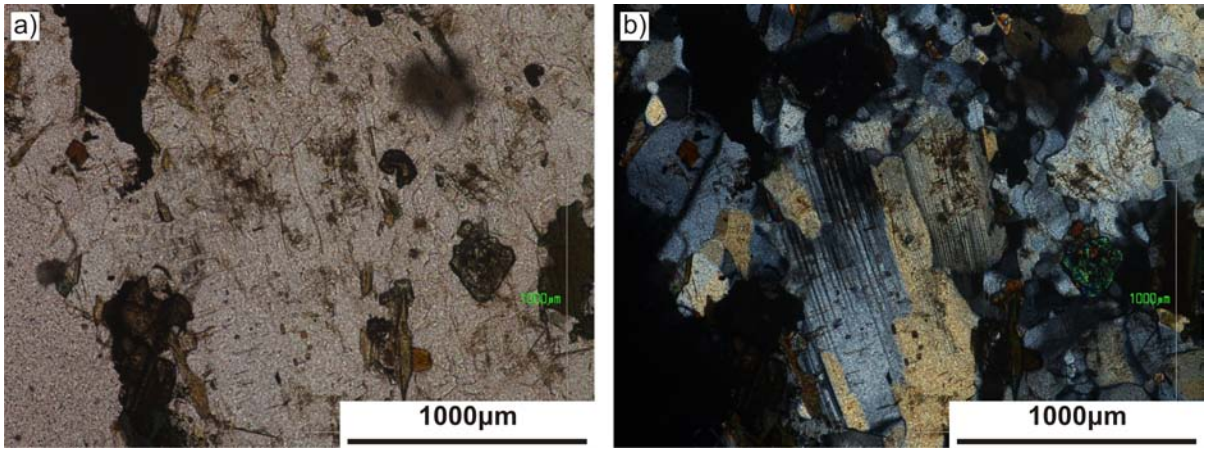

Figure 3.23: Photomicrographs of sample 10JA28-02: (a) Plane polarized light; (b) Crossed polarized light. Note discontinuous deformation twins in plagioclase.

All zircons in the Telegraph Passage sample (10JA28-02) have few inclusions and are transparent, although three appear orange from oxidized iron on their surfaces and along fractures. They are euhedral to subhedral, including both near equant and very elongate prisms. They range 50-200 µm in width and 100-400 µm in length. CL images of polished grains exhibit oscillatory zoning with no evidence for xenocrystic cores (Figure 3.22b). The 44 LA-ICP-MS data yielded a weighted average $^{206}Pb/^{238}U$ age of 99.69 ± 0.99 Ma (Figure 3.17e,f). Two grains with concordant LA-ICP-MS ages were selected for ID-TIMS analysis. One of these lies left of Concordia suggesting an error with the common lead correction. Interference at mass 204, which would lead to an overestimation of the common lead correction, was observed during analysis. Given the lower concentration of ^{207}Pb than ^{206}Pb, such an error will have a greater impact on the $^{207}Pb/^{235}U$ ratio and result in the data point shifting left of Concordia. The $^{206}Pb/^{238}U$ value for the data point which lies on Concordia is taken as the best estimate of the age of the dyke at 97.6 ± 0.2 Ma (Figure 3.18c). The Telegraph Passage sample (10JA28-02) suggests that dextral transpression in domain 2 also occurred during the mid-Cretaceous, coming to a close shortly after ~97 Ma.

3.4.2.4 11JA18-02 Marrack Island

Sample 11JA18-02 is from a granodiorite dyke on Marrack Island (Figure 3.3) which is interpreted to postdate a component of sinistral deformation (D_{3a}) and predate formation of conjugate shear bands (D_{3b}). The dyke crosscuts the main foliation, as well as S-folds which affect that foliation, but is offset by a sinistral shear zone (Figure 3.24). The shear zone has the same orientation as the local

sinistral shear bands and larger scale sinistral shear zones. The outcrop contains numerous 5-20 cm C' shear bands (both sinistral and dextral) which define the conjugate geometry characteristic of domain 3.

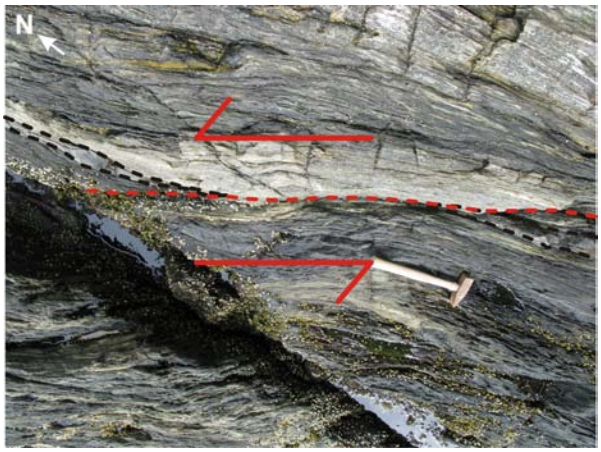

Figure 3.24: Mesoscale sinistral shear zone that offsets granodiorite dyke sample 11JA18-02. The two segments of the dyke are outlined by black dashed lines and the shear zone is outlined by the dashed red line. Red arrows indicate shear sense.

Zircons extracted from Marrack Island sample (11JA18-02) range from anhedral to euhedral with both concentric zoning and irregular domains visible in CL (Figure 3.22c). They range 25-100μm in width and 50-200 μm in length. Ages range from 495 Ma to 90 Ma with distinct concentrations at 100 Ma and at 92 Ma (Figure 3.19a, inset). The weighted average $^{206}Pb/^{238}U$ age of 92.6 ± 4.9 Ma for the three youngest grains is reported as the crystallization age of the dyke, with older ages representing xenocrysts and antecrysts. Alternately, the few younger ages may be the result of lead loss with the concentration of analyses at ~100 Ma indicating the emplacement age but, once again, this is unlikely given the pristine condition of the zircons. Regardless of whether the Marrack Island sample (11JA18-01) is 100 Ma or 92 Ma, it constrains shear bands as mid-Cretaceous structures. The two oldest xenocrysts are expected as the dyke is observed in intrusive contact with the latest Cambrian to Ordovician Descon Formation.

3.4.2.5 10JA26-03 Grenville Channel

Sample 10JA26-03 was collected from the largest of a suite of dykes at the mouth of Kumealon Inlet which crosscut foliation but are also folded and boudinaged indicating sinistral motion associated with the Grenville Channel shear zone (Figure 3.3)(Figure 3.25). The dykes are comprised of

medium grained granodiorite and intrude into very strongly deformed pillow basalts and flows. Relict pillows have aspect ratios of approximately 20:1 on the horizontal plane (Figure 3.14c). This sample is interpreted to be synkinematic with respect to sinistral shear in domain 4.

Figure 3.25: Sample 10JA26-03 associated dyke, displaying boudinage consistent with sinistral motion. Actual dyke sampled not shown.

The zircons recovered from this sample are transparent to honey coloured, euhedral, stubby prisms with variable morphology. Inclusions and fractures range from few to many. They range 50-175 μm in width and 75-300 μm in length. Three grains from this sample in the polished mount contained complex zoning patterns possibly indicating the presence of inherited cores (Figure 3.22d). Nineteen LA-ICP-MS analyses fall near Concordia (Figure 3.17g) but range from 100-913 Ma. The two youngest analyses provided a weighted average $^{206}Pb/^{238}U$ age of 103 ± 32 Ma which is interpreted as the crystallization age for the dyke (Figure 3.17g(inset),h). Given the range of ages and evidence for cores in CL images, all older grains are ascribed to inheritance. The largest cluster of analyses are Early Permian, around 290 Ma. These zircons are likely inherited from the nearby Kumealon unit or related dikes, which extensively intrude rocks of the Descon and Mathieson Channel formations (Nelson *et al*., 2012).

The Grenville Channel dyke sample (10JA26-03) suggests only that sinistral deformation within domain 4 was a Cretaceous structure owing to the large reported uncertainty (103 ± 32 Ma). It does however conform remarkably well with a 102.6 ± 3.7 Ma Lu-Hf age of prograde garnet growth reported as synkinematic to sinistral deformation within Kumealon Inlet (Wolf *et al*., 2010). Both of these constraints support the interpretation that sinistral transpression along the Grenville Channel shear zone was occurring at ca. 102 Ma.

3.4.2.6 11JA13-01 Kumealon Inlet

Sample 11JA13-01 was collected from a medium grained granodiorite dyke within Kumealon Inlet (Figure 3.3). It crosscuts northeast-vergent folds and is crosscut by another dyke that is weakly folded (Figure 3.26). It is therefore interpreted as late synkinematic with respect to upright to northeast-vergent folding.

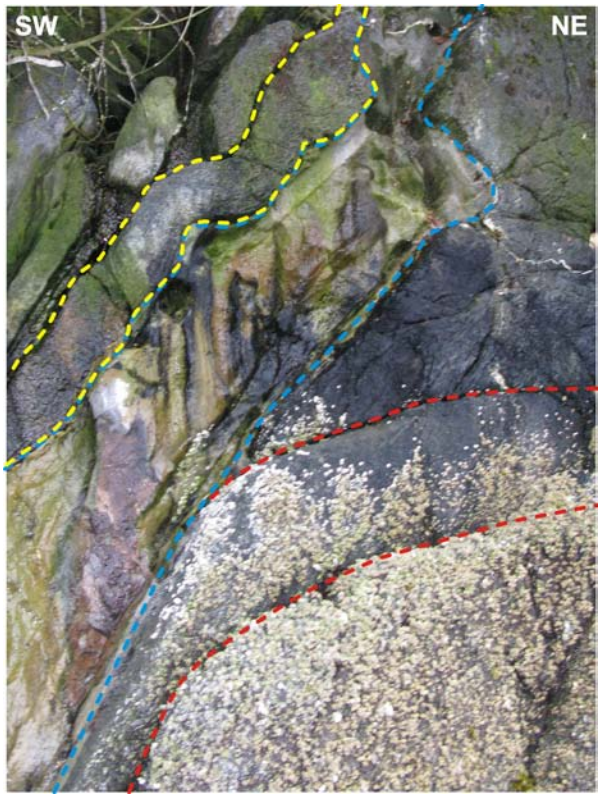

Figure 3.26: Sampling location for 11JA13-01. Upright to northeast-vergent folds (folded contacts outlined in red) are cut by sampled dyke (outlined in blue). The sampled dyke is cut by another dyke (outlined in yellow) that is also weakly folded. The vertical streaks visible in the photo are a surface stain due to runoff. Dyke outlined in yellow is approximately 30 cm wide.

The Kumealon Inlet sample (11JA13-01) contains both equant and elongate, euhedral to subhedral zircons. They range 50-100 μm in width and 100-300 μm in length. CL images exhibit oscillatory zoning, sometimes with an associated change in luminescence at the very edge of the grain (Figure 3.22e). In some zircons, zoning appears modified, potentially indicating the presence of xenocrystic cores. In grains with clear core and rim structures, the rims exhibit oscillatory zoning and as such are

interpreted as magmatic overgrowths on xenocrystic cores. Grains with rims too narrow to be analyzed separately (<25 um) were not selected. Ten concordant and near-concordant SHRIMP-RG analyses yielded a weighted average $^{206}Pb/^{238}U$ age of 92.6 ± 1.9 Ma (Figure 3.19c,d). This age indicates that upright to northeast-vergent folding occurred through 92.6 ± 1.9 Ma. It should be noted that this age is similar to constraints on west to southwest-vergent shear in the Prince Rupert area (Crawford *et al*., 1987; 2000).

3.4.3 Geochronology Discussion

The late synkinematic Swede Point sample (10JA27-02) along the Useless shear zone as well as the late synkinematic Peninsula Point sample (10JA27-03) in between the Salt Lagoon and Barrett shear zones provide constraints on the end of sinistral transpression, indicating that it ended shortly after 96 Ma. The 104.5 ± 0.9 Ma age from a mylonitized dyke within the Barrett shear zone confirms that significant deformation occurred during the mid-Cretaceous (J.B. Mahoney, unpublished data). This dyke crosscuts folded foliation so sinistral deformation was ongoing prior to 104.5 ± 0.9 Ma as well.

The late synkinematic Telegraph Passage dyke sample (97.6 ± 0.2 Ma) constrains dextral deformation along Telegraph Passage as mid-Cretaceous. This age is coeval, within uncertainties, with the Peninsula Point sample (97.1 ± 0.4 Ma), and falls between the earliest and latest synkinematic ages from domain 1, so the deformation events are considered coeval. The age constraints outlined above support the conclusion drawn from kinematic data and geometry that the northwest-striking sinistral shear zones and the north-striking dextral shear zone represent a coeval conjugate set. Furthermore, they constrain this conjugate set as a mid-Cretaceous structure. The corresponding strain field, of ENE-WSW directed shortening and NNW-SSE directed extension, must have been in place prior to 97.6 ± 0.2 Ma as the above constraints are late synkinematic. If the mesoscale shear band which offsets the Marrack Island dyke (sample 11JA18-02) is assumed to have initiated along with the conjugate sets, it constrains shear bands as post 92.6 ± 4.9 Ma. Therefore, ENE-WSW shortening continued through that time.

Upright to northeast vergent folding in domain 4 is constrained as active at ca. 92.6 ± 1.9 Ma by the Kumealon Inlet sample (11JA13-01). Given that S_3 is axial planar to these folds and accommodated sinistral shear, some shearing must have occurred after (or along with) folding. When combined with the ca. 102.6 ± 3.7 Ma synkinematic constraint on sinistral transpression in the form of the Lu-Hf garnet age reported by Wolf et al. (2010), this suggests that folding and sinistral shear likely overlapped in time supporting the hypothesis that the deformation regime was transpressional.

3.5 Overall significance of local Cretaceous structures

3.5.1 D3a: Early Cretaceous sinistral transpression

The D3a sinistral transpression described herein is interpreted to be coeval with early motion along the Grenville Channel shear zone farther south, which records deformation as early as 123 Ma near Klemtu (Nelson *et al*., 2012), as well as sinistral shear on the Kitkatla and Principe-Laredo shear zones between ~150 and 106 Ma (Chardon *et al*., 1999). This deformation may relate to proposed large scale Early Cretaceous sinistral translation of terranes within the Coast Belt (Monger *et al*., 1994; Israel *et al*., 2006; Gehrels *et al*., 2009). The interpreted shortening direction for D_{3a} is nearly E-W (Figure 3.15b). If this is extrapolated to the orogen scale, it would be sinistral oblique with respect to the margin; in agreement with relative plate motion models which support a sinistral component to Farallon – North America convergence during the Early Cretaceous (Engebretson *et al*., 1985).

3.5.2 D3b: mid-Cretaceous lateral extension

Structures associated with D_{3b} indicate lateral extension during overall sinistral transpression. They include the conjugate shear zones represented by the Porcher Island sinistral domain (1) and the Telegraph Passage dextral domain (2), the conjugate shear bands of the Marrack Island domain (3), and the characteristic horizontal lineations within the Grenville Channel shear zone domain (4). The interpreted shortening direction for all of these structures is ENE-WSW (Figure 3.15b). When this is extrapolated to the orogen scale, it would be orogen perpendicular. The associated extensional direction would be orogen parallel. The only known tectonic setting associated with significant lateral extension is tectonic escape (Kuiper *et al*., 2011).

The transition from D_{3a} to D_{3b} indicates a transition from oblique to orthogonal shortening and the onset of lateral extension. While exact timing of this transition is unclear, it is interpreted as late Early Cretaceous. It was well underway by ~97 Ma, as indicated by coeval, synkinematic ages from conjugate shear zones. Relative plate motion models, while notoriously inconclusive during the mid-Cretaceous due to the lack of magnetic reversals, do indicate a transition from sinistral oblique to near orthogonal convergence between North America and Farallon plates at ~100 Ma (Engebretson *et al*., 1985).

3.6 Conclusion

Detailed structural mapping has documented and dated shearing and folding related to the northwest striking sinistral transpressional Grenville Channel shear zone system, including the Useless, Barrett, Salt Lagoon, and Lamppost shear zones which feed into it from the northwest. The north-striking Telegraph Passage shear zone was identified and characterized as a dextral transpressional structure. The geometry of these shear zones as well as new U-Pb geochronology supports the hypothesis that they were active, at least in part, as a conjugate set during the mid-Cretaceous indicating horizontal, north-northwestward extension. Shear zone boundary parallel extension within the Grenville Channel shear zone proper also indicates a similar component of NW-SE extension.

Conjugate shear bands observed in outcrop reflect the geometry of map scale conjugate shear zones; both corresponding to a strain field of ENE-WSW shortening and NNW-SSE extension. The horizontal stretch observed for the Grenville Channel shear zone similarly indicates NW-SE extension. If the same strain field is extrapolated to the orogen scale, it indicates orogen-parallel extension and orogen perpendicular shortening. The geometry of mid-Cretaceous shear zone systems in the Coast and Omineca belts outlining the proposed Intermontane escape block are somewhat reminiscent of a conjugate set, and would be the result of a similar strain field since tectonic escape is defined as lateral (or orogen parallel) extension out of a convergent orogen. From outcrop scale, to map scale, to orogen scale similar structures were operating during the mid-Cretaceous exemplifying the scale independence of structural geology.

Chapter 4
The Ogden Channel complex: lower crustal root of the Klakas Orogeny

4.1 Introduction

The North American Cordillera is the type example of an accretionary orogen, with much of its volume comprised of accreted 'suspect terranes' (Coney *et al*, 1980). Subsequent studies have established that the Intermontane terranes formed in proximity to the western, proto-Pacific margin of Laurentia, whereas the geological evidence from the Alexander and other terranes display far-travelled paleogeographic histories (Nelson *et al*., 2006; Nelson and Colpron, 2007; Colpron *et al*., 2007; Colpron and Nelson, 2009). The Alexander, Arctic Alaska and Farewell terranes (Figure 4.1), are part of a group of terranes whose faunal, detrital zircon and paleomagnetic records indicate that they evolved somewhere in proximity to Baltica, Siberia and northeast Laurentia up to the Middle Paleozoic (Soja, 1994, 2008; Bazard *et al*., 1995; Gehrels *et al*., 1996; Soja & Antoshkina 1997; Blodgett *et al*., 2002; Dumoulin *et al*., 2002; Antonishka & Soja 2006; Pedder, 2006; Bradley *et al*., 2007; Amato *et al*., 2009; Beranek *et al*., 2012a, b). Also included in this group are the Okanagan subterrane of Quesnellia in southeastern BC (Figure 4.1), the Trinity and Yreka terranes in northwestern California, and the Shoo-Fly complex of the Northern Sierra terrane in northeastern California (Colpron and Nelson, 2009; 2011a). Colpron and Nelson, (2009; 2011a) suggested migration of these terranes into Panthalassa occurred by west-directed protrusion of a Scotia style arc situated north of Laurentia during the Late Silurian to Late Devonian. This model is referred to as the 'northwest passage' (Figure 4.2).

The Alexander terrane, one of the terranes of Baltican and Siberian affinity in figure 4.1, provides an excellent laboratory to study the Paleozoic history of these terranes as it records a near continuous geological record through that time (Gehrels *et al*., 1996). In particular, it records a Late Silurian to Early Devonian orogenic event referred to as the Klakas orogeny (Gehrels 1983; Gehrels *et al*., 1987, 1996). The timing of the Klakas orogeny corresponds to the Scandian phase of the Caledonian orogeny and amalgamation of Laurussia, as well as the proposed timing of initiation of the northwest passage. Accurately dating and characterizing the Klakas orogeny will aid in correlating it to events elsewhere and provide further paleogeographic constraints on the Alexander terrane, potentially providing more insight into the mechanism by which terranes of Siberian and Baltican affinity ended

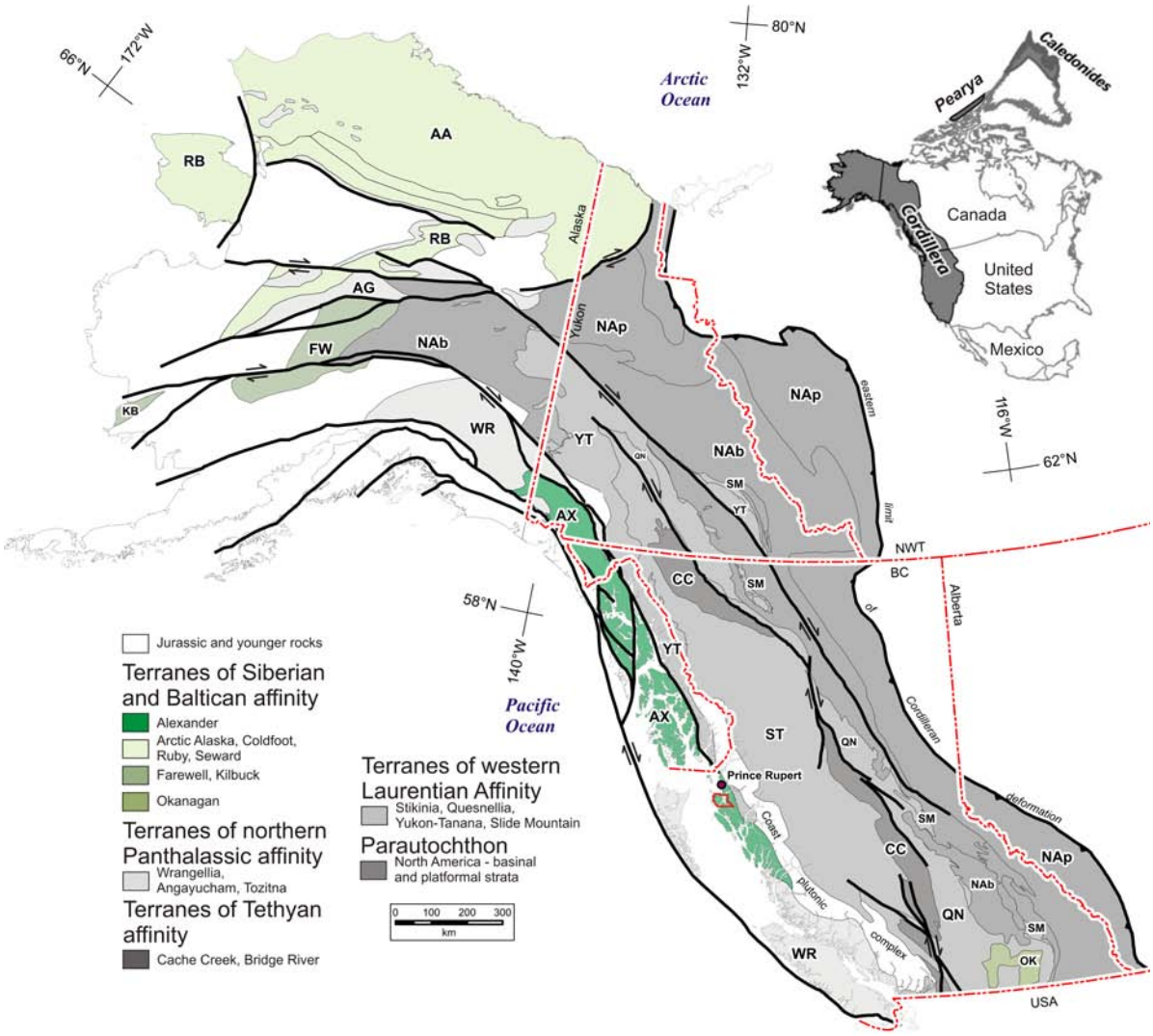

Figure 4.1: Paleozoic to early Mesozoic terranes of the Northern Cordillera with emphasis on terranes of Siberian and Baltican affinity. Red box immediately south of Prince Rupert outlines map area of current study presented in Figure 4.5. Inset map shows the current geographic relationship between the Cordillera, the Greenland Caledonides, and Pearya. Terrane abbreviations: AX – Alexander, AA – Arctic Alaska, RB – Ruby, FW – Farewell, KB – Kilbuck, OK – Okanagan, WR – Wrangellia, AG – Angayucham, CC – Cache Creek, ST – Stikinia, QN – Quesnellia, YT – Yukon Tanana, SM – Slide Mountain, NAp – North America platformal strata, NAb – North America basinal strata (modified after Colpron and Nelson, 2009; 2011a; 2011b; Beranek *et al.*, 2012a).

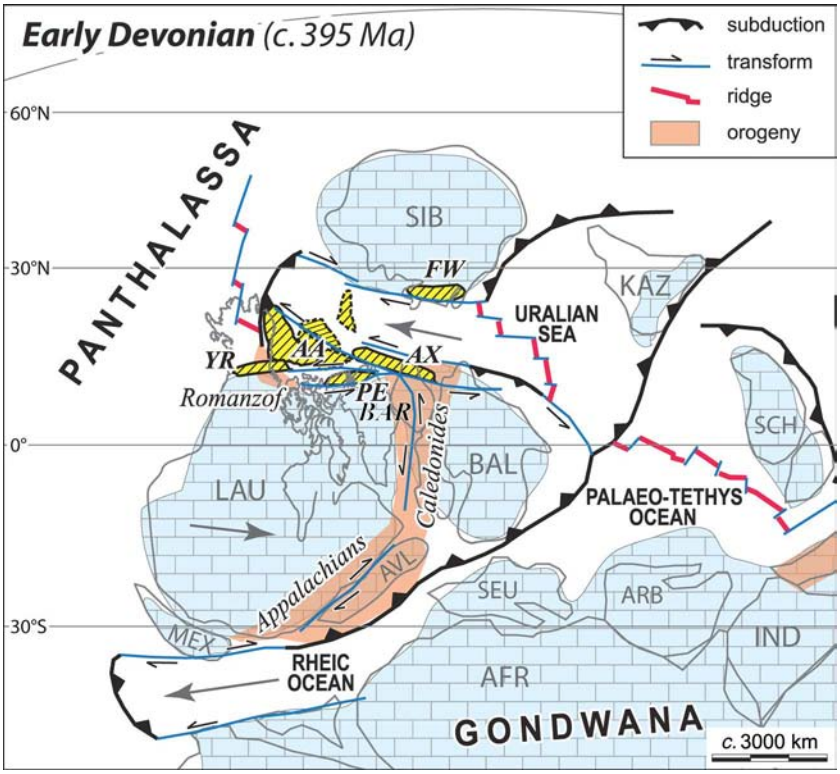

Figure 4.2: Tectonic reconstruction proposed to explain the translation of the Alexander terrane from the Uralian seaway into Panthalassa through a 'Northwest Passage'. Abbreviations: AA – Arctic Alaska, AX – Alexander, PE – Pearya, FW – Farewell, YR – Yreka, BAR – Barentsia (modified after Colpron and Nelson, 2011a).

up in the North American Cordillera. Furthermore, the Pb isotopic signature of VMS showings within the southern Alexander terrane suggest an association with Ordovician VMS deposits in Eastern Canada and Scandanavia (Nelson *et al*., 2013). A better understanding of the paleogeography of the Alexander terrane will lead to more effective mineral exploration within the terrane.

The Ogden Channel complex is a metaplutonic-metamorphic complex on southern Porcher Island and adjacent Pitt Island in north coastal British Columbia (Figure 4.3). New U-Pb geochronology and structural observations from the complex has constrained it as a Late Silurian to Early Devonian plutonic complex, which formed synkinematically with respect to dominantly southwest-vergent deformation with a minor sinistral component. It is interpreted to represent the mid-crustal root of a compressive magmatic arc (Dewey, 1980) active during the Klakas orogeny.

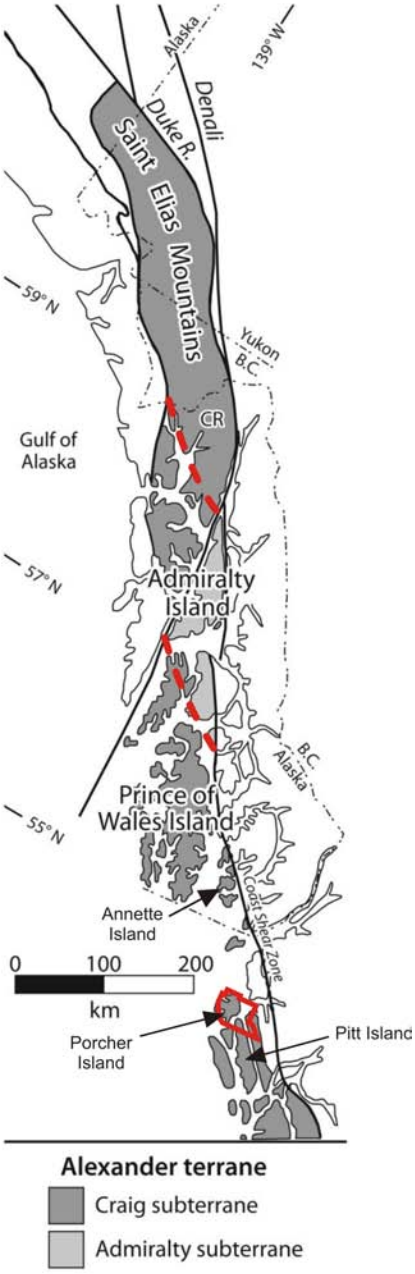

Figure 4.3: Location of subterranes within the Alexander terrane. Study area is outlined in red. The dotted red line represents the approximate break between arc and back-arc associated Ordovician stratigraphy and between proximal and distal facies clastic strata during the Devonian. The offset corresponds to approximately 150 km of dextral displacement along the Chatham Straight fault (Hudson *et al.*, 1981), (modified after Gehrels and Saleeby, 1987a; Beranek *et al.*, 2012a).

4.2 Tectonic Setting

4.2.1 Geology of the Alexander terrane

4.2.1.1 Major subdivisions of Alexander terrane

The Alexander terrane underlies much of southeast Alaska as well as portions of north coastal and northwestern British Columbia, southwestern Yukon, and adjacent mainland Alaska (Figure 4.1; 4.3). It is comprised of the Craig and Admiralty subterranes on the basis of stratigraphic and tectonic contrasts (Gehrels and Saleeby, 1987a; after Berg *et al*., 1978). The Craig subterrane is further subdivided into the Prince of Wales and St. Elias sections (Figure 3; Beranek *et al*., 2012a). The Craig subterrane on Prince of Wales Island is characterized by Neoproterozoic as well as Upper Cambrian to Lower Silurian arc volcanic strata and Middle Devonian proximal facies clastic strata (Figure 4.4). The St. Elias section of the Craig subterrane includes Late Cambrian to Early Silurian strata associated with a back-arc and continental shelf setting overlain by Devonian shallow marine to terrigenous distal facies clastic strata (Figure 4.4). The Admiralty Subterrane is characterized by Ordovician through Devonian deep marine strata, with a transition from chert-dominated (clastic-starved) in the Ordovician to argillite dominated in the Silurian to Devonian (Figure 4.4). The geographic distribution of these subterranes is suggestive of a southwest facing arc (present coordinates) during the Latest Cambrian to Early Silurian and subsequent northeast tapering clastic wedge during the Late Silurian and Early Devonian (Figure 4.3)(Gehrels and Saleeby, 1987a). Evidence for the Klakas orogeny is dominantly recorded by the Prince of Wales component of the Craig subterrane, described below. A review of the Neoproterozoic through Devonian stratigraphy of all three divisions of the Alexander terrane are available in appendix B.

4.2.1.2 Craig Subterrane: Prince of Wales – Neoproterozoic to Late Devonian strata

The oldest rocks assigned to the Craig subterrane consist of metavolcanic rocks, minor metasedimentary rocks, and orthogneisses of the latest Proterozoic to Cambrian Wales Group, interpreted to have formed in an arc setting (Gehrels and Saleeby, 1987b; Gehrels *et al*., 1987; Gehrels, 1990). The Wales Group was pervasively deformed and metamorphosed to greenschist and amphibolite grade during the Middle to Late Cambrian Wales orogeny (Gehrels and Saleeby, 1987a).

The Wales Group is overlain by the Upper Cambrian to Lower Silurian arc derived strata of the Descon Formation (Eberlein and Churkin, 1970; Gehrels and Saleeby, 1987a,b; Gehrels *et al*., 1996;

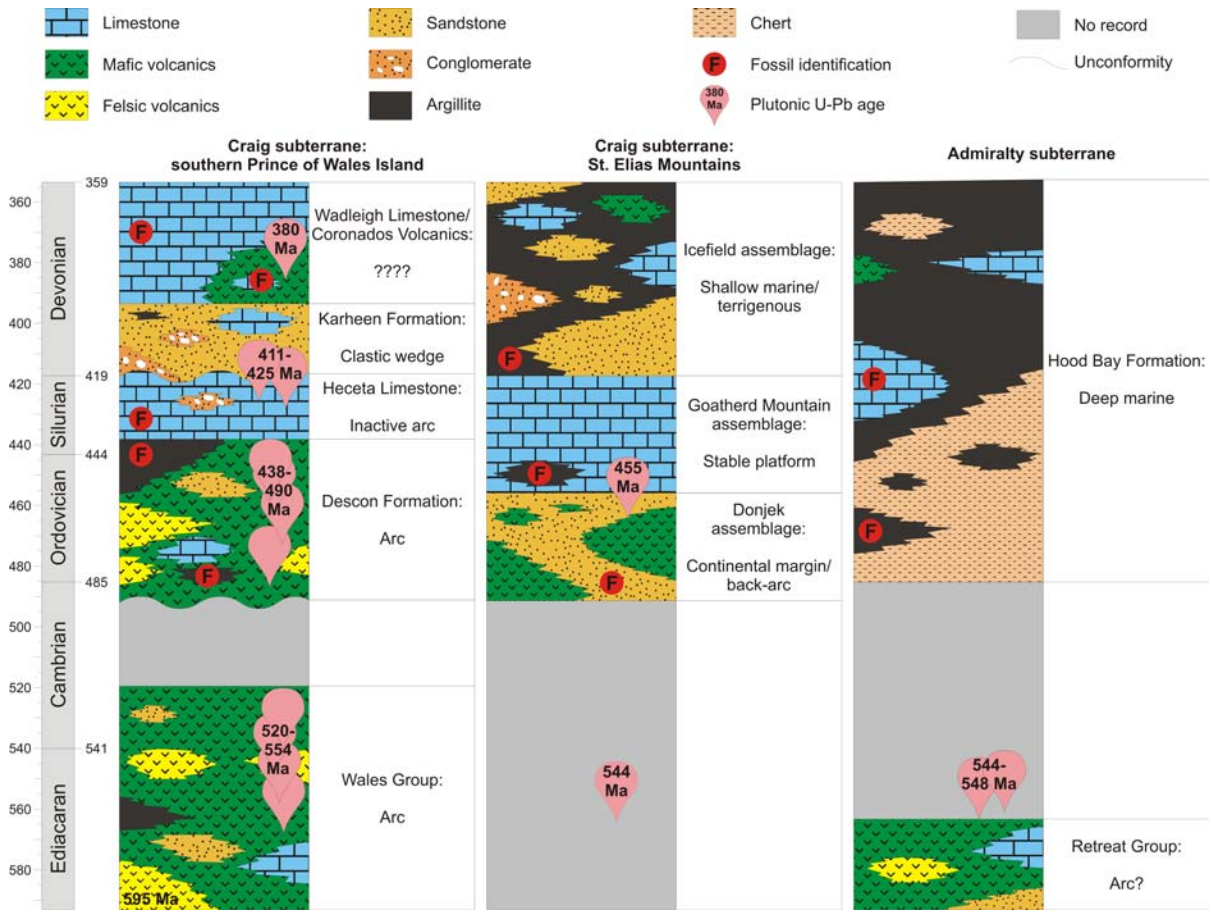

Figure 4.4: Schematic Ediacaran through Devonian stratigraphy of the major subterranes within the Alexander terrane. Modified after Gehrels and Saleeby, (1987a); Colpron and Nelson (2009); Karl *et al.* (2010); Beranek *et al.* (2012a); and supplementary references discussed in the appendix B. Geologic timescale of Walker *et al.* (2012).

Grove *et al.*, 2008). The youngest age from a Middle Ordovician to Early Silurian suite of ultramafic to intermediate plutons interpreted as consanguineous with the Descon Formation records the end of Descon arc magmatism at 438 ± 5 Ma (U-Pb zircon, ID-TIMS; Gehrels and Saleeby, 1987b).

The Descon Formation is conformably overlain by the Silurian Heceta Limestone and turbidites of the Bay of Pillars Formation (Eberlein and Churkin, 1970; Gehrels and Saleeby, 1987a). Conglomeratic lenses within the upper part of the Heceta Limestone record the onset of the Klakas orogeny during the Silurian (Gehrels and Saleeby, 1987a). Paleobiogeographic studies on the Heceta Limestone suggest a correlation with rocks within the Ural Mountains (i.e. Baltica) (Soja, 1994; Soja & Antoshkina 1997; Antonishka & Soja 2006).

Silurian strata are discontinuous, which is attributed to subsequent erosion (Eberlein and Churkin, 1970); this major unconformity separates Silurian and older strata from the Lower Devonian Karheen Formation and its equivalents: the Cedar Cove Formation and the Mathieson Channel Formation (Loney *et al*., 1975; Gehrels and Saleeby, 1987a; Nelson *et al*., 2011a, 2012). The Karheen Formation is a fining-upwards sequence with conglomeratic redbeds at the base, followed by siltstone, limestone and laminated mudstone at the top (Gehrels and Saleeby, 1987b). It forms a northeastward tapering clastic wedge (Ovenshine *et al*., 1969; Gehrels and Saleeby, 1987a; Gehrels *et al*., 1996). The major unconformity as well as the presence of clasts with varied lithologies including Silurian plutonic clasts is interpreted to indicate significant uplift and erosion during the Late Silurian-Early Devonian Klakas orogeny (Gehrels *et al*., 1983; Gehrels and Saleeby, 1987a; Gehrels *et al*., 1996). It is tectonically modelled as a collision between the Craig subterrane and a pericratonic block to the southwest (present coordinates; Gehrels *et al*., 1996). This orientation is supported by an increase in metamorphic grade from north to south, southwest- and, locally, northeast-vergent thrust faults, and northeastward taper of the Lower Devonian Karheen Formation (and Cedar Cove Formation) clastic wedge which was deposited during the waning stages of the orogeny (Ovenshine *et al*., 1969; Loney *et al*., 1975; Gehrels *et al*., 1983; Gehrels and Saleeby, 1987a; Gehrels *et al*., 1996). The end of Klakas deformation in southeast Alaska is constrained to the Late Silurian or Early Devonian by a 426 ± 15 Ma deformed metadiorite and 415 ± 5 Ma undeformed trondhjemite on Annette Island in southeast Alaska (Figure 4.3)(U-Pb zircon, ID-TIMS; Gehrels *et al*., 1987).

The detrital zircon spectrum for the Karheen Formation is dominated by grains between ~410 and 490 Ma, and also includes grains as old as 3 Ga (Gehrels *et al*., 1996; Grove *et al*., 2008). The Paleozoic peak is interpreted to record rapid uplift and erosion of the Descon Formation and associated plutons, while the presence of Precambrian grains indicates that the Alexander terrane was adjacent to a continental landmass during deposition. Furthermore, some of these Precambrian zircons fall between 1.49 – 1.61 Ga: the North American Magmatic Gap (NAMG) as identified by van Schmus *et al*., (1993) and therefore the continental landmass to which it was adjacent was probably not western North America. Only two regions are known which could have sourced the entire suite of zircons and also record Klakas age (Late Silurian to Early Devonian) orogenesis: the paleo-Pacific margin of Australia and Scandanavian Baltica (Gehrels *et al*., 1996). Paleobiogeographic studies (Soja, 1994; Soja & Antoshkina 1997; Antonishka & Soja 2006; Pedder, 2006) suggest much stronger ties to Baltica than Australia. It has been suggested that the Karheen

Formation is a correlative of the Old Red Sandstone in northeastern United States and Canada, Greenland, Svalbard, Norway, and Great Britain (Bazard *et al*., 1995; Gehrels *et al*., 1996).

The Karheen Formation is overlain in part by the Wadleigh Limestone which contains coral fossils of Middle to Late Devonian age (Eberlein and Churkin, 1970). Pedder (2006) reports a correlation of Late Devonian corals in the upper Wadleigh Limestone with those in the Western Canada Sedimentary Basin, suggesting the Alexander terrane was close enough to northwestern North America to exchange coral larvae at that time.

4.3 Geological Setting

4.3.1 Geology of southern Porcher Island and western Pitt Island

4.3.1.1 The Ogden Channel complex

The Ogden Channel complex is separated from the supracrustal strata to the north by the Salt Lagoon shear zone, an extension of the Grenville Channel shear zone (Figure 4.5). It is a variably deformed, amphibolite-grade, metaplutonic-metamorphic suite which occupies much of southern Porcher Island and western Pitt Island (Figure 4.5). It is characterized by a series of compositionally and texturally heterogeneous small plutons and dikes. They are predominantly mafic to intermediate, ranging from gabbro to granodiorite, but dominated by diorite, quartz diorite and tonalite. Many are porphyritic, with plagioclase or hornblende phenocrysts. Numerous pendants of metavolcanic and metasedimentary rocks are incorporated into the complex. Separately mappable metamorphic inliers consist of laminated mylonitic metatuff, calc-silicate, and pelite. Within the complex, some deformed volcanic protoliths are probably Descon equivalents. A metamorphosed and deformed dacite lapilli tuff in Billy Bay has yielded a Late Silurian U-Pb age (J.B. Mahoney, unpublished data), indicating that it is coeval with the plutonic bodies that make up most of the complex (see below).

In the most highly deformed sections of the complex, such as along the Barrett shear zone, grain size reduction has obliterated nearly all original textures, aside from a few plagioclase porphyroclasts demonstrating its igneous origin. In thin section, the mafic rocks are fine-grained aggregates of green amphiboles and plagioclase, whereas felsic rocks exhibit quartz ribbons surrounding feldspar phenocrysts. In less deformed zones, the synkinematic nature of the complex is more easily observed by the wide range of fabric development, with younger intrusions of the complex crosscutting foliation in older bodies (Figure 4.6).

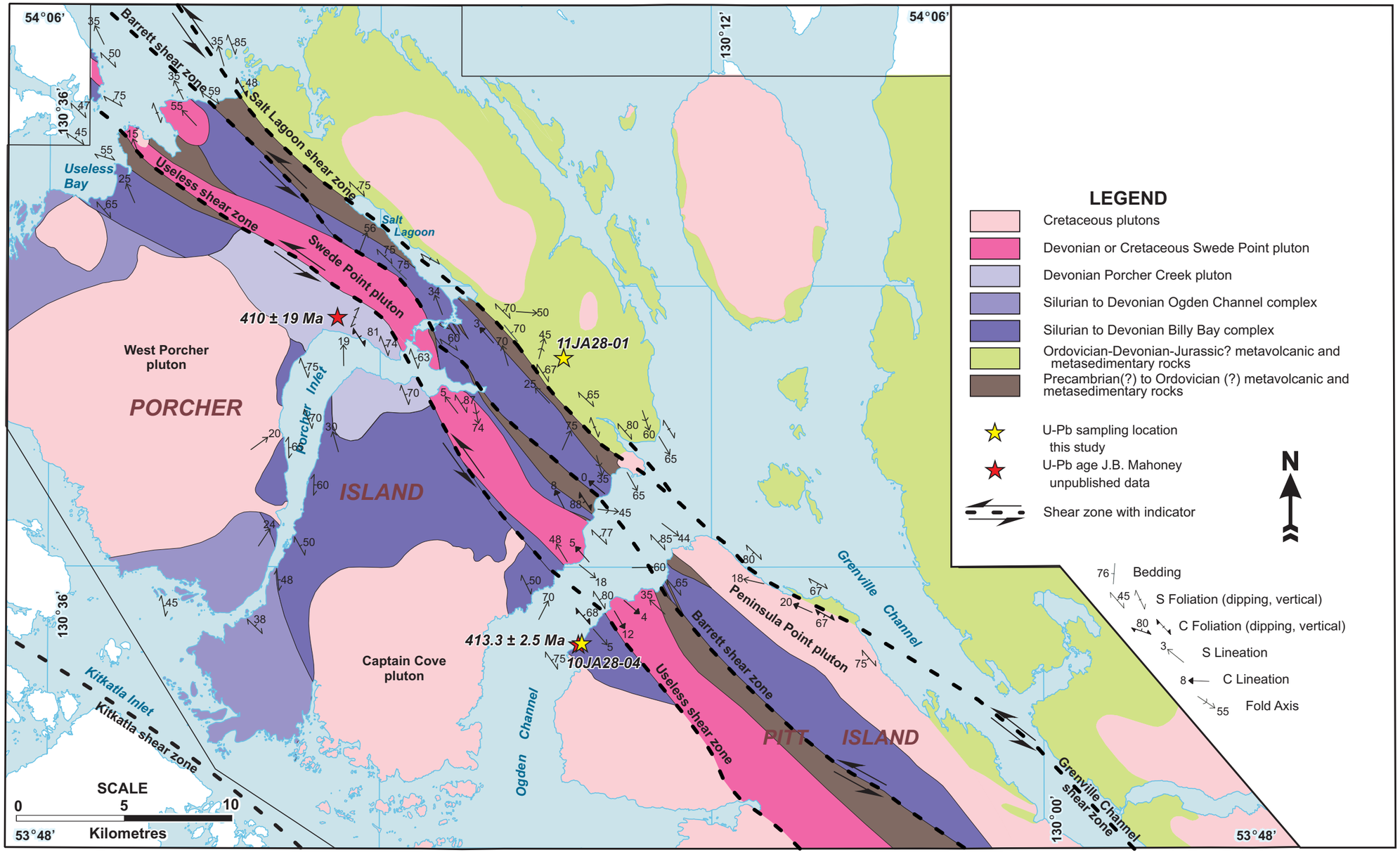

Figure 4.5: Simplified geological map of Porcher Island and western Pitt Island, northwestern British Columbia. (modified after Nelson *et al*., 2010b; 2012; Angen *et al*., 2012).

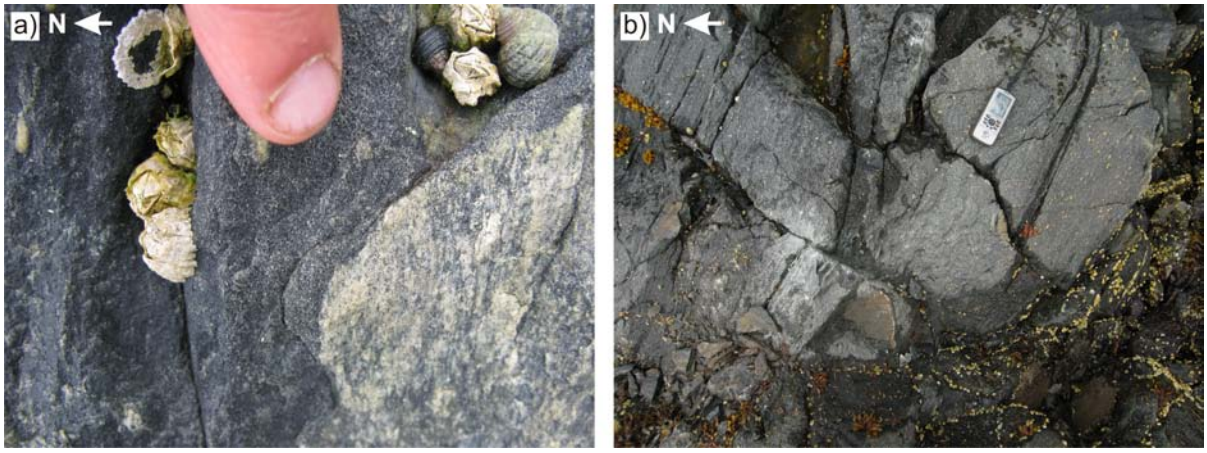

Figure 4.6: Crosscutting relationship in the Ogden Channel complex; (a) photograph of the crosscutting relationship between two dykes sampled for U-Pb geochronology, the mylonitic tonalite on the right yielded an age of 412.3 ± 1.4 Ma (J.B. Mahoney, unpublished data), the fine grained quartz diorite on the left which truncates fabric in the tonalite was sampled as 10JA28-04 and yielded an age of 413.3 ± 2.5 Ma; (b) photograph showing foliation within the quartz diorite dyke sampled as U-Pb sample 10JA28-04.

4.3.1.2 The Porcher Creek pluton

The Porcher Creek pluton, as defined by Nelson *et al*. (2010), is an intermediate dyke complex including diorite, andesite, tonalite, and leucotonalite phases. It is interpreted as late synkinematic to post kinematic as most dykes exhibit no homogeneous fabric, but often contain minor shear bands of variable orientation associated with chlorite and epidote alteration (Figure 4.7). One of the post kinematic intrusions contains deformed xenoliths (Nelson *et al*., 2012). Considering its variable, intermediate composition and relationship to deformation, the Porcher Creek pluton is herein considered to be a concentration of later phase intrusions within the Ogden Channel complex.

4.3.1.3 Billy Bay complex

The Billy Bay complex is a mafic to felsic intrusive and extrusive complex that is variably deformed, similar to the Ogden Channel complex. The intrusive component of the Billy Bay complex is slightly more felsic than the Ogden Channel complex, including diorite, tonalite, and granodiorite. The supracrustal component of the complex is dominantly volcanic, including andesite and basalt flows, andesitic and dacitic tuff and breccia as well as minor metasedimentary rocks including meta-argillite,

Figure 4.7: Sinistral shear band in the Porcher Creek pluton. Note the abundant chlorite and epidote alteration.

metachert, and metasandstone (Nelson *et al*., 2010a). The Billy Bay complex is interpreted as the extrusive and hypabyssal equivalent of the Ogden Channel complex.

4.3.1.4 Swede Point Pluton:

The Swede Point pluton is a planar body of dominantly granodiorite with minor tonalite and diorite. It is ubiquitously well foliated, commonly exhibiting S-C fabric indicating sinistral shear (Figure 2.5b). It yielded a U-Pb zircon age of 382 ± 14 Ma (ID-TIMS; van der Heyden, 1989); this represents the upper intercept of a Discordia line with a lower intercept at 73 ± 11 Ma. The possibility remains that this is a composite of Devonian (or older) cores with younger rims representing the emplacement age. The highly planar geometry of this pluton suggests that it was either emplaced along a previous anisotropy (Nelson *et al*., 2010a), or along an active shear zone. If the Late Devonian age is correct, it may be following a planar Klakas age structure.

4.3.1.5 Cretaceous Plutons:

The study area is intruded by several dominantly granodioritic Cretaceous plutons of the Coast Plutonic Complex including the Captain Cove pluton (108.5 ± 1.0 Ma -107.5 ± 1.5 Ma; U-Pb zircon, ID-TIMS; Butler *et al*., 2006), Peninsula Point pluton (97.1 ± 0.4 Ma; this study, see Chapter 3), and the undated West Porcher pluton (Figure 4.5).

4.4 Structural Geology

4.4.1 Structural Observations

4.4.1.1 Ogden Channel Complex

The strong transposition foliation observed within the Ogden Channel complex north of the Useless shear zone is interpreted as the result of mid-Cretaceous shear zone deformation (see Chapter 3). A 410 ± 19 Ma age (Figure 4.5)(U-Pb zircon, LA-ICP-MS; J.B. Mahoney, unpublished data) from an undeformed granodiorite of the Porcher Creek pluton immediately south of the Useless shear zone indicates that this area was relatively unaffected by the mid-Cretaceous event. A similar conclusion was reported by Nelson *et al*. (2011a) along the southern Grenville Channel shear zone where undeformed Jurassic plutons are present southwest of the shear zone and a highly deformed ca. 123.3 ± 1.4 Ma pluton (U-Pb zircon, LA-ICP-MS; Gehrels *et al*., 2009; Nelson *et al*., 2011a) is present to the northeast. Chardon *et al*. (1999) report high strain fabrics along the Kitkatla shear zone within and immediately south of Kitkatla Inlet (Figure 4.5). This deformation does not appear to affect the Ogden Channel complex, based on the observation that where the Captain Cove pluton is observed in intrusive contact with the Ogden Channel complex on Pitt and Porcher Islands it is undeformed; whereas, gneissic foliation is observed within the Captain Cove pluton proximal to the Kitkatla shear zone (Chardon *et al*., 1999). All structures described for the Ogden Channel complex herein come from southwest of the Useless shear zone (Figure 4.5) and are assumed to be Early Devonian or older.

The foliations from this domain vary from east dipping to north dipping, with lineations generally oriented down-dip (Figure 4.8). The poles to foliation form a weak great circle girdle oriented at $138^{o}/30^{o}$. This may indicate that the foliation has been folded about a northeast plunging axis, similar to the observed northeast plunging hinge lines of observed S folds (Figure 4.8). Where observed, shear bands suggest a sinistral shear component to deformation (Figure 4.9a,b). The steeply plunging lineations in figure 4.8 may either be a result of transpression as described in Chapter 2 or southwest-vergent reverse shear in accordance with other structures assigned to the Klakas orogeny (Gehrels *et al*., 1996).

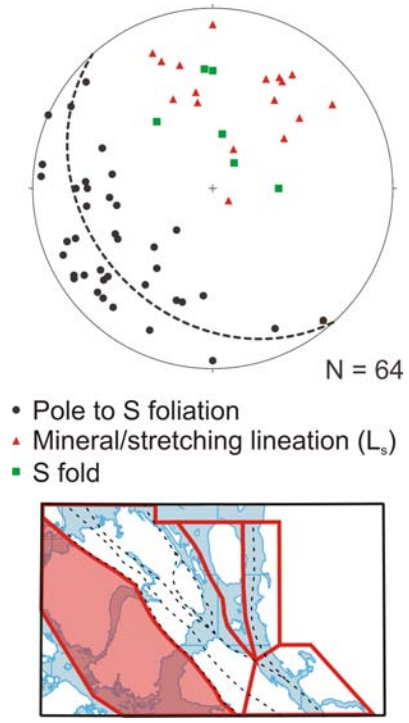

Figure 4.8: Lower hemisphere stereonet projection of structural data from south of the Useless shear zone. Dashed great circle at 138°/30° represents best fit girdle of foliation data potentially indicating large scale folding around a northeast plunging hinge line.

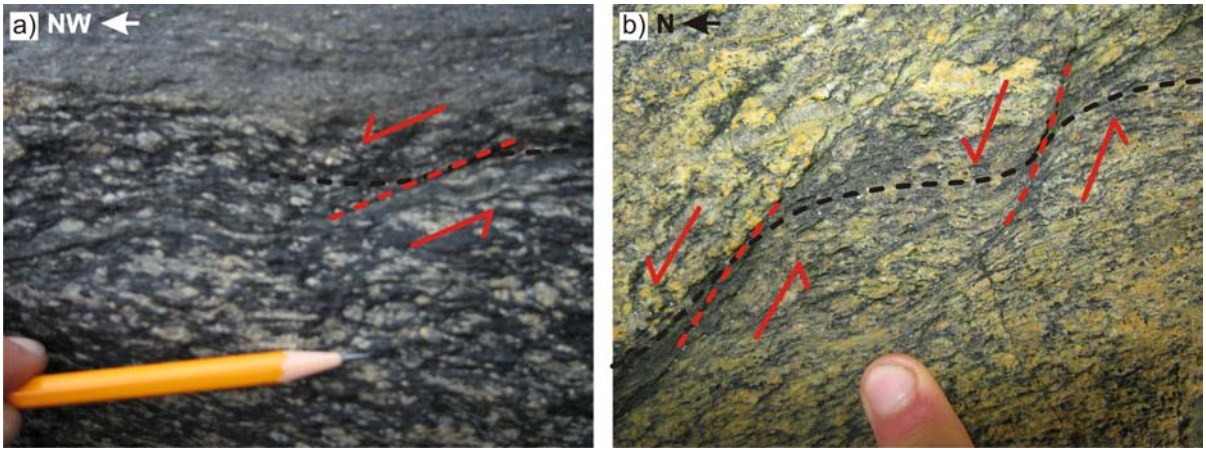

Figure 4.9: Shear sense indicators within the Ogden Channel complex. (a) sinistral C' shear band along the eastern shore of Ogden Channel, approximately 50 metres south of the dyke collected as U-Pb sample 10JA28-04; (b) sinistral C' shear band from the eastern shore of Porcher Inlet.

4.4.1.2 Paleozoic deformation of the Descon Formation

As previously noted, much of the fabric north of the Useless shear zone is the result of Cretaceous deformation (see Chapter 3). However, sample 11JA28-01 (356.1 ± 4.3 Ma; see below) crosscuts a pre-existing, heterogeneously developed fabric within the Descon Formation (Figure 4.10a). Locally, this fabric indicates sinistral shear, consistent with structures observed within the Ogden Channel complex (Figure 4.10b).

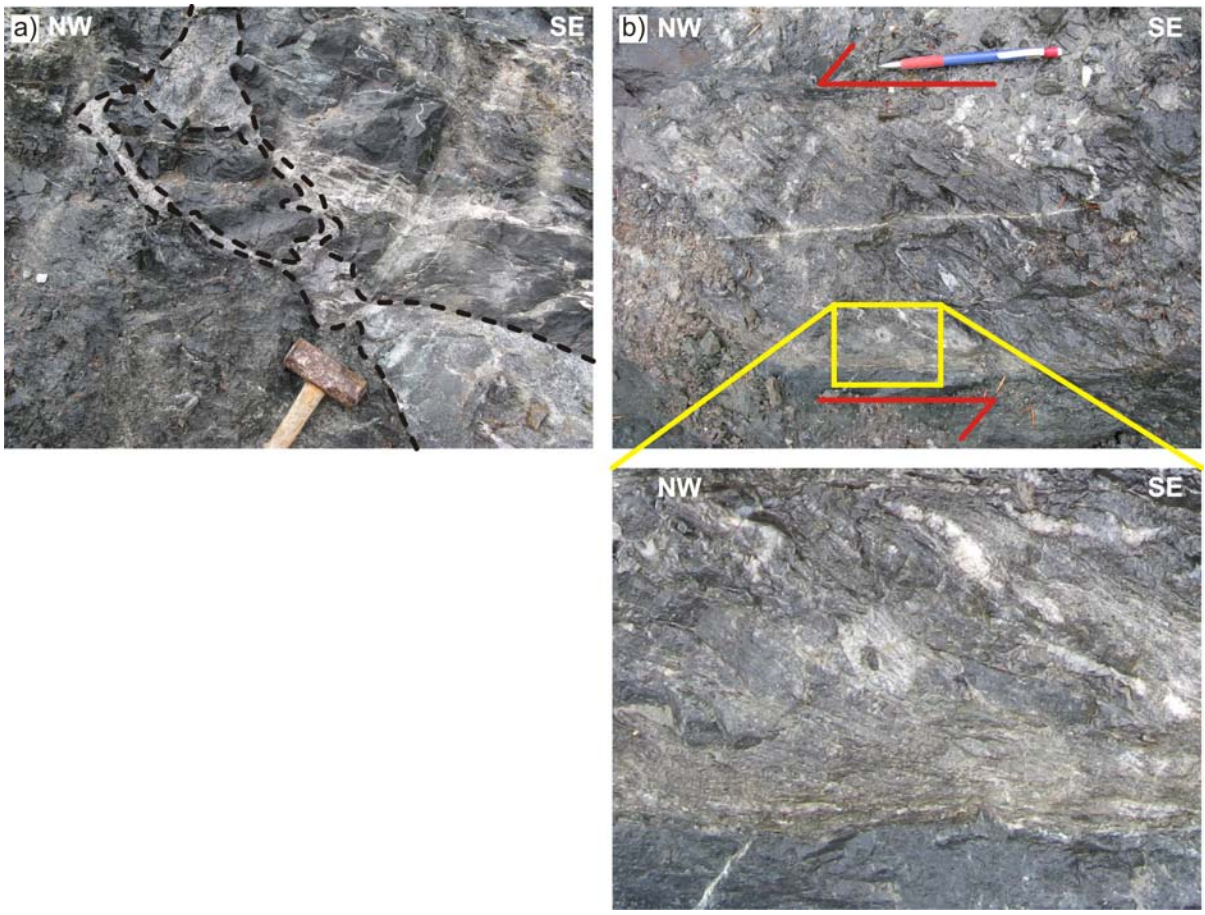

Figure 4.10: Photographs from U-Pb 11JA28-01 sampling locality: (a) Photograph of the dyke sampled as U-Pb 11JA28-01; (b) A localized zone of sinistral deformation has developed a strong fabric in which some quartz veins have been transposed. Sense of motion is sinistral. Basaltic material adjacent to the zone of deformation (at the bottom of the photograph) contains very weak fabric.

4.4.2 Structural Interpretation

Overall, deformation within the Ogden Channel complex is ambiguous. At present, it cannot be confirmed whether it was dominantly southwest-vergent, consistent with observations assigned to the Klakas orogeny elsewhere in the Alexander terrane (Gehrels and Saleeby, 1987a,b; Gehrels *et al*., 1987), or dominantly sinistral in accordance with locally observed shear sense indicators. The evidence for a sinistral component to Late Silurian – Early Devonian deformation within the Ogden Channel complex is an important new contribution, as it has not previously been observed within the Alexander terrane.

4.5 Geochronology

New LA-ICP-MS and SHRIMP-RG analyses for two geochronological samples provide constraints on the Paleozoic history of the Alexander terrane. Sample 10JA28-04 is from a typical, synkinematic, Ogden Channel complex dyke located along the eastern shore of Ogden Channel (Figure 4.5). It provides an age both for emplacement of a typical phase of the Ogden Channel complex and for coeval deformation. Sample 11JA28-01 is from a synkinematic or interkinematic dyke that intrudes the Descon Formation north of the Salt Lagoon shear zone on Porcher Island, northwest of Oona River (Figure 4.5). It crosscuts fabric that indicates sinistral shear, and is boudinaged consistent with sinistral shear.

4.5.1 Analytical methods:

The data presented herein represent LA-ICP-MS analyses carried out at the Jack Satterly Geochronology Laboratory and SHRIMP-RG analyses carried out at the Stanford USGS Micro Analysis Centre. For all methods, zircon was separated from up to 20 kg samples following standard methods and hand picked under alcohol. All graphical plots and age calculations were produced using Isoplot 3.7 (Ludwig, 2009).

4.5.1.1 LA-ICP-MS METHODS

Whole zircons from sample 10JA28-04 (Ogden Channel) were mounted on a glass slide using double-sided tape and imaged under reflected light. LA-ICP-MS methods are described in more detail in section 3.4.1.1. U-Pb isotopic composition was calibrated to DD 91-1 (2682.4 ± 1.0 Ma; Davis, 2002). Data reduction for LA-ICP-MS analyses was completed using the program of Davis (1982).

4.5.1.2 SHRIMP-RG METHODS

Zircons from sample 11JA28-01 (Oona River) were mounted in a 2.54 cm epoxy resin round and polished to expose cross sections. The grains were imaged via transmitted light, reflected light, and cathodoluminesence in order to identify potential core and rim structures. The procedure for SHRIMP-RG analyses followed that of Williams (1998), with data reduction completed using the SQUID program (Ludwig, 2005). U-Pb isotopic composition was calibrated to zircon standard R33 (419 ± 1 Ma; Black *et al*., 2004).

4.5.2 Data and results

Isotopic analyses are presented in appendix A. Uncertainty ellipses in graphical representations are plotted at 2σ and age uncertainties are reported at 95% confidence levels. Decay constants used are from Jaffey *et al*. (1971), and common Pb isotope compositions were estimated from Stacey and Kramers (1975).

4.5.2.1 Sample 10JA28-04: Ogden Channel quartz diorite

4.5.2.1.1 Sample description and field relationships

Sample 10JA28-04 is a weakly deformed plagioclase porphyritic quartz diorite dyke. It displays a weak foliation and demonstrably crosscuts foliation in an adjacent dyke (Figure 4.6a,b). It is interpreted as a late synkinematic phase of the Ogden Channel complex. It provides an emplacement age for the Ogden Channel complex and a constraint on the end of deformation within the complex. Shear sense indicators were not observed within the sampled dyke but shear bands observed nearby record sinistral shear (Figure 4.9a).

4.5.2.1.2 Data and results

The Ogden Channel quartz diorite sample contains translucent to very pale yellow, stubby prismatic, euhedral zircons ranging 25-75 μm in width and 75-150 μm in length. Of 21 near concordant LA-ICP-MS analyses, 15 cluster to yield a weighted average $^{206}Pb/^{238}U$ age of 413.3 ± 2.5 Ma (Figure 11a,b). One grain (23.1) provided a concordant result, with a $^{206}Pb/^{238}U$ age of 295.9 ± 1.1 Ma. While this grain was morphologically indistinguishable, it is ascribed to contamination based on the strong agreement of all other grains analyzed, and the quartz diorite composition of the dyke which is unlikely to have significant inheritance. A further argument for discounting 23.1 is its anomalously low Th/U ratio of 0.2 (see appendix A). While this is still in the range commonly attributed to

igneous zircon (Rubatto, 2002), it's at the low end of the range observed for mafic to intermediate intrusions (Wang *et al*., 2011). The crystallization age of the dyke is thus interpreted as 413.3 ± 2.5 Ma.

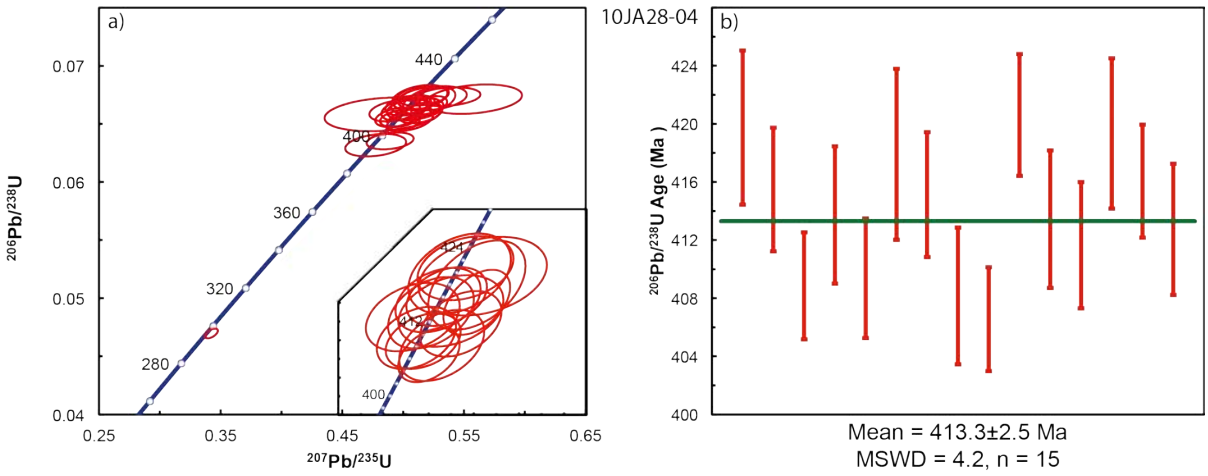

Figure 4.11: Concordia and $^{206}Pb/^{238}U$ weighted average plots for LA-ICP-MS analyses of sample 10JA28-04. Inset in (a) includes only the 15 analyses plotted in (b). Data point uncertainties are 2σ. Reported age from weighted average $^{206}Pb/^{238}U$ ages at 95% confidence, with uncertainties calculated from data point uncertainties only. Analytical data are presented in table A.4.

4.5.2.1.3 Interpretation

The weakly deformed Ogden Channel sample (10JA28-04) indicates that the complex was emplaced, in part, during the Early Devonian. The mylonitic tonalite in figure 4.6a yielded a U-Pb zircon age of 412.3 ± 1.4 Ma (LA-ICP-MS; J.B. Mahoney unpublished data). The crosscutting relationship, with fabric in the mylonitic tonalite crosscut by the weakly deformed quartz diorite, combined with geochronology indicating that the samples are essentially coeval (within uncertainty of one another), confirms that deformation was ongoing during the Early Devonian. The limited deformation recorded by sample 10JA28-04 further suggests that this event was coming to a close during the Early Devonian; an interpretation which is supported by the 410 ± 19 Ma age (J.B. Mahoney, unpublished data) from a postkinematic phase of the Porcher Creek pluton (Figure 4.5)

4.5.2.2 Sample 11JA28-01: Oona River sample

4.5.2.2.1 Sample description and field relationships

Sample 11JA28-01 was collected from a light grey granodiorite dyke north of the Salt Lagoon shear zone on Porcher Island (Figure 4.5). It is stretched and boudinaged consistent with sinistral shear, but also crosscuts an existing fabric in the surrounding country rock (Figure 4.10a). Brittle-ductile features locally define a strong fabric indicating sinistral shear (Figure 4.10b).

4.5.2.2.2 11JA28-01 data and results

The Oona River sample (11JA28-01) contains predominantly equant, subhedral zircon grains and lesser elongate prisms. They range in width from 50-100 μm and in length from 100-250 μm. All grains exhibit some degree of concentric zoning in CL (Figure 4.12a). Ten concordant and nearly concordant SHRIMP-RG analyses fall in the range from 335 Ma to 385 Ma (Figure 4.12b); eight of those which overlap yield a weighted average $^{206}Pb/^{238}U$ age of 356.1 ± 4.3 Ma (Figure 4.12c).

4.5.2.2.3 Interpretation

The significance of Oona River sample (11JA28-01) is that it indicates the Descon Formation on northern Porcher Island underwent a phase of deformation prior to and/or during 356.1 ± 4.3 Ma. This is interpreted to record Klakas age deformation. Furthermore, the brittle-ductile structural style is very different from that exhibited by the Ogden Channel complex, suggesting that the area north of the Salt Lagoon shear zone was at a higher structural level during the Devonian and, by extension, that the Salt Lagoon shear zone represents a significant structural break.

The age of this sample is also significant in that it is not a common magmatic age within the Alexander terrane. It is, however, a typical age for the Sicker Group: the volcanic arc assemblage at the base of the Wrangellia terrane (Yorath *et al*., 1999). Van der Heyden (1989) suggested that the Swede Point pluton indicates a Devonian linkage between the Alexander and Wrangellia terranes. Sample 11JA28-01 contributes to a growing body of evidence suggesting a late Paleozoic link between the Alexander and Wrangellia terranes (Gardner *et al*., 1986; van der Heyden, 1989; Nelson *et al*., 2012).

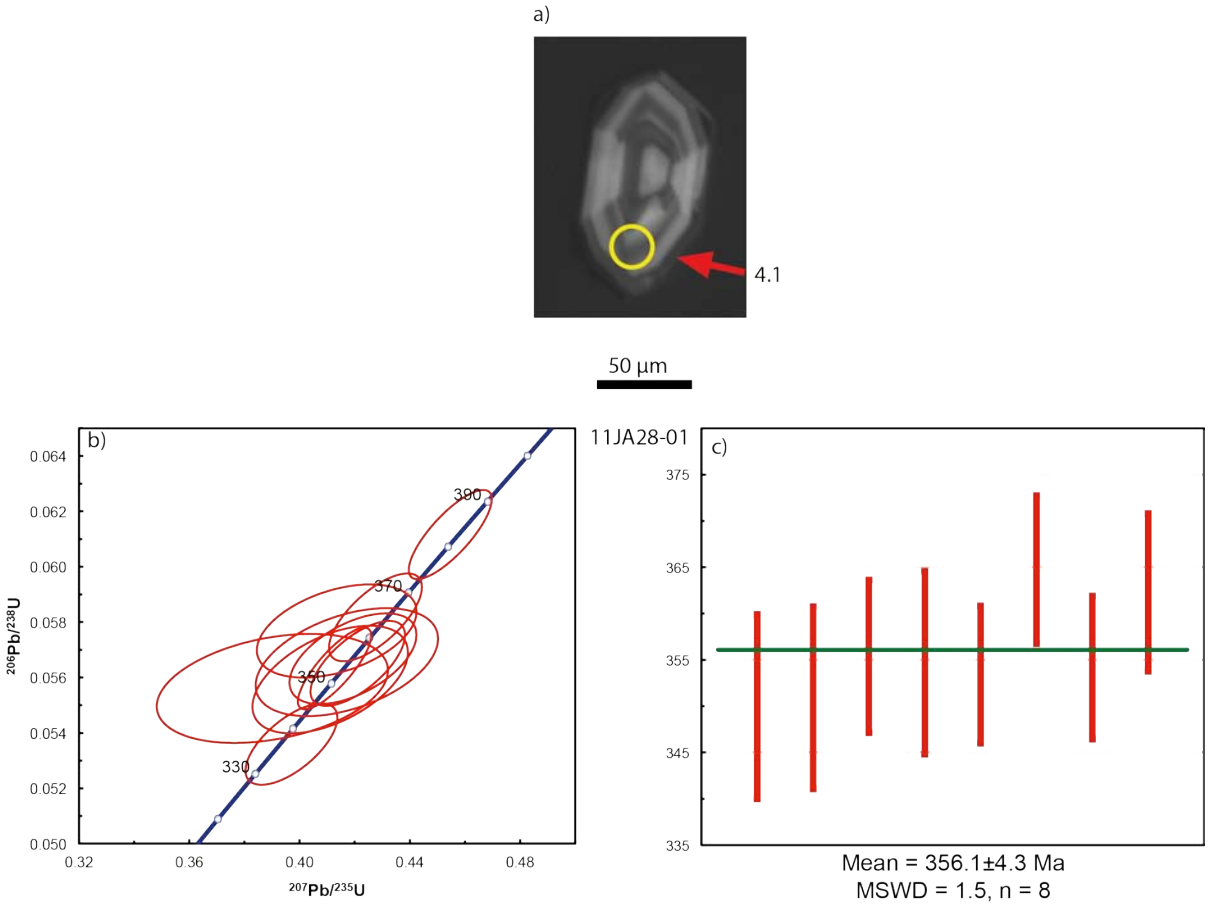

Figure 4.12: SEM image and graphical representation of geochronological data associated with sample 11JA28-01: (a) CL image of zircon 10.1 exhibiting typical concentric oscillatory zoning; (b) Concordia plot of all SHRIMP-RG analyses; (c) $^{206}Pb/^{238}U$ weighted average of overlapping data, note that the oldest and youngest grains in b have been removed. Data point uncertainties are 2σ. Reported age from weighted average $^{206}Pb/^{238}U$ at 95% confidence, with uncertainties calculated from data point uncertainties only. Analytical data are presented in Table A.5.

4.6 Discussion

The lithological, geochronological, and structural characteristics of the Ogden Channel complex have important implications for the tectonic setting of the Alexander terrane during the Klakas orogeny. Age constraints, including the 413.3 ± 2.5 Ma age reported herein for a comparatively weakly deformed quartz diorite (sample 10JA28-04), indicate that the Ogden Channel complex was emplaced during the Late Silurian to Early Devonian. The late synkinematic to post-kinematic 410 ± 19 Ma granodiorite from the Porcher Creek pluton (J.B. Mahoney, unpublished data) indicates that

deformation was coming to a close in this part of the Alexander terrane during the earliest Early Devonian. The 412.3 ± 1.4 Ma age (J.B. Mahoney, unpublished data) from the mylonite crosscut by the dyke sampled as 10JA28-04 indicates that a significant amount of deformation occurred during the Early Devonian. These timing constraints on the end of deformation are consistent, within uncertainty, with constraints from southern Annette Island in southeast Alaska where a 426 ± 15 Ma metadiorite with semi-schistose foliation is crosscut by an undeformed 415 ± 5 Ma trondhjemite dyke (U-Pb zircon, ID-TIMS; Gehrels *et al*., 1987).

The dominantly mafic to intermediate composition of the Ogden Channel complex suggests that it formed in an arc setting. This is in contrast with Late Silurian to Early Devonian magmatism in southeast Alaska which has been interpreted as the result of anatectic melting based on leucodiorite to trondhjemite composition as well as syn- to post-kinematic emplacement (Gehrels and Saleeby, 1987b); however, the compositional differences could be the result of differing percentages of partial melting. The paucity of xenocrystic cores in the samples analyzed during this study argue against an anatectic origin. Geochemical characterization of these two plutonic suites may help to clarify the tectonic setting of the Alexander terrane during the Late Silurian to Early Devonian.

Regardless of the origin of the magma, structural observations within the Ogden Channel complex indicate a sinistral component to Klakas age deformation, in addition to previously reported southwest-vergent deformation attributed to the Klakas orogeny elsewhere in the Alexander terrane (Gehrels *et al*., 1983; Gehrels and Saleeby, 1987a,b; Gehrels *et al*., 1987; Gehrels *et al*., 1996). As described above, the Klakas orogeny is hypothesized to be the result of interaction between the Craig subterrane and a continental fragment to the southwest. The dominantly southwest-vergent deformation implies that the Alexander terrane was emplaced above the colliding continental fragment. This is consistent with an upper plate setting for the Alexander terrane as would be the case if Silurian to Early Devonian magmatism was arc-related. The evidence for a sinistral component to deformation reported herein is important as it has not previously been reported for Klakas age deformation and may aid in identifying the continental fragment to which the Alexander terrane accreted during the Klakas orogeny.

The Pearya terrane of northern Ellesmere Island (Figure 4.1, inset; Figure 4.2) was accreted to the Franklinian belt along the northern margin of Laurentia by sinistral transpression during the Late Silurian to Early Devonian (Trettin, 1987). The Caledonian terranes of Svalbard (Barentsia, Figure 4.2) are similarly interpreted to have undergone sinistral transpression during the Silurian to Early

Devonian (Gee *et al*., 2008). Colpron and Nelson (2009; 2011a) suggested that this sinistral transpression is related to the southern edge of the Scotia style arc responsible for transporting terranes of Caledonian affinity into Panthalassa. The evidence for sinistral transpression of Late Silurian to Early Devonian age within the Alexander terrane described herein is consistent with a location near the southern margin of the proposed Scotia style arc perhaps in proximity to Pearya and/or Barentsia. The detrital zircon record of the Karheen Formation suggests that the Alexander terrane was still in proximity to Baltica (or at least a crustal fragment capable of producing the same zircon spectrum as Baltica) during the Early Devonian. This is consistent with the paleogeographic reconstruction presented in figure 4.2, where the Alexander terrane is located along the northern extent of the Baltican Caledonides, adjacent to both Pearya and Barentsia during the Early Devonian (Colpron and Nelson, 2011a).

4.7 Conclusion:

The Ogden Channel complex on southern Porcher Island and adjacent Pitt Island in north coastal British Columbia is a metaplutonic/metamorphic complex in which multiple gabbroic to granodioritic intrusions were emplaced syn- to post-kinematically. New U-Pb geochronology, including the 413.3 ± 2.5 Ma age reported for sample 10JA28-04 indicates that it was emplaced during the Late Silurian to Early Devonian, corresponding to the Klakas orogeny identified elsewhere in the Alexander terrane. Lithological observations suggest calc-alkaline, potentially subduction related origin for the suite of Ogden Channel plutons and dikes, in contrast with previous interpretations of synkinematic Late Silurian to Early Devonian plutons on Annette Island as anatectic in origin. Evidence for a sinistral component to Klakas age deformation within the Ogden Channel complex is important as it has previously been interpreted as strictly southwest-vergent. Constraining Klakas age deformation as sinistral reverse suggests a correlation with Pearya and Svalbard, both of which underwent sinistral transpression during the Devonian.

The 356.1 ± 4.3 Ma age reported for a dike one km north of the Salt Lagoon shear zone (sample 11JA28-01) which crosscuts a pre-existing fabric suggests that the effects of Klakas age deformation extended beyond the Ogden Channel complex into the zone occupied by the Early Cretaceous Grenville Channel fault. Later transpressional shear may have nucleated on a pre-existing mid-Paleozoic structure.

A detailed study of the Ogden Channel complex and Late Silurian to Early Devonian magmatism on and near Annette Island in southeast Alaska, including whole rock geochemical analyses and further structural investigation, is warranted to indicate the tectonic setting of the Alexander terrane during the Klakas orogeny. If the tectonic fragment which the Alexander terrane interacted with during the Klakas orogeny can be identified, it will further constrain the model for translation of terranes of Baltican, Siberian, and Caledonian affinity that are now found in the North American Cordillera; it will also contribute to our understanding of the metallogeny of the Alexander terrane and lead to more effective exploration programs. Determining the extent to which sinistral shear recorded by the Ogden Channel complex is of Silurian to Devonian age, as opposed to the result of younger deformation, would be important for reconstructing the tectonic history of the Alexander terrane.

Chapter 5
Discussion and Conclusion

5.1 Tectonic escape

Tectonic escape is commonly considered a feature of collisional orogenies such as is the case in the Himalayan and Anatolian regions (Burke and Sengor, 1986). Not only is the northern Cordillera not a collisional orogeny, the timing of proposed tectonic escape in the northern Cordillera does not match any of the major terrane accretion events, which are generally assigned to the Jurassic. Therefore, if tectonic escape did occur in the northern Cordillera, it must not be restricted to collisional orogenies. If tectonic escape is considered based on stress and strain relationships alone, it follows from Anderson's theory of faulting (Anderson, 1951) that the fundamental requirement is that the vertical stress is greater than the horizontal confining stress (i.e. orogen parallel). This can be achieved by either dramatic thickening of the lithosphere as in the Himalayas, or by reducing the orogen parallel stress. The latter is achieved in the Anatolian region by slab rollback and associated trench suction along the Hellenic arc (Burke and Sengor, 1986). England and McKenzie (1982; 1983) suggest that the basic requirement of tectonic escape is that the vertical stress must be great enough to cause strain. However, if the horizontal, orogen-perpendicular stress is great enough to cause strain, that strain will occur regardless of the vertical stress. It will take place in the form of orogen perpendicular shortening, and will be accommodated by extension against the minimum stress. If the minimum stress is vertical, it will be accommodated by thickening; if the minimum stress is orogen parallel, it will be accommodated by horizontal, orogen-parallel extension (ie. tectonic escape). Therefore, we argue that the basic requirement for tectonic escape is not that the vertical stress is great enough to cause strain, but rather that it is greater than the orogen parallel stress.

5.1.1 Orogen perpendicular shortening

If the above interpretation is correct, a significant orogen perpendicular stress is required to initiate deformation within the orogen. According to a study of modern subduction zones, the intensity of deformation within the upper plate exhibits strong correlations with slab dip and the (subduction zone orthogonal component of) absolute velocity of the overriding plate; as compared to other factors including age of the subducting slab and absolute velocity of the lower plate, which both exhibit weak correlations with upper plate deformation (Lallemand *et al*., 2005). The apparent polar wander path

for North America indicates a significant change in direction from northwestward to southwestward during the late Early Cretaceous (Besse and Courtillot, 1991; Elston *et al*., 2002). This transition would correspond to an increase in subduction zone orthogonal absolute motion of the northern Cordilleran upper plate. As previously mentioned, the magmatic front associated with the Coast Plutonic Complex is interpreted to have migrated eastward at a rate of 2.0 to 2.7 km/My between 120 and 80 Ma (Gehrels *et al*., 2009). This may record a shallowing of the slab dip starting at ca. 120 Ma; a hypothesis corroborated by the onset of thickening and high grade metamorphism in the Coast Belt during the mid-Cretaceous (Crawford *et al*., 1987; 2000; Rusmore *et al*., 2005; Wolf *et al*., 2010). These two events correlate to the onset of deformation in the relatively weak and deformable parts of the upper plate (ie. the back arc region in what is to become the Coast Plutonic Complex, as well as the Omineca belt in Figure 3.1).

5.1.2 Rheological control on deformation

Hyndman *et al*., (2005) presented a model for back-arc heating across the entire width of an orogen leading to high topography and reduced lithospheric strength. They point out that deformation is commonly constrained to the margins of the back-arc with little internal deformation as is observed in the Cordillera during the mid-Cretaceous. Their interpretation is that a sufficiently weak detachment surface transfers deformation across the back arc. An alternative hypothesis is that these two regions are the hottest, and therefore weakest, regions within the back arc. In nearly all of their heat flow cross sections there are two spikes in heat flow, one that corresponds to the arc and one near the margin between the back arc and craton. If there is an overall convection cell overprinted on turbulent convection as depicted in figure 5.1, the hottest asthenospheric material would be present at the point of upwelling of the large convection cell (ie. the back of the back arc). As it moves towards the arc it would lose heat into the overlying crust/lithosphere and become cooler. Release of volatiles and production of magma explains the high heat flow within the arc (Hyndman *et al*., 2005). The concentration of deformation along the Coast and Omineca Belts may therefore be the thermal effects of the asthenospheric wedge.

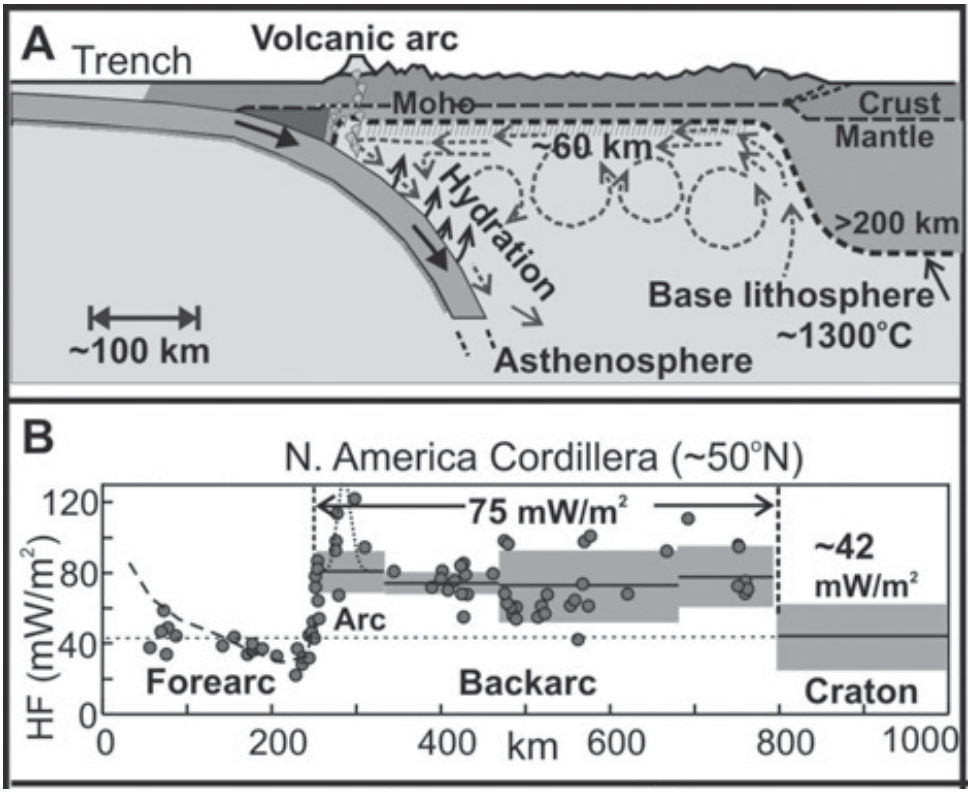

Figure 5.1: (a) Schematic cross section of asthenospheric convection beneath a back-arc. Note the multiple smaller convection cells within one large convection cell; (b) modern heat flow (HF) values across the North American Cordillera. Note that the highest values are present at the arc and at the back-arc to craton transition (from Hyndman and Currie, 2011).

5.1.3 Deviation from ideal conjugate orientation

While the sense of shear on orogen scale shear zone systems matches that observed for shear zones and shear bands observed in this study, their orientation deviates significantly from the theoretical geometry of ductile conjugate sets. Where the two shear zone systems merge in southern British Columbia they are close to the idealized value, but both curve towards parallelism with the strike of the orogen to the north (Figure 3.1 inset). The same curvature is observed for shear zones associated with escape of the Tibetan plateau. Tapponnier *et al*. (1982) carried out studies on plasticine concluding that faults utilize existing anisotropies. These anisotropies are in the form of contacts between layers in their plasticine model, and terrane boundaries in tectonic escape. As previously mentioned, the shear zone systems outlining the escape block within the northern Cordillera do correspond to major terrane boundaries.

5.2 Conclusions

This research has recorded structures and geochronology related to two tectonic events. They are the Late Silurian to Early Devonian Klakas orogeny and mid-Cretaceous tectonic escape:

1) The Ogden Channel complex is a synkinematic magmatic record of the Late Silurian to Early Devonian Klakas orogeny. Structures suggest a component of sinistral shear during this event, supporting a probable paleogeography for the Alexander terrane at the northern extent of the Caledonian orogeny at that time, in proximity to Barentsia, Pearya, and the Greenland Caledonides. Petrology of the Ogden Channel complex suggests it is subduction related, in contrast with observations of coeval plutons within the Alexander terrane in southeast Alaska. This relationship has yet to be worked out.

2) The structural grain of the study area is dominated by mid-Cretaceous shear zones. Their geometry and associated age constraints suggest they formed, in part, as a ductile conjugate set. These conjugate shear zones, along with similar conjugate shear bands and the horizontal stretch recorded in the Grenville Channel shear zone, correspond to a strain field of orogen perpendicular shortening and orogen parallel extension. The mid-Cretaceous shear zones across the northern Cordillera also have a similar geometry, suggesting that a similar strain field was present at all three scales. The evidence presented herein suggests that the northern Cordillera underwent tectonic escape during the mid-Cretaceous, corresponding to the timing of a transition between sinistral oblique and dextral oblique subduction beneath western North America.

5.3 Future work

The results of this research have provided significant insight into the tectonic history of the region, but have also raised several new questions. A few ideas for future research are as follows:

1) The relationship between dextral, west-side-up shearing documented for the Telegraph Passage shear zone herein and east-side-up shearing on the Prince Rupert shear zone immediately to the north is unclear. A detailed structural study linking these two areas would be a great asset; however, emplacement of younger plutons may have obliterated any structural relationships.

2) The metamorphic history of the study area is complex and not always easily integrated with structural observations. For example, the increase in metamorphic grade from west to east across the Telegraph Passage shear zone does not readily fit the structural interpretation that it accommodated a

component of west side up motion. A detailed study of the metamorphic history would undoubtedly provide further insight into the tectonic history of the region.

3) A further study of Late Silurian to Early Devonian magmatism in the southern Alexander terrane is warranted as it will likely provide better constraints on the Klakas orogeny. Geochemical studies of Late Silurian to Early Devonian plutons, both in the study area and in the vicinity of Annette Island in southeast Alaska, would aid in correlating this magmatism to a specific tectonic setting.

4) A more in-depth comparison of the proposed tectonic escape for the northern Cordillera with known modern examples of tectonic escape including the Tibetan plateau and the Aegean region will contribute to our understanding of the controls on tectonic escape and provide insight into the tectonic conditions within the northern Cordillera during the mid-Cretaceous. Of particular interest to the author is what may have caused the orogen parallel stress to be less than the vertical stress in the northern Cordillera at that time.

Appendix A

Geochronological data

Table A.1: U-Pb isotopic data from LA-ICP-MS analyses on zircon presented in Chapter 3.

Spot	U	^{206}Pb	Th/U	Isotopic ratios (1σ)		Age(1σ) /Ma
	ppm	ppm		^{207}Pb/^{235}U	^{206}Pb/^{238}U	^{206}Pb/^{238}U
10JA26-03						
1.1	650	25	0.29	0.2804 (0.0030)	0.0388 (0.00022)	245.7 (1.4)
2.1	260	17	0.01	0.5358 (0.0059)	0.0673 (0.00031)	420.1 (1.9)
3.1	883	134	0.51	1.4853 (0.0082)	0.1521 (0.00050)	912.8 (2.8)
1.1	216	15	0.08	0.5682 (0.0100)	0.0711 (0.00052)	442.7 (3.1)
2.1	255	12	0.45	0.3429 (0.0048)	0.0455 (0.00029)	287.1 (1.8)
3.1	404	18	0.37	0.3206 (0.0033)	0.0450 (0.00028)	283.5 (1.7)
4.1	288	13	0.52	0.3327 (0.0053)	0.0462 (0.00034)	291.0 (2.1)
5.1	391	18	0.17	0.3463 (0.0050)	0.0467 (0.00026)	294.2 (1.6)
6.1	487	23	0.52	0.4252 (0.0045)	0.0481 (0.00028)	302.6 (1.7)
7.1	226	11	0.39	0.3431 (0.0066)	0.0471 (0.00028)	296.6 (1.7)
8.1	265	12	0.62	0.3286 (0.0054)	0.0456 (0.00024)	287.7 (1.5)
9.1	399	19	0.34	0.3376 (0.0049)	0.0473 (0.00023)	298.1 (1.4)
11.1	959	16	0.23	0.1129 (0.0018)	0.0163 (0.00009)	104.5 (0.6)
13.1	734	11	0.56	0.1035 (0.0025)	0.0156 (0.00010)	99.7 (0.7)
14.1	2712	141	0.15	0.3700 (0.0021)	0.0520 (0.00019)	327.1 (1.2)
15.1	253	12	0.42	0.3513 (0.0056)	0.0488 (0.00028)	307.0 (1.7)
16.1	1225	55	0.45	0.3182 (0.0033)	0.0449 (0.00028)	282.8 (1.7)
17.1	910	41	0.37	0.3281 (0.0034)	0.0451 (0.00023)	284.1 (1.4)
18.1	1506	94	0.04	0.4712 (0.0047)	0.0623 (0.00032)	389.8 (1.9)
10JA27-02						
1.1	210	3	0.46	0.1080(0.0053)	0.0156(0.00016)	99.5(1.0)
2.2	275	7	0.05	0.1765(0.0059)	0.0243(0.00028)	154.9(1.8)
3.1	72	1	0.26	0.1157(0.0061)	0.0157(0.00019)	100.5(1.2)
4.1	472	8	0.17	0.1239(0.0030)	0.0166(0.00015)	106.0(1.0)
5.1	452	11	0.05	0.1825(0.0037)	0.0253(0.00024)	160.9(1.5)
8.1	911	15	0.53	0.1089(0.0042)	0.0166(0.00012)	106.3(0.7)
9.1	181	3	0.29	0.1095(0.0054)	0.0162(0.00018)	103.7(1.2)
10.1	296	8	0.79	0.1872(0.0045)	0.0282(0.00020)	179.0(1.3)
11.1	1033	22	0.96	0.1483(0.0020)	0.0215(0.00013)	137.1(0.8)
12.1	838	20	0.41	0.1617(0.0030)	0.0233(0.00011)	148.7(0.7)
13.1	721	15	0.14	0.1312(0.0025)	0.0202(0.00011)	128.7(0.7)

14.1	645	21	0.72	0.2244(0.0031)	0.0327(0.00014)	207.5(0.9)
15.1	243	4	0.61	0.1053(0.0034)	0.0161(0.00012)	103.1(0.8)
16.1	118	2	0.29	0.1152(0.0062)	0.0154(0.00018)	98.8(1.1)
17.1	294	5	0.20	0.1055(0.0039)	0.0153(0.00016)	98.2(1.0)
18.1	370	8	0.68	0.1506(0.0040)	0.0223(0.00021)	142.0(1.3)
20.1	275	4	0.44	0.0985(0.0035)	0.0156(0.00014)	99.5(0.9)
21.1	916	22	0.14	0.1668(0.0033)	0.0238(0.00016)	151.4(1.0)
22.1	1017	23	1.58	0.1561(0.0046)	0.0222(0.00020)	141.4(1.2)
25.1	789	17	0.96	0.1516(0.0037)	0.0218(0.00013)	138.9(0.8)
26.1	318	5	0.75	0.10610.0060)	0.0154(0.00021)	98.5(1.3)
27.1	315	5	0.26	0.1031(0.0046)	0.0153(0.00015)	97.8(1.0)
10JA27-03						
1.1	216	3	0.26	0.1017(0.0024)	0.0152(0.00012)	97.5(0.7)
2.1	337	5	0.46	0.0997(0.0017)	0.0150(0.00007)	96.1(0.5)
4.1	241	4	0.50	0.1025(0.0022)	0.0151(0.00009)	96.6(0.6)
4.2	368	6	0.26	0.1013(0.0016)	0.0150(0.00007)	96.1(0.5)
5.1	385	6	0.54	0.1015(0.0020)	0.0154(0.00007)	98.5(0.5)
6.1	144	2	0.32	0.1095(0.0033)	0.0160(0.00012)	102.6(0.8)
7.1	161	3	0.24	0.1091(0.0030)	0.0159(0.00015)	101.5(1.0)
8.1	239	4	0.30	0.1043(0.0022)	0.0160(0.00011)	102.2(0.7)
9.1	200	3	0.33	0.1025(0.0027)	0.0154(0.00011)	98.4(0.7)
10.1	280	4	0.49	0.1039(0.0022)	0.0153(0.00011)	97.9(0.7)
11.1	120	2	0.30	0.1040(0.0031)	0.0155(0.00013)	98.9(0.8)
12.1	268	4	0.37	0.1023(0.0022)	0.0150(0.00009)	96.1(0.6)
13.1	313	5	0.54	0.0973(0.0020)	0.0148(0.00011)	94.4(0.7)
14.1	201	3	0.36	0.1003(0.0028)	0.0149(0.00010)	95.0(0.6)
16.1	277	4	0.38	0.1011(0.0025)	0.0150(0.00009)	96.0(0.6)
17.1	172	3	0.42	0.0974(0.0027)	0.0149(0.00011)	95.1(0.7)
18.1	190	3	0.52	0.1003(0.0042)	0.0154(0.00011)	98.5(0.7)
19.1	195	3	0.59	0.1008(0.0028)	0.0152(0.00012)	97.3(0.8)
22.1	144	2	0.35	0.1008(0.0030)	0.0150(0.00014)	95.8(0.9)
22.2	351	5	0.48	0.0975(0.0020)	0.0144(0.00008)	92.4(0.5)
23.1	302	5	0.55	0.1093(0.0022)	0.0155(0.00009)	99.3(0.6)
24.1	372	6	0.59	0.1068(0.0020)	0.0148(0.00008)	95.0(0.5)
25.1	222	3	0.37	0.1032(0.0027)	0.0149(0.00012)	95.2(0.8)
26.1	162	2	0.28	0.1111(0.0031)	0.0152(0.00012)	97.3(0.8)
10JA28-02						
1.1	62	1	0.57	0.1050(0.0047)	0.0153(0.00017)	97.7(1.1)
3.1	44	1	0.54	0.1303(0.0069)	0.0162(0.00022)	103.3(1.4)

4.1	54	1	0.37	0.1013(0.0052)	0.0153(0.00020)	98.1(1.3)
5.1	115	2	0.56	0.1016(0.0039)	0.0148(0.00012)	94.6(0.8)
6.1	40	1	0.41	0.1123(0.0061)	0.0147(0.00022)	94.0(1.4)
7.1	57	1	0.53	0.0995(0.0049)	0.0145(0.00017)	92.7(1.1)
8.1	69	1	0.60	0.1015(0.0049)	0.0150(0.00018)	96.2(1.1)
9.1	72	1	0.56	0.1230(0.0058)	0.0157(0.00018)	100.4(1.1)
1.1	205	3	0.49	0.1500(0.0070)	0.0150(0.00023)	96.1(1.5)
2.1	364	6	0.36	0.1113(0.0042)	0.0157(0.00016)	100.3(1.0)
3.1	202	3	0.38	0.1181(0.0063)	0.0161(0.00023)	102.7(1.4)
4.1	360	6	0.56	0.1113(0.0043)	0.0161(0.00016)	102.9(1.0)
5.1	511	8	0.63	0.1077(0.0037)	0.0161(0.00017)	103.1(1.1)
6.1	429	7	0.67	0.1058(0.0044)	0.0152(0.00016)	97.0(1.0)
7.1	256	4	0.47	0.1077(0.0049)	0.0155(0.00021)	99.3(1.3)
8.1	126	2	0.43	0.1099(0.0058)	0.0160(0.00024)	102.6(1.5)
9.1	116	2	0.52	0.1201(0.0061)	0.0160(0.00023)	102.0(1.5)
10.1	103	2	0.47	0.1166(0.0060)	0.0162(0.00027)	103.4(1.7)
11.2	152	2	0.52	0.1196(0.0053)	0.0158(0.00020)	101.0(1.3)
12.1	199	3	0.56	0.1129(0.0054)	0.0158(0.00018)	101.1(1.2)
13.1	229	4	0.54	0.1188(0.0048)	0.0160(0.00020)	102.3(1.3)
14.1	131	2	0.37	0.1183(0.0064)	0.0160(0.00025)	102.5(1.6)
15.1	136	2	0.36	0.1187(0.0060)	0.0163(0.00028)	104.4(1.8)
16.1	200	3	0.57	0.1198(0.0053)	0.0159(0.00021)	102.0(1.3)
17.1	123	2	0.49	0.1111(0.0050)	0.0161(0.00023)	102.8(1.4)
18.1	107	2	0.52	0.1155(0.0086)	0.0156(0.00024)	99.9(1.5)
1.2	48	1	0.42	0.16367(0.0148)	0.0155(0.00028)	99.1(1.8)
2.2	70	1	0.40	0.1294(0.0088)	0.0152(0.00021)	97.0(1.4)
3.2	82	1	0.42	0.1483(0.0085)	0.0159(0.00026)	101.5(1.6)
4.2	75	1	0.41	0.1470(0.0089)	0.0156(0.00024)	100.1(1.5)
5.2	156	2	0.50	0.1160(0.0063)	0.0154(0.00020)	98.3(1.3)
6.2	81	1	0.55	0.1326(0.0082)	0.0162(0.00025)	103.7(1.6)
7.2	88	1	0.49	0.1168(0.0072)	0.0157(0.00024)	100.4(1.5)
8.2	49	1	0.42	0.0966(0.0217)	0.0161(0.00032)	103.0(2.1)
9.2	70	1	0.40	0.1458(0.0088)	0.0157(0.00027)	100.6(1.7)
10.2	70	1	0.42	0.1393(0.0095)	0.0160(0.00029)	102.5(1.8)
11.2	69	1	0.52	0.1462(0.0094)	0.0157(0.00027)	100.4(1.7)
12.2	52	1	0.36	0.1616(0.0111)	0.0161(0.00032)	102.8(2.1)
13.2	92	1	0.51	0.1201(0.0073)	0.0158(0.00024)	100.9(1.5)
14.2	44	1	0.42	0.2229(0.0154)	0.0153(0.00033)	97.9(2.1)
15.2	86	1	0.44	0.1114(0.0068)	0.0151(0.00025)	96.3(1.6)

16.2	61	1	0.48	0.1556(0.0111)	0.0164(0.00033)	105.1(2.1)
17.2	86	1	0.50	0.1209(0.0069)	0.0155(0.00023)	98.9(1.5)
18.2	44	1	0.38	0.2158(0.0139)	0.0170(0.00036)	108.5(2.3)

Table A.2: U-Pb isotopic data from ID-TIMS analyses on zircon presented in Chapter 3.

	Fraction	Weight (mg)	U (ppm)	Th/U	Pbtot (pg)	PbCom (pg)	$^{206}Pb/^{204}Pb$ measured	Isotopic ratios (2σ) $^{207}Pb/^{235}U$	$^{206}Pb/^{238}U$	Age (2σ) $^{206}Pb/^{238}U$	% Disc
1	**10JA27-02**										
1	1 CA, lpr, incl, clr	0.0009	415	0.06	5.1	0.4	816.54	0.1021(0.0021)	0.01502(0.00004)	96.1(0.3)	41
2	2 CA, lpr, incl, clr	0.0013	361	0.29	6.9	0.8	585.44	0.1013(0.0030)	0.01506(0.00008)	96.3(0.5)	30
2	**10JA27-03**										
3	1 CA, spr frag, crks,	50	383	0.25	282	1.0	19257	0.1007(0.0003)	0.01521(0.00003)	97.3(0.2)	2.0
4	1 CA zr, euh spr, not etched	4.5	2688	0.20	175	0.6	20957	0.1007(0.0002)	0.01519(0.00002)	97.2(0.2)	6.2
5	1 CA zr, euh prism frag, sl. etched	5.2	2168	0.28	166	0.9	11593	0.1002(0.0004)	0.01513(0.00006)	96.8(0.4)	4.8
6	1 CA zr, euh prism frag, sl. etched	13	1246	0.26	238	1.0	15395	0.1001(0.0006)	0.01510(0.00009)	96.6(0.6)	6.9
7	1 CA zr, spr, clr,	14	529	0.21	107	0.8	8584	0.0997(0.0005)	0.01505(0.00006)	96.3(0.4)	6.0
3	**10JA28-02**										
8	1 CA, lpr, incl, clr	0.014	98	0.40	21.3	0.9	1597.00	0.0984(0.0012)	0.01531(0.00004)	98.0(0.3)	-243
9	1 CA, spr, incl, few crk	0.009	54	0.39	7.5	0.4	1111.58	0.1004(0.0013)	0.01525(0.00002)	97.6(0.2)	-14

Errors are given at 2 sigma. Lpr, long prism; spr, short prism, euh, euhedral, frag, fragment; incl, inclusions; crks, cracks; clr, clear; Pbtot, total lead; Pcom, common lead (assuming all has blank isotopic composition). % Disc, percent discordance of 207/206 age?. Decay constants are from Jaffey et al. (1971).

Table A.3: U-PB isotopic data from SHRIMP-RG analyses on zircon presented in Chapter 3.

Spot	U (ppm)	^{206}Pb*b (ppm)	Th/U	Isotopic ratios (1σ) ^{207}Pb/^{235}U		^{206}Pb/^{238}U		Age (1σ, Ma) ^{206}Pb/^{238}U	
11JA18-02									
1.1	117	8	0.3	0.5827	(0.0214)	0.0793	(0.00117)	494.3	(7.2)
2.1	303	4	0.5	0.0884	(0.0094)	0.0154	(0.00024)	99.1	(1.5)
3.1	1,258	17.1	0.8	0.0997	(0.0042)	0.0158	(0.00019)	101.2	(1.2)
4.1	582	7.8	0.7	0.0915	(0.0058)	0.0156	(0.00021)	100.5	(1.3)
5.1	175	10.3	0.4	0.5414	(0.0153)	0.0686	(0.00088)	426.8	(5.4)
6.1	498	6.2	0.7	0.0931	(0.0033)	0.0144	(0.00018)	92.4	(1.2)
7.1	207	2.5	0.3	0.0952	(0.0044)	0.0141	(0.00022)	90.3	(1.4)
8.1	771	20.7	0.1	0.2246	(0.0052)	0.0311	(0.00036)	197.1	(2.3)
9.1	556	7.1	0.8	0.0992	(0.0029)	0.0148	(0.00018)	94.4	(1.2)
10.1	1,598	21.6	0.7	0.1017	(0.0022)	0.0157	(0.00018)	100.6	(1.1)
11JA13-01									
1.1	51	0.7	0.5	0.0782	(0.0703)	0.0141	(0.00073)	91.0	(3.0)
2.1	77	1	0.4	0.0863	(0.0219)	0.0151	(0.00041)	97.1	(2.4)
3.1	54	0.7	0.6	err		0.0139	(0.00051)	92.8	(2.4)
4.1	49	0.7	0.4	err		0.0125	(0.00087)	91.8	(2.5)
5.1	61	0.8	0.4	0.0327	(0.0306)	0.0143	(0.00043)	94.8	(2.3)
6.1	74	0.9	0.6	0.0949	(0.0077)	0.0144	(0.00032)	92.2	(2.1)
7.1	430	5.7	0.4	0.0971	(0.0056)	0.0154	(0.00021)	99.1	(1.3)
8.1	79	1	0.4	0.0851	(0.0127)	0.0144	(0.00032)	92.9	(2.0)
9.1	200	2.7	0.5	0.0724	(0.0093)	0.0153	(0.00024)	99.7	(1.5)
10.1	114	1.3	0.7	0.1000	(0.0081)	0.0138	(0.00029)	87.8	(1.8)
11.1	62	0.8	0.6	0.0715	(0.0176)	0.0144	(0.00037)	93.4	(2.3)
12.1	62	0.8	0.6	0.0378	(0.0275)	0.0142	(0.00040)	94.1	(2.2)

Table A.4: U-Pb isotopic data from LA-ICP-MS analyses on zircon presented in Chapter 4.

Spot	U	^{206}Pb	Th/U	Isotopic ratios (1σ)				Age(1σ) /Ma	
	ppm	ppm		^{207}Pb/^{235}U		^{206}Pb/^{238}U		^{206}Pb/^{238}U	
10JA28-04									
1.1	103	7	0.60	0.5137	(0.0093)	0.0673	(0.00044)	419.7	(2.7)
2.1	241	16	0.57	0.5042	(0.0077)	0.0666	(0.00035)	415.5	(2.1)
3.1	268	18	0.71	0.4976	(0.0068)	0.0655	(0.00030)	408.8	(1.8)
5.1	345	23	0.59	0.5099	(0.0095)	0.0663	(0.00039)	413.7	(2.4)
6.1	164	11	0.51	0.4831	(0.0195)	0.0658	(0.00059)	410.9	(3.6)
7.1	226	14	0.74	0.4774	(0.0102)	0.0632	0.00040)	394.8	(2.4)
9.1	199	13	0.77	0.4946	(0.0072)	0.0656	(0.00034)	409.4	(2.1)
10.1	235	16	0.67	0.5214	(0.0088)	0.0670	(0.00049)	417.9	(2.9)
11.1	297	20	0.76	0.5213	(0.0060)	0.0665	(0.00036)	415.1	(2.2)
12.1	197	13	0.70	0.5058	(0.0077)	0.0654	(0.00039)	408.1	(2.4)
15.1	348	23	0.75	0.5002	(0.0055)	0.0651	(0.00030)	406.6	(1.8)
17.1	138	9	0.49	0.5163	(0.0087)	0.0674	(0.00035)	420.6	(2.1)
19.1	190	13	0.50	0.5010	(0.0078)	0.0662	(0.00039)	413.4	(2.4)
20.1	184	12	0.45	0.5143	(0.0074)	0.0659	(0.00036)	411.6	(2.2)
21.1	126	8	0.40	0.5240	(0.0116)	0.0672	(0.00043)	419.3	(2.6)
22.1	172	11	0.63	0.5080	(0.0073)	0.0667	(0.00032)	416.1	(1.9)
23.1	1617	76	0.20	0.3424	(0.0022)	0.0470	(0.00017)	295.9	(1.1)
24.1	141	9	0.49	0.4930	(0.0085)	0.0661	(0.00037)	412.7	(2.3)
25.1	71	5	0.29	0.5581	(0.0162)	0.0671	(0.00052)	418.8	(3.1)
26.1	234	15	0.40	0.4893	(0.0079)	0.0635	(0.00030)	397.1	(1.8)
27.1	244	16	0.41	0.5368	(0.0109)	0.0673	(0.00033)	420.1	(2.0)

Table A.5: U-PB isotopic data from SHRIMP-RG analyses on zircon associated with Chapter 4.

Spot	U (ppm)	^{206}Pb*b (ppm)	Th/U	Isotopic ratios (1σ)				Age (1σ, Ma)	
				^{207}Pb/^{235}U		^{206}Pb/^{238}U		^{206}Pb/^{238}U	
11JA28-01									
1.1	153	7.3	0.8	0.3902	(0.0171)	0.0556	(0.00080)	349.9	(5.0)
2.1	202	9.7	0.5	0.4111	(0.0115)	0.0559	(0.00079)	350.9	(4.9)
3.1	488	23.8	1.2	0.4194	(0.0094)	0.0567	(0.00067)	355.4	(4.1)
4.1	169	8.2	0.5	0.4172	(0.0135)	0.0566	(0.00080)	354.7	(4.9)
5.1	2,232	108	1.6	0.4127	(0.0054)	0.0563	(0.00060)	353.4	(3.7)
6.1	1,245	62.2	0.9	0.4276	(0.0069)	0.0582	(0.00065)	364.7	(4.0)
7.1	731	35.5	1.7	0.4211	(0.0070)	0.0565	(0.00063)	354.2	(3.9)
8.1	296	14.7	1.3	0.4135	(0.0118)	0.0577	(0.00069)	362.3	(4.3)
9.1	622	28.7	1.3	0.3971	(0.0068)	0.0536	(0.00060)	336.3	(3.7)
10.1	1,347	70.8	1.4	0.4547	(0.0062)	0.0612	(0.00066)	382.9	(4.0)

Appendix B

Expanded Proterozoic to Devonian stratigraphy of the Alexander terrane

Craig Subterrane: Prince of Wales

The oldest rocks assigned to the Craig subterrane consist of metavolcanic and metasedimentary rocks of the latest Proterozoic to Cambrian Wales Group, which is interpreted to have formed in an arc setting (Gehrels and Saleeby, 1987b). A felsic metavolcanic unit yielded a U-Pb zircon age of 595 ± 20 Ma (Gehrels *et al*., 1996). The Wales metamorphic suite is intruded by orthogneisses ranging in age from 554-520 Ma (Gehrels, 1990; Gehrels and Saleeby, 1987b; Gehrels *et al*., 1987). The Wales Group, and the Proterozoic to Cambrian plutonic suite interpreted as syngenetic with it, were pervasively deformed and metamorphosed to greenschist and, locally, amphibolite grade during the Middle to Late Cambrian Wales orogeny (Gehrels and Saleeby, 1987a). Note that they considered it to last until Early Ordovician, but evidence described below indicates that the Descon arc initiated in the latest Cambrian.

The Wales Group is overlain by the Upper Cambrian to Lower Silurian arc derived strata of the Descon Formation (Eberlein and Churkin, 1970; Gehrels and Saleeby, 1987a,b). A Descon Formation sandstone sample includes detrital zircon grains as old as 490 Ma suggesting that arc magmatism had resumed by then (Gehrels *et al*., 1996; Grove *et al*., 2008; Beranek *et al*., 2012a). Eberlein and Churkin (1970) report Early Ordovician graptolites low within the Descon Formation stratigraphy. While the lower contact of the Descon formation is not observed, it is interpreted as an unconformity based on the higher degree of deformation and metamorphism observed in the Wales Group on Prince of Wales Island (Gehrels and Saleeby, 1987a,b). The Descon Formation and the underlying Wales metamorphic suite are intruded by numerous intermediate to ultramafic plutons of Middle Ordovician to Early Silurian age, confirming that the Wales metamorphic suite forms the basement to the Descon Formation (Gehrels and Saleeby, 1987a). The youngest age published for this suite is 438 ± 5 Ma, and is considered to record the end of Descon arc magmatism (Gehrels and Saleeby, 1987b).

The Descon Formation is conformably overlain by the Silurian Heceta Limestone and turbidites of the Bay of Pillars Formation (Eberlein and Churkin, 1970; Gehrels and Saleeby, 1987a). The Heceta

Limestone includes conglomeratic lenses that contain volcanic derived clasts dissimilar to the Descon Formation, containing common plagioclase and amphibole phenocrysts as opposed to clinopyroxene phenocrysts found in the Descon Formation (Eberlein and Churkin, 1970). Paleobiogeographic studies on the Heceta Limestone suggest a correlation with the Ural Mountains (i.e. Baltica) (Soja, 1994; Soja & Antoshkina 1997; Antonishka & Soja 2006). Silurian strata are discontinuous, which is attributed to subsequent erosion (Eberlein and Churkin, 1970).

A major unconformity separates Silurian and older strata from the Lower Devonian Karheen Formation (Gehrels and Saleeby, 1987a). The Karheen Formation is a fining-upwards sequence with conglomeratic redbeds at the base, followed by siltstone, limestone and laminated mudstone at the top (Gehrels and Saleeby, 1987b). It is observed in depositional contact with both the Heceta Limestone and the Descon Formation (Eberlein and Churkin, 1970; Gehrels and Saleeby, 1987b). Along with the correlative Cedar Cove Formation described by Loney *et al*., (1975), it forms a northeastward tapering clastic wedge (Ovenshine *et al*., 1969; Gehrels and Saleeby, 1987a; Gehrels *et al*., 1996). The major unconformity as well as the presence of clasts with varied lithologies including Silurian plutonic clasts indicates significant uplift and erosion during the Late Silurian-Early Devonian. This event was named the Klakas orogeny (Gehrels *et al*., 1983; Gehrels and Saleeby, 1987a; Gehrels *et al*., 1996). It is tectonically modelled as a collision between the Craig subterrane and a pericratonic block to the southwest (present coordinates; Gehrels *et al*., 1996). The detrital zircon spectrum for the Karheen Formation is dominated by grains between ~410 and 490 Ma, as well as grains as old as 3 Ga (Gehrels *et al*., 1996; Grove *et al*., 2008).

In coastal northwestern BC, the Mathieson Channel Formation is temporally equivalent to the Karheen Formation but with generally finer grain size and greater limestone content (Nelson *et al*. 2011a, 2012). Nelson *et al*., (2012) report a detrital zircon spectrum for the Mathieson Channel formation ranging from 400 to 460 Ma (J.B. Mahoney, unpublished data). Nelson *et al*. (2010a) report a detrital zircon spectrum including Precambrian ages (G. Gehrels, unpublished data). The Banks Island assemblage, which outcrops west of known Alexander terrane rocks, is comprised of quartzite, marble, metapelite, and metabasalt (Gehrels and Boghossian, 2000). A characteristic feature is thin, pure quartzite layers interbedded with marble or metapelite. The Nd and Sr isotopic signature of the Banks Island assemblage is consistently continental (Boghossian and Gehrels, 2000). Nelson *et al*. (2012) propose a lateral transition between the Banks Island assemblage and the Mathieson Channel Formation indicating a change in provenance from dominantly continental to

dominantly arc derived detritus. The detrital zircon spectra for the Karheen Formation, Mathieson Channel Formation, and Banks Island assemblage all contain Late Silurian to Early Devonian ages; more than 10 My younger than the youngest magmatic activity related to the Descon arc (see above).

The Karheen Formation is overlain by both the Coronados Volcanics and the Wadleigh Limestone. The Coronados volcanics are comprised of greenish grey pillow basalts and fossiliferous limestone which has yielded Middle Devonian corals (Eberlein and Churkin, 1970). The Wadleigh Limestone is observed in gradational contact with the Karheen Formation but also overlies the Coronados Volcanics indicating a lateral facies change. Coral fossils indicate a Middle to Late Devonian age (Eberlein and Churkin, 1970). Pedder (2006) reports a correlation of Late Devonian corals in the upper Wadleigh Limestone with those in the Western Canada Sedimentary Basin suggesting the Alexander terrane was close enough to northwestern North America to exchange coral faunas at that time.

Craig Subterrane: St. Elias

The St. Elias component of the Craig subterrane underlies southwest Yukon and adjacent portions of northwestern British Columbia, southeast Alaska, and mainland Alaska (Figure 4.3). The St. Elias component has a continuous record of dominantly platformal sedimentary rocks from the Upper Cambrian through the Devonian (Figure 4.4). Evidence for an unexposed Wales Group equivalent in the St. Elias area is 544 Ma xenocrystic cores in an Ordovician pluton in northern southeast Alaska (Karl *et al*., 2006).

The oldest known rocks of the Alexander terrane in the St. Elias mountains belong to the Donjek Assemblage which is coeval with the Descon Formation, as recorded by Late Cambrian to Early Ordovician conodonts and bivalves (Dodds *et al*., 1993). It is comprised dominantly of quartzose to calcareous siltstone and sandstone (Dodds and Campbell, 1992). Basalt is locally a significant component of the Donjek Formation (Mihalynuk *et al*., 1993). Rift related geochemistry of these basalts has led to the interpretation that the Donjek Formation was deposited in a back-arc setting associated with the Descon arc (Beranek *et al*., 2012a).

The Donjek Formation is overlain by limestone, limestone conglomerate, argillite, and calcareous sandstone with common turbidite sequences referred to as the Goatherd Mountain Assemblage of Ordovician to Silurian age (Dodds and Campbell, 1992; Mihalynuk *et al*., 1993; Beranek *et al*., 2012a). Argillite layers have yielded Middle Ordovician graptolites suggesting a correlation between

the lower Goatherd Mountain assemblage and the upper Descon Formation (Norford and Mihalynuk, 1994). The upper portion of the Goatherd Mountain Assemblage is likely in part correlative with the Heceta Limestone and Bay of Pillars Formation.

The Goatherd Mountain Assemblage is overlain by the Devonian to Triassic Icefield Assemblage, comprised of lithic sandstone, polymictic conglomerate, and minor argillite and limestone with a characteristic orange weathering colour, similar to the Karheen Formation defined further south (Mihalynuk *et al*., 1993; Beranek *et al*., 2012a).

Admiralty subterrane

The Admiralty subterrane underlies Admiralty Island as well as smaller portions of nearby islands in southeast Alaska(Figure 4.3). The oldest known rocks of the Admiralty subterrane are greenschists and quartzites belonging to the Retreat Group; their age is uncertain but they are intruded by Precambrian plutons (544.2 ± 1.3 Ma and 547.6 ± 1.3 Ma U-Pb zircon ages; Karl *et al*., 2006). The Retreat Group may be a correlative of the Wales Group (Karl *et al*., 2006).

The next oldest unit in the Admiralty subterrane is the Ordovician-Devonian Hood Bay Formation, comprised of quartz veined black chert and argillite containing Ordovician graptolites at the base (Carter, 1977) which grades up into carbonaceous argillite, chert, greywacke, minor basalt, and thinly-laminated black limestone which has yielded Silurian-Devonian conodonts (Karl *et al*., 2010; Loney, 1964). Angular clasts of quartz veined black chert are observed in the overlying Cannery Formation of Mississippian age, suggesting a phase of deformation, uplift, and erosion occurred during the Devonian (Karl *et al*., 2010). Loney (1964) reports chert and argillite grains in greywacke layers of the upper Hood Bay Formation that texturally resemble chert and argillite within the Hood Bay Formation, possibly indicating that uplift and erosion occurred prior to deposition of the upper-most Hood Bay Formation. If the Craig and Admiralty subterranes were connected during the mid Paleozoic, the Hood Bay Formation may record deep basinal sedimentation within the back-arc to the Descon arc (Beranek *et al*., 2012a).

Bibliography

Abbott, J. G. and Turner, R. J. W., 1991. Mineral deposits of the northern Canadian Cordillera, Yukon - northeastern British Columbia [Field Trip 14]. Geological Survey of Canada, Open File 2169; Ottawa, Ontario, CA. Calgary, AB, Canada: *Geological Survey of Canada*, 320 p

Amato, J. M., Toro, J., Miller, E. L., Gehrels, G. E., Farmer, G. L., Gottlieb, E. S., and Till, A. B., 2009. Late Proterozoic–Paleozoic evolution of the Arctic Alaska–Chukotka terrane based on U-Pb igneous and detrital zircon ages: implications for Neoproterozoic paleogeographic reconstructions; *Geological Society of America Bulletin*, v. 121, p. 1219–1235.

Anderson, E.M., 1951. The Dynamics of Faulting, 2nd ed., Oliver and Boyd, Edinburgh.

Andronicos, C. L., Hollister, L.S., Davidson, C., and Chardon, D., 1999. Kinematics and tectonic significance of transpressive structures within the Coast plutonic complex, British Columbia, *Journal of Structural Geology*, v. 21, p. 229–243.

Andronicos, C. L., Chardon, D. H., Hollister, L. S., Gehrels, G. E., and Woodsworth, G. J., 2003. Strain partitioning in an obliquely convergent orogen, plutonism, and synorogenic collapse: Coast Mountains Batholith, British Columbia, Canada; *Tectonics*, v. 22, no. 2, 24 p.

Angen, J., van Staal, C., Lin, S., 2012, Structural geology of the Alexander Terrane in the vicinity of Porcher Island, northwestern British Columbia; *BC Geological Survey*; Geological Fieldwork 2011, Paper 2012-1, p. 135-148.

Antoshkina, A., and Soja, C., 2006. Late Silurian Reconstruction Indicated by Migration of Reef Biota between Alaska, Baltica (Urals), and Siberia (Salair); *GFF* v. 128, no. 2, p. 75-78.

Bazard, D. R., Butler, R. F., Gehrels, G. E., and Soja, C. M., 1995. Early Devonian paleomagnetic data from the lower Devonian Karheen Formation suggest Laurentia-Baltica connection for the Alexander terrane; Geology, v. 23, p. 707–710.

Bentley, C., 2004. Rock Fabric Analysis of the Sierra Crest Shear Zone System, California: Implications for Crustal-Scale Transpressional Shear Zones: MSc Thesis, College Park, Maryland. 159 p.

Beranek, L.P., van Staal, C.R., Gordee, S.M., McClelland, W.C., Israel, S., and Mihalynuk, M.G., 2012a. Tectonic significance of Upper Cambrian-Middle Ordovician mafic volcanic rocks on the Alexander terrane, Saint Elias Mountains, northwestern Canada; *Journal of Geology*, v. 120, p. 293-314.

Beranek, L.P., Mortensen, J.K., Lane, L.S., Allen, T.L., Fraser, T.A., Hadlari, T., and Zantvoort, W.G., 2012b, Detrital zircon geochronology of the western Ellesmerian clastic wedge, northwestern Canada: Insights on Arctic tectonics and the evolution of the northern Cordilleran miogeocline; *Geological Society of America Bulletin* v.122, no. 11-12, p. 1899-1911.

Berg, H. C., Jones, D. L., and Coney, P. J., 1978. Map showing pre-Cenozoic tectonostratigraphic terranes of southeastern Alaska and adjacent areas; *U.S. Geological Survey* Open File Report 78-1085.

Berthé, D., 1979. Orthogneiss, mylonite and non-coaxial deformation of granites: the example of South Armorican shear zone; *Journal of Structural Geology*, v. 1, p. 31-42.

Besse, J., and Courtillot, V., 1991. Revised and synthetic apparent polar wander paths of the African, Eurasian, North American and Indian plates, and true polar wander since 100 Ma; *Journal of Geophysical Research*, v. 96, p. 4029–4050.

Black, L. P., Kamo, S. L., Allen, C. M., Davis, D. W., Aleinikoff, J. N., Valley, J. W., Mundil, R., Campbell, I.H., Korsch, R.J., Williams, I.S.,and Foudoulis, C., 2004. Improved 206Pb/238U microprobe geochronology by the monitoring of a trace-element-related matrix effect: SHRIMP, ID-TIMS, ELA-ICP-MS and oxygen isotope documentation for a series of zircon standards; Chemical Geology, v. 205, p. 115–140.

Blodgett, R. B., Rohr, D. M., and Boucot, A. J., 2002. Paleozoic links among some Alaskan accreted terranes and Siberia based on megafossils. *In* Miller, E. L., Grantz, A., and Klemperer, S., eds. Tectonic evolution of the Bering Shelf–Chukchi Sea–Arctic Margin and adjacent landmasses; *Geological Society of America* Special Paper 360, p. 273–280.

Boghossian, N.D., and Gehrels, G.E., 2000, Nd isotopic tracing of terranes and other sedimentary assemblages through roof pendants of the Coast Plutonic Complex between Prince Rupert and Bella Coola, British Columbia. *In* Stowell, H.H., and McClelland, W.C., eds. Tectonics of the Coast Mountains, SE Alaska and Coastal British Columbia; *Geological Society of America Special Paper* 343, p. 77–88.

Bradley, D. C., McClelland, W. C., Wooden, J. L., Till, A. B., Roeske, S. M., Miller, M. L., Karl, S. M., and Abbott, J. G., 2007. Detrital zircon geochronology of some Neoproterozoic to Triassic rocks in interior Alaska. *In* Ridgway, K. D., Trop, J. M., Glen, J. M. G., and O'Neill, J. M., eds. Tectonic growth of a collisional continental margin: crustal evolution of southern Alaska; *Geological Society of America* Special Paper 431, p. 155–189.

Brew, D.A., 1995. Description and regional setting of the Silver Bay segment of the Sitka fault zone, southeastern Alaska, and evidence for possible sinistral separation. *In* Dumoulin, J.A., and Gray, J.E., eds. Geologic studies in Alaska by the U.S. Geological Survey, 1995; *U.S Geological Survey* Professional Paper 1574, p. 307-316.

Brew, D. A., and Ford, A. B., 1978. Megalineament in southeastern Alaska marks southwest edge of Coast Range batholithic complex; *Canadian Journal of Earth Sciences*, v. 15, p. 1763–1772.

Burke, K., and Şengor, A.M.C., 1986. Tectonic escape in the evolution of the continental crust. *In* Barazangi, M., ed. Reflection Seismology, Continental Crust, Geodynamic Series, 14; *American Geophysical Union* Special Publication, p. 41–51.

Butler, R.F., Gehrels, G.E., Hart, W., Davidson, C., and Crawford, M.L., 2006. Paleomagnetism of Late Jurassic to mid-Cretaceous plutons near Prince Rupert, British Columbia. *In* Haggart, J.W., Enkin, R.J., and Monger, J.W.H., eds. Paleogeography of the North American Cordillera: Evidence For and Against Large-Scale Displacements; *Geological Association of Canada*, Special Paper 46, p. 171-200.

Carter, C. 1977. Age of the Hood Bay Formation, Alaska. *In* Sohl, N. F., and Wright, W. B., eds. Changes in stratigraphic nomenclature by the U.S. Geological Survey, 1976. U.S. Geological Survey Bulletin 1435-A, p. A117–A118.

Chardon, D., Andronicos, C.L., and Hollister, L.S., 1999. Large-scale transpressive shear zone patterns and displacements within magmatic arcs: The Coast Plutonic Complex, British Columbia; *Tectonics*, v. 18, p. 278-292.

Chardon, D., 2003. Strain partitioning and batholith emplacement at the root of a transpressive magmatic arc; *Journal of Structural Geology,* v. 25, p. 91-97.

Colpron, M., 2006. Geology and mineral potential of Yukon-Tanana Terrane in the Livingstone Creek area (NTS 105E/8), south-central Yukon. *In* Emond, D.S., Bradshaw, G.D., Lewis, L.L., and Weston, L.H. eds. Yukon Exploration and Geology 2005; *Yukon Geological Survey*, p. 93-107.

Colpron, M. and Nelson, J., 2009. A Palaeozoic Northwest Passage: incursion of Caledonian, Baltican and Siberian terranes into eastern Panthalassa, and the early evolution of the North American Cordillera. *In* Cawood, P.A. and Kroner, A., eds. Earth Accretionary Systems in Space and Time; *The Geological Society of London,* Special Publication 318, p. 273-307.

Colpron, M., and Nelson, J.L., 2011a. A Palaeozoic NW Passage and the Timanian, Caledonian and Uralian connections of some exotic terranes in the North American Cordillera. *In* Spencer, A. M., Embry, A. F., Gautier, D. L., Stoupakova, A. V. and Sørensen, K. eds., Arctic Petroleum Geology; *The Geological Society of London*, Memoirs, v. 35, p. 463–484

Colpron, M., and Nelson, J.L., 2011b. A Digital Atlas of Terranes for the Northern Cordillera; *British Columbia Ministry of Energy and Mines*, BCGS GeoFile 2011-11.

Colpron, M., Nelson, J.L., and Murphy, D.C., 2006. A tectonostratigraphic framework for the pericratonic terranes of the northern Cordillera. *In* Colpron, M., and Nelson, J., eds. Paleozoic Evolution and Metallogeny of Pericratonic Terranes at the Ancient Pacific Margin of North America; *Geological Association of Canada* Special Paper 45, p. 1–23.

Colpron, M., Nelson, J., and Murphy, D., 2007. Northern Cordilleran terranes and their interactions through time; *GSA Today*, v. 17, p. 4-10.

Colpron, M., Murphy, D., and Nelson, J.L., 2011a. Cretaceous crustal structures in Yukon and implications for gold mineralization in the northern Cordillera; Poster, *AME BC Mineral Exploration Roundup* 2011.

Colpron, M., Murphy, D., and Nelson, J.L., 2011b. Crustal structures in Yukon and implications for gold mineralization in the northern Cordillera: Abstract, *Cordilleran Tectonics Workshop* 2011, p. 6-7.

Condie, K. C., 2007. Accretionary orogens in space and time. *Geological Society of America Memoir* 200, p. 145-158

Coney, P. J., Jones, D. L., and Monger, J. W. H., 1980. Cordilleran suspect terranes; *Nature,* v. 288, p. 329–333.

Crawford, M.L., Hollister, L.S. and Woodsworth, G.J., 1987. Crustal deformation and regional metamorphism across a terrane boundary, Coast Plutonic Complex, British Columbia; *Tectonics,* v. 6, p. 343-361.

Crawford, M.L., Crawford, W.A. and Gehrels, G.E., 2000. Terrane assembly and structural relationships in the eastern Prince Rupert quadrangle, British Columbia. *In* Stowell, H.H., McClelland, W.C., eds. Tectonics of the Coast Mountains, Southeastern Alaska and British Columbia; *Geological Society of America*, Special Paper 343, pages 1-21.

Crawford, M.L., and Crawford, W.A., 1991. Magma emplacement in a convergent tectonic orogen, southern Revillagigedo Island, southeastern Alaska; *Canadian Journal of Earth Sciences*, v. 28, p. 929–938.

Crawford, M. L., and Hollister, L. S., 1982. Contrast of metamorphic and structural histories across the Work Channel lineament, Coast Plutonic Complex, British Columbia; *Journal of Geophysical Research*, v. 87, p. 3849–3860.

Czeck, D.M., and Hudleston, P.J., 2003. Testing models for obliquely plunging lineations in transpression: a natural example and theoretical discussion; *Journal of Structural Geology*, v. 25, p. 959-982.

Davidson, J. P., Morgan, D.J., Charlier, B. L. A., Harlou, R., and Hora, J. M., 2007. Microsampling and isotopic analysis of igneous rocks: Implications for the study of magmatic systems; *Annual Reviews of Earth and Planetary Sciences*, v. 35, p. 273-311.

Davis, D.W., 1982. Optimum linear regression and error estimation applied to U–Pb data; *Canadian Journal of Earth Sciences*, v. 19, p. 2141–2149.

Davis. D.W., 2002. U-Pb geochronology of Archean metasedimentary rocks in the Pontiac and Abitibi subprovinces, Quebec, constraints on timing, provenance and regional tectonics; *Precambrian Research*, v. 115, p. 97-117.

Demerse, D. 2008. Sinistral high strain in the coast mountains near Bella Coola, west central British Columbia: M.Sc. thesis, University of British Columbia, Vancouver, 201 p.

Dewey, J.F., 1980. Episodicity, sequence and style at convergent plate boundaries. *In* Strangeway, D.W., ed. The Continental Crust and its Mineral Deposits; *Geological Association of Canada* Special Paper 20, p. 553-573

Dodds, C. J., Campbell, R. B., Read, P. B., Orchard, M. J., Tozer, E. T., Bamber, E. W., Pedder, A. E. H., et al., 1993. Macrofossil and conodont data from SW Kluane Lake

(115G & F[E1/2]), Mount Saint Elias (115B & C[E1/2]), SW Dezadeash (115A), NE Yakutat (114O), and Tatshenshini (114P) map areas, Yukon Territory and British Columbia; *Geological Survey of Canada*, Open File 2731, 137 p.

Dodds, C. J., and Campbell, R. B., 1992. Overview, legend, and mineral deposit tabulations for geology of SW Kluane Lake (115G & F[E1/2]), Mount Saint Elias (115B & C[E1/2]), SW Dezadeash (115A), NE Yakutat (114O), and Tatshenshini (114P) map areas, Yukon Territory and British Columbia; *Geological Survey of Canada*, Open Files 2188–2191, 85 p.

Dumoulin, J. A., Harris, A. G., Gagiev, M., Bradley, D. C., and Repetski, J. E., 2002. Lithostratigraphic, conodont, and other faunal links between lower Paleozoic strata in northern and central Alaska and northeastern Russia. *In* Miller, E. L., Grantz, A., and Klemperer, S., eds. Tectonic evolution of the Bering Shelf–Chukchi Sea–Arctic Margin and adjacent landmasses; *Geological Society of America* Special Paper 360, p. 291–312.

Eberlein, G.D. and Churkin, M.J., 1970. Paleozoic stratigraphy in the northwest coastal area of Prince of Wales Island, southeastern Alaska; *U.S. Geological Survey*, Bulletin 1284, 67 p.

Elston, D.P., Enkin, R.J., Baker, J., Kisilevsky, D.K., 2002. Tightening the Belt: Paleomagnetic-stratigraphic constraints on deposition, correlation, and deformation of the Middle Proterozoic (ca. 1.4 Ga) Belt-Purcell Supergroup, United States and Canada; *Geological Society of America* Bulletin, v. 114, no. 5, p. 619-638.

Engebretson, D.C., Cox, A., and Gordon, R.G., 1985. Relative motions between oceanic and continental plates in the Pacific basin; *Geological Society of America*, Special Paper 206, p. 1-59.

England, P. C., and McKenzie, D. P., 1982. A thin viscous sheet model for continental deformation, *Geophys. J. R. Astr.* Soc., 70,295-321.

England, P. C. & McKenzie, D. P., 1983. Correction to: a thin viscous sheet model for continental deformation; *Geophysical Journal of the Royal* Astronomical Society, v. 73, p. 525-532.

Eshelby, J.D., 1957. The determination of the elastic field of an ellipsoidal inclusion, and related problems; *Proceedings of the Royal Society of London*, v. A241, p. 376-396.

Evenchick, C.A., McMechan, M.E., McNicoll, V.J., Carr, S.D., 2007. A synthesis of the Jurassic-Cretaceous tectonic evolution of the central and southeastern Canadian Cordillera: Exploring links across the orogen. *In* Sears, J.W., Harms, T.A., and Evenchick, C.A., eds. Whence the Mountains? Inquiries into the Evolution of Orogenic Systems: A Volume in Honour of Raymond A. Price; *Geological Society of America Special Paper 433*, p. 117-145.

Fossen, H., and Tikoff, B., 1993. The deformation matrix for simultaneous simple shearing, pure shearing, and volume change, and its application to transpression/transtension tectonics; *Journal of Structural Geology*, v. 15, p. 413-422.

Gabrielse, H., 1969. Geology of Jennings River map area, British Columbia (104O); *Geological Survey of Canada*, Paper 68-55, 37 p.

Gabrielse, H., 1998. Geology of the Cry Lake and Dease Lake map area, north-central British Columbia; *Geological Survey of Canada* Bulletin 504, 147 p.

Gabrielse, H., Murphy, D.C., and Mortensen, J.K., 2006. Cretaceous and Cenozoic dextral orogen-parallel displacements, magmatism, and paleogeography, north-central Canadian Cordillera. *In* Haggart, J.W., Enkin, R.J., and Monger, J.W.H., eds. Paleogeography of the North American Cordillera: Evidence For and Against Large-Scale Displacements; *Geological Association of Canada*, Special Paper 46, p. 255-276.

Gabrielse, H., 1985. Major Dextral Transcurrent Displacements Along the Northern Rocky Mountain Trench and Related Lineaments in North-Central British Columbia; *Geological Society of America Bulletin* 96, no. 1, p. 1-14.

Gardner, M.C., Bergman, S.C., Cushing, G.W., MacKevett, E.M. Jr., Plafker, G., Campbell, R.B., Dodds, C.J., McClelland, W.C. and Mueller, P.A., 1988. Pennsylvanian pluton stitching of Wrangellia and the Alexander terrane, Wrangell Mountains, Alaska; *Geology*, v. 16, p. 967-971.

Gee, D. G., Fossen, H., Henriksen, N., and Higgins, A. K., 2008. From the early Paleozoic platforms of Baltica and Laurentia to the Caledonide orogen of Scandinavia and Greenland. *Episodes*, v. 31, p. 44–51.

Gehrels, G. E., 1990. Late Proterozoic-Cambrian metamorphic basement to the Alexander terrane on Long and Dall Islands, southeastern Alaska; *Geological Society of America* Bulletin 102, p. 760–767.

Gehrels, G.E., 2001. Geology of the Chatham Sound region, southeast Alaska and coastal British Columbia; *Canadian Journal of Earth Sciences*, v. 38, p. 1579-1599.

Gehrels, G.E., and Boghossian, N.D., 2000, Reconnaissance geology and U-Pb geochronology of the west flank of the Coast Mountains between Bella Coola and Prince Rupert, coastal British Columbia. *In* Stowell, H.H., and McClelland, W.C., eds. Tectonics of the Coast Mountains, SE Alaska and Coastal British Columbia; *Geological Society of America Special Paper* 343, p. 61–76.

Gehrels, G.E. and Saleeby, J.B., 1987a. Geologic framework, tectonic evolution, and displacement history of the Alexander terrane; *Tectonics*, v. 6, p. 151-173.

Gehrels, G.E., and Saleeby, J.B., 1987b. Geology of Southern Prince of Wales Island, Southeastern Alaska; *Geological Society of America* Bulletin 98, no. 2, p. 123-137.

Gehrels, G. E., Butler, R. F. and Bazard, D. R., 1996. Detrital zircon geochronology of the Alexander terrane, southeastern Alaska; *Geological Society of America Bulletin*, v. 108, p. 722-734.

Gehrels, G.E., Saleeby, J.B. and Berg, H.C., 1983. Preliminary description of the Klakas orogeny in the southern Alexander terrane, southeastern Alaska. *In* Stephens, C.H., ed.

Pre-Jurassic Rocks in Western North American Suspect Terranes; *Pacific Section, Society of Economic Paleontologists and Mineralogists*, p. 131-141.

Gehrels, G. E., Saleeby, J.B., and Berg, H.C., 1987. Geology of Annette, Gravina, and Duke islands, southeastern Alaska; *Canadian Journal of Earth Sciences*, v. 24, p. 866-881.

Gehrels, G.E., McClelland, W.C., Samson, S.D., Patchett, J.P. and Orchard, M.J., 1992. Geology of the western flank of the Coast Mountains between Cape Fanshaw and Taku Inlet, southeastern Alaska; *Tectonics*, v. 11, p. 567-585.

Gehrels, G.E., Rusmore, M., Woodsworth, G., Crawford, M., Andronicos, C., Hollister, L., Patchett, J., Ducea, M., Butler, R., Klepeis, K., Davidson, C., Friedman, R., Haggart, J., Mahoney, B., Crawford, W., Pearson, D. and Girardi, J., 2009. U-Th-Pb geochronology of the Coast Mountains batholith in north-coastal British Columbia: constraints on age and tectonic evolution; *Geological Society of America* Bulletin, v. 121, p. 1341-1361.

Greene, D.C., Schweickert, R.A., 1995. The Gem Lake shear zone: Cretaceous dextral transpression in the Northern Ritter Range pendant, eastern Sierra Nevada, California; *Tectonics*, v. 14, p. 945-961.

Greig, C., 1992. Jurassic and Cretaceous Plutonic and Structural Styles of the Eagle Plutonic Complex, Southwestern British Columbia, and their Regional Significance; *Canadian Journal of Earth Sciences*, v. 29, no. 4, p. 793-811.

Greig, C. J., R. L. Armstrong, J. E. Harakal, D. Runkle, and van der Heyden, P., 1992. Geochronometry of the Eagle Plutonic Complex and the Coquihalla Area, Southwestern British Columbia; *Canadian Journal of Earth Sciences*, v. 29, no. 4, p. 812-829.

Grove, M., Gehrels, G. E., Cotkin, S. J., Wright, J. E., and Zou, H., 2008. Non-Laurentian cratonal provenance of Late Ordovician eastern Klamath blueschists and a link to the Alexander terrane. *In* Wright, J. E., and Shervais, J. W., eds. Ophiolites, arcs, and batholiths; *Geological Society of America* Special Paper 438, p. 223–250.

Haeussler, P.J., 1992. Structural evolution of an arc-basin: The Gravina Belt in central southeastern Alaska; *Tectonics*, v. 11, p. 1245-1265.

Harland, W.B., 1971. Tectonic transpression in Caledonian Spitsbergen; *Geological Magazine,* v. 108, p. 27-42.

Hobbs, B.E., Means, W.D., and Williams, P.F., 1976. An Outline of Structural Geology; John Wiley, New York.

Hollister, L. S., and C. L. Andronicos, 1997. A candidate for the Baja British Columbia fault system in the Coast Plutonic Complex; *GSA Today*, v. 7, p. 1–7.

Hollister, L. S., and C. Andronicos, 2000. The Central Gneiss Complex, Coast Mountains, British Columbia. *In* H. H. Stowell, H.H., and McClelland, W.C., eds. Tectonics of the Coast Mountains, Southeastern Alaska and British Columbia; *Geological Society of America* Special Paper 343, p. 45-59.

Hollister, L.S., and Andronicos, C., 2006. Formation of new continental crust in Western British Columbia during transpression and transtension; *Earth and Planetary Science Letters*, v. 249, p. 29-38

Hoskin, P.W.O. and Schaltegger, U., 2003. The composition of zircon and igneous and metamorphic petrogenesis. *In* Hanchar, J.M., and Hoskin, P.W.O., eds. Zircon; *Reviews in Mineralogy and Geochemistry,* v. 53, p.27-62. Mineralogical Society of America.

Hudleston, P. J., Schultz-Ela, D., and Southwick, D. L., 1988. Transpression in an Archean greenstone belt. northern Minnesota; *Canadian Journal of Earth Sciences,* v. 25, p. 1060-1068.

Hudson, T., Plafker G., and Dixon, K., 1981. Horizontal offset history of the Chatham Strait fault; *U.S. Geological Survey Circular*, v. 844 p. 128-132.

Hurlow, H.A., 1993. Mid-Cretaceous strike-slip and contractional fault zones in the western Intermontane terrane, and their relation to the North Cascades-southeastern Coast Best orogen; *Tectonics*, v. 12, p. 1240-1257.

Hutchison, W.W., 1982. Geology of the Prince Rupert – Skeena map area, British Columbia; *Geological Survey of Canada* Memoir 394, 115 p., with 1:250 000 scale geological map, GSC Map 1427A.

Hyndman, R.D., Currie, C.A., and Mazzotti, S.P., 2005. Subduction zone backarcs, mobile belts, and orogenic heat; *GSA Today*, v. 15, p. 4–10

Hyndman, R.D. and Currie, C.A., 2011. Why is the North America Cordillera high? Hot backarcs, thermal isostasy, and mountain belts; *Geology*, v. 39, p. 783-786.

Israel, S., 2001. Structural and stratigraphic relationships within the Tchaikazan River area, southwestern British Columbia: Implications for the tectonic evolution of the southern Coast belt: M.Sc. thesis, University of British Columbia, Vancouver, 129 p.

Israel, S. 2008. Tectonic significance of the Atnarko Complex, Coast Mountains, British Columbia: Ph.D. thesis, University of British Columbia, Vancouver, 192 p.

Israel, S., Schiarizza, P., Kennedy, L.A., Friedman, R.M., and Villeneuve, M., 2006. Evidence for Early to Late Cretaceous sinistral deformation in the Tchaikazan River area, southwestern British Columbia: Implications for the tectonic evolution of the southern Coast belt. *In* Haggart, J.W., Enkin, R.J., and Monger, J.W.H., eds. Paleogeography of the North American Cordillera: Evidence For and Against Large-Scale Displacements; *Geological Association of Canada*, Special Paper 46, p. 331-350.

Jaffey, A.H., Flynn, K.F., Glendenin, L.E., Bentley, W.C., and Essling, A.M., 1971. Precision measurements of half-lives and specific activities of 235U and 238U; *Physical Reviews,* v. 4, p. 1889-1906.

Jiang, D., 2012. The motion of deformable ellipsoids in power-law viscous materials: Formulation and numerical implementation of a micromechanical approach applicable to

flow partitioning and heterogeneous deformation in Earth's lithosphere; *Journal of Structural Geology*, in press.

Jiang, D., and Bentley, C., 2012. A micromechanical approach for simulating multiscale fabrics in large-scale high-strain zones: Theory and application; *Journal of Geophysical Research*, v. 117, B12201

Jiang, D., and Williams, P.F., 1998. High-strain zones: a unified model; *Journal of Structural Geology*, v. 20, p. 1105-1120.

Jiang, D. and Williams, P.F., 1999. When do drag folds not develop into sheath folds in shear zones?; *Journal of Structural Geology,* v. 21, p. 577-583.

Kapp, P. and Gehrels, G., 1998. Detrital Zircon Constraints on the Tectonic Evolution of the Gravina Belt, Southeastern Alaska; *Canadian Journal of Earth Sciences,* v. 35, no. 3, p. 253-268.

Karl, S.M., Haeussler, P.J., Friedman, R.M.. Mortensen, J.K., Himmelberg, G.R., and Zumsteg, C.L., 2006. Late Proterozoic ages for rocks on Mount Cheetdeekahyu and Admiralty Island, Alexander terrane, southeast Alaska; *Geological Society of America Abstract with Programs*, v. 38, p. 20.

Karl, S. M., Layer, P. W., Harris, A. G., Haeussler, P. J., and Murchey, B. L., 2010. The Cannery Formation: Devonian to Early Permian arc-marginal deposits within the Alexander terrane, southeastern Alaska. *In* Dumoulin, J. A., and Galloway, J. P., eds. Studies by the U.S. Geological Survey in Alaska 2008–2009. *U.S. Geological Survey* Professional Paper 1776-B, 45 p.

Klepeis, K. A., and Crawford, M. L., 1999. High-temperature arc-parallel normal faulting and transtension at the roots of an obliquely convergent orogen; *Geology*, v. 27, p. 7–10.

Klepeis, K. A., Crawford, M. L., and Gehrels, G. A., 1998. Structural history of the crustal-scale Coast shear zone near Portland Inlet, SE Alaska and British Columbia; *Journal of Structural Geology*, v. 20, p. 883–904.

Krogh T. E., 1973. A low contamination method for the hydrothermal decomposition of zircon and extraction of U and Pb for isotopic age determinations; *Geochimica. Cosmochimica Acta,* v. 37, p. 485-494.

Krogh, T. E., 1982. Improved accuracy of U Pb zircon ages by the creation of more concordant systems using an air abrasion technique; *Geochimica Cosmochimica Acta,* v. 46, p. 637 – 649.

Kuiper, Y.D., Jiang, D., Lin, S., 2007. Relationship between non-cylindrical fold geometry and the shear direction in monoclinic and triclinic shear zones; *Journal of Structural Geology* v. 29, p.1022-1033.

Kuiper, Y.D., Lin, S., Jiang, D., 2011. Deformation partitioning in transpressional shear zones with an along-strike stretch component: An example from the Superior Boundary Zone, Manitoba, Canada; *Journal of Structural Geology*, v. 33, p. 192-202.

Lallemand, S., Heuret, A., and Boutelier, D., 2005. On the relationships between slab dip, back-arc stress, upper plate absolute motion, and crustal nature in subduction zones; *Geochemistry, Geophysics, Geosystems*, v. 6, no. 9, 18 p.

Lawrence, R.D., 1978. Tectonic Significance of Petrofabric Studies Along the Chewack-Pasayten Fault, North-Central Washington; *Geological Society of America* Bulletin 89, no. 5, p. 731-743.

Leitch, C.H.B., Godwin, C.I., and Dawson, K.M., 1989. Early Late Cretaceous-Early Tertiary Gold Mineralization: a Galena Lead Isotope Study of the Bridge River Mining Camp, Southwestern British Columbia, Canada; *Economic Geology,* v. 84, no. 8, p. 2226-2236.

Lin, S., Williams, P.F., 1992a. The origin of ridge-in-groove slickenside striae and associated steps in an S-C mylonite; *Journal of Structural Geology,* v. 14, p. 315-321.

Lin, S., Jiang, D., and Williams, P.F., 1998. Transpression (or transtension) zones of triclinic symmetry: natural example and theoretical modelling. *In* Holdsworth, R.E., Strachan, R.A. and Dewey, J.F., eds. Continental transpressional and transtensional tectonics; *Geological Society of London*, Special Publications, no. 135, p. 41-57.

Lin, S., Jiang, D., and Williams, P.F., 2007. Importance of differentiating ductile slickenside striations from stretching lineations and variation of shear direction across a high strain zone; *Journal of Structural Geology*, v. 29, p. 850-862.

Lister, G. and Williams, P.F., 1983. The partitioning of deformation in flowing rock masses. *Tectonophysics*, v. 92, no. 1-3, p. 1-33.

Loney, R.A., 1964, Stratigraphy and petrography of the Pybus-Gambier Bay area, Admiralty Island, Alaska; *U.S. Geological Survey Bulletin* 1178, 104 p.

Loney, R. A., Brew, D.A., Muffler, L.J.P., and Pomeroy, J.S., 1975. Reconnaissance geology of Chichagof, Baranof, and Kruzof islands, southeastern Alaska; *U.S. Geological Survey* Professional Paper 792, p.1-105,

Ludwig , K.R., 2005. SQUID, version 1.13b: a user's manual; *Berkeley Geochronology Center* Special Publication, v. 2, 22 p.

Ludwig, K. R., 2009. Isoplot v.3.7 – A geochronological toolkit for Excel; *Berkeley Geochronology Centre*. Berkeley, California

Mahoney, J. B., Gordee, S.M., Haggart, J.W., Friedman, R.M., Diakow, L.J., and Woodsworth, G.J., 2009. Magmatic Evolution of the Eastern Coast Plutonic Complex, Bella Coola Region, West-Central British Columbia; *Geological Society of America Bulletin* 121, no. 9-10, p. 1362-1380.

McClelland, W.C., and Gehrels, G.E, 1990. Geology of the Duncan Canal shear zone: Evidence for Early to Middle Jurassic deformation of the Alexander terrane, southeastern Alaska; *Geological Society of America* Bulletin, v. 102, p. 1378–1392.

McClelland and Mattinson, J.M., 2000. Cretaceous-Tertiary evolution of the western Coast Mountains, central southeastern Alaska. *In* Stowell, H.H., McClelland, W.C., eds. Tectonics of the Coast Mountains, Southeastern Alaska and British Columbia; *Geological Society of America,* Special Paper 343, p. 159-182.

McClelland, W.C., Gehrels, G.E., Samson, S.D. and Patchett, P.J., 1992. Structural and geochronologic relations along the western flank of the Coast Mountains Batholith: Stikine River to Cape Fanshaw, central southeastern Alaska; *Journal of Structural Geology*, v. 14, p. 475-489.

McClelland, W.C., Tikoff, B., Manduca, C.A., 2000. Two-phase evolution of accretionary margins: examples from the North American Cordillera; *Tectonophysics*, v. 326, p. 37-55.

McGroder, M. F., and Umhoefer, P. J., 1989. Comment on "Escape hypothesis for the Stikine block"; *Geology*, v. 17, p. 1161-1162.

Mihalynuk, M.G., Smith, M.T., MacIntyre, D.G., and Deschenes, M., 1993. Tatshenshini project, part B: stratigraphic and magmatic setting of mineral occurrences; *British Columbia Ministry of Energy, Mines, and Petroleum Resources* Paper 1993-1, p. 189–228.

Miller, M.G., 1988. Possible Pre-Cenozoic Left-Lateral Slip on the Yalakom Fault, Southwestern British Columbia; *Geology*, v. 16, no. 7, p. 584-587.

Molinari, A., Canova, G.R., and Ahzi, S., 1987. A self consistent approach of the large deformation polycrystal viscoplasticity; *Acta Mettalurigica*, v. 35, p. 2983-2994.

Monger, J.W.H., Price, R.A., and Tempelman-Kluit, D.J., 1982. Tectonic Accretion and the Origin of the Two Major Metamorphic and Plutonic Welts in the Canadian Cordillera; *Geology*, v. 10, no. 2, p. 70-75.

Monger, J.W.H., van der Heyden, P., Journeay, J.M., Evenchick, C.A., and Mahoney, J.B., 1994. Jurassic-Cretaceous basins along the Canadian Coast belt: Their bearing on pre-mid-Cretaceous sinistral displacements; *Geology*, v. 22, p. 175-178.

Monger, J. W. H., Souther, J.G., and Gabrielse, H., 1972. Evolution of the Canadian Cordillera: a Plate-Tectonic Model; *American Journal of Science*, v. 272, no. 7, p. 577-602.

Morozov, I.B., Smithson, S.B., Hollister, L.S., and Diebold, J.B., 1998. Wide-angle seismic imaging across accreted terranes, southeastern Alaska and western British Columbia; *Tectonophysics*, v. 299, p. 281-296.

Mortensen, J.K., Sluggett, C., Liverton, T. and Roots, C.F., 2006. U-Pb zircon and monazite ages for the Seagull and Cassiar batholiths, Wolf Lake map area, southern Yukon. *In* Emond, D.S., Bradshaw, G.D., Lewis, L.L., and Weston, L.H., eds. *Yukon Exploration and Geology 2005*, Yukon Geological Survey, p. 257-266.

Mortensen, J.K. and Hansen, V.L., 1992. U-Pb and 40Ar-39Ar geochronology of granodioritic orthogneiss in the western Pelly Mountains, Yukon Territory. *In* Radiogenic Age and Isotopic Studies: Report 6; *Geological Survey of Canada*, Paper 1992-2, p. 125-128.

Mortimer, N., 1986. Late Triassic, arc-related, potassic igneous rocks in the North American Cordillera; *Geology*, v. 14, p. 1035-1038.

Mura, T., 1987. Micromechanics of defects in solids. Kluwer Academic Publishers, Dordrecht, 587 p.

Murphy, D.C., 1997. Preliminary geological map of Grass Lakes area, Pelly Mountains, SE Yukon (105G/7); *Exploration and Geological Services Division, Yukon Region, Indian and Northern Affairs Canada*, Open File 1997-3, 1:50 000 scale.

Nelson, J.L., and Diakow, J.L., 2013. Geology of the northern coastal area of British Columbia; *BC Ministry of Energy, Mines and Petroleum Resources*, Open File 2013-XX, 1:150,000 scale.

Nelson, J., and Colpron, M., 2007. Tectonics and metallogeny of the British Columbia, Yukon and Alaskan Cordillera, 1.8 Ga to present. *In* Goodfellow, W.D., ed. Mineral Deposits of Canada: A synthesis of Major Deposit-Types, District Metallogeny, the Evolution of Geological Provinces, and Exploration Methods; *Geological Association of Canada, Mineral Deposits Division*, Special Publication 5, p. 755-791.

Nelson, J., Colpron, M., Piercey, S.J., Dusel-Bacon, C., Murphy, D.C., and Roots, C., 2006. Paleozoic tectonic and metallogenetic evolution of pericratonic terranes in Yukon, northern British Columbia and eastern Alaska. *In* Colpron, M., and Nelson, J.L., eds. Paleozoic Evolution and Metallogeny of Pericratonic Terranes at the Ancient Pacific Margin of North America, Canadian and Alaska Cordillera. *Geological Association of Canada*, Special Paper 45, p. 323-360.

Nelson, J.L., Mahoney, J.B., Gehrels, G.E., van Staal, C., Potter, J.J., 2010a. Geology and mineral potential of Porcher Island, northern Grenville Channel and vicinity, northwestern British Columbia; *BC Ministry of Energy, Mines and Petroleum Resources* Geological Fieldwork 2009, Paper 2010-1, p. 19-42.

Nelson, J.L., Mahoney, J.B., Gehrels, G.E., 2010b. Geology and mineral potential of the Porcher Island–Grenville Channel area, northwestern British Columbia (parts of 103G/15,16, H/13, J/1 and 2); *BC Ministry of Energy and Mines*, Open File 2010-03, scale 1:50 000.

Nelson, J.L., Diakow, J.L., Karl, S., Mahoney, J.B., Gehrels, G.E., Pecha, M., van Staal, C., 2011a. Geology and Mineral Potential of the Southern Alexander Terrane and western Coast Plutonic Complex near Klemtu, Northwestern British Columbia; *BC Ministry of Energy, Mines and Petroleum Resources* Geological Fieldwork 2010, Paper 2011-1, p. 73-97.

Nelson, J.L., Colpron, M., Murphy, D., Israel, S., Angen, J., 2011b. Mid-Cretaceous dextral and sinistral fault systems in the northern Cordillera, northward escape of the Intermontane block, and the search for a plate tectonic moose-gooser; *Cordilleran Tectonics Workshop 2011 Program with Abstracts*, p. 20-23.

Nelson, J.L., Diakow, J.B., Mahoney, J.B., van Staal, C., Pecha, M., Angen, J., Gehrels, G. and Lau, T., 2012. North Coast project: Tectonics and metallogeny of the Alexander terrane, and Cretaceous sinistral shearing of the western Coast belt; *BC Geological Survey* Geological Fieldwork 2011, 2012-1, p. 157-180.

Nelson, J., Diakow, L., van Staal, C., and Chipley, D., 2013. Ordovician volcanogenic sulphides in southern Alexander terrane, coastal NW British Columbia: Geology, Pb isotopic signature, and a case for correlation with Appalachian and Scandinavian deposits; *BC Ministry of Energy, Mines and Petroleum Resources*; Geological Fieldwork 2012, Paper 2013-1, in press.

Norford, B.S., and Mihalynuk, M.G., 1994. Evidence of the Pacific Faunal Province in the northern Alexander Terrane, recognition of two Middle Ordovician graptolite zones in northwestern British Columbia. Canadian Journal of Earth Sciences, v. 31, p. 1389–1396.

Ovenshine, A. T., Eberlein, G. D., and Churkin, M., 1969. Paleotectonic significance of a Silurian-Devonian clastic wedge, southeastern Alaska; *Geological Society of America* Abstract with Programs, v. 1, p. 50.

Passchier, C.W., 1997. The fabric attractor; *Journal of Structural Geology,* v. 19, p. 113-127.

Pedder, A. E. H., 2006. Zoogeographic data from studies of Paleozoic corals of the Alexander terrane, southeastern Alaska and British Columbia. *In* Haggart, J. W., Enkin, R. J. and Monger, J. W. H., eds. Paleogeography of the North American Cordillera: Evidence For and Against Large-scale Displacements; *Geological Association of Canada*, Special Papers 46, p. 29–57.

Platt, J.P., 1979. Extensional crenulation cleavage; *Journal of Structural Geology,* v. 1, p. 95-96.

Pupin, J.P., 1980. Zircon and granite petrology; *Contributions to Mineralogy and Petrology*, v. 73, p. 207-220.

Ramberg, H., 1975, Particle paths, displacement and progressive strain applicable to rocks: *Tectonophysics*, v. 28, p. 1-37.

Ramsay, J.G., 1980. Shear zone geometry: a review; *Journal of Structural Geology*, v. 2: p. 83-101.

Ramsay, J., and Graham, R., 1970. Strain variation in shear belts; *Canadian Journal of Earth Sciences*, v. 7, p. 786-813.

Ramsay, J.G., and Huber, M.I., 1983. The techniques of modern structural geology, Vol 1: Strain analysis. *Academic Press*, London.

Robin, P.F., and Cruden, A.R., 1994. Strain and vorticity patterns in ideally ductile transpression zones; *Journal of Structural Geology*, v. 16, p. 447-466.

Roddick, J.A., 1970. Douglas Channel-Hecate Straight map area, British Columbia; *Geological Survey of Canada*, Paper 70-41, 70 pages.

Rubatto, D., 2002. Zircon trace element geochemistry: Partitioning with garnet and the link between U-Pb ages and metamorphism; *Chemical Geology*, v. 184, p. 123-138.

Rubin, C.M. and Saleeby, J.B., 1992. Tectonic history of the eastern edge of the Alexander terrane, southeast Alaska; *Tectonics*, v. 11, p. 586-602.

Rubin, C.M., Saleeby, J.B, Cowan, D.S., Brandon, M.T. and McGroder, M.F., 1990. Regionally extensive mid-Cretaceous west-vergent thrust system in the northwestern Cordillera: Implications for continental margin tectonism; *Geology,* v. 18, p. 276-280.

Rusmore, M.E., 1985. Geology and Tectonic Significance of the Cadwallader Group and its Bounding Faults: Ph.D. Thesis, University of Washington, 174 p.

Rusmore, M.E., Gehrels, G., and Woodsworth, G.J., 2001. Southern continuation of the Coast shear zone and Paleocene strain partitioning in British Columbia – southeast Alaska; *Geological Society of America* Bulletin, v. 113, p. 961-975.

Rusmore, M.E., Woodsworth, G.J., and Gehrels, G.E., 2005. Two-stage exhumation of midcrustal arc rocks, Coast Mountains, British Columbia; *Tectonics*, v. 24, 25 p.--, doi: 10.1029/2004TC001750.

Sanderson, D.J., and Marchini, W.R.D., 1984. Transpression; *Journal of Structural Geology*, v. 6, p. 449-458.

Schiarizza, P., Gaba, R.G., Coleman, M., Garver, J.I., and Glover, J.K., 1990. Geology and mineral occurrences of the Yalakom River area (92O/1, 92J/15,16), British Columbia; *Geological Fieldwork 1989: British Columbia Ministry of Energy, Mines and Petroleum Resources* Paper 1990-1, p. 53-72.

Schiarizza, P., Gaba, R.G., Glover, J.K., Garver, J.I., and Umhoefer, P.J., 1997. Geology and mineral occurrences of the Taseko – Bridge River area; *British Columbia Ministry of Employment and Investment*, Bulletin 100, 291 p.

Schwerdtncr, W.M., 1989. The solid-body tilt of deformed paleohorizontal planes: application to an Archean transpression zone, southern Canadian Shield; *Journal of Structural Geology,* v. 11, p. 1021-1027.

Simpson, C. and Schmid, S.M., 1983. An evaluation of criteria to deduce the sense of movement in sheared rocks; *Geological Society of America* Bulletin, v. 94, p. 1281-1288.

Stacey, J.S., and Kramers, J.D., 1975. Approximation of terrestrial lead isotope evolution by a two-stage model; *Earth and Planetary Science Letters*, v. 26, p. 207–221.

Soja, C.M., 1994. Significance of Silurian Stromatolite-Sphinctozoan Reefs; *Geology,* v. 22, no. 4, p. 355-358.

Soja, C.M., 2008. Silurian-bearing terranes of Alaska. *In* Blodgett, R.B., and Stanley, G.D., Jr., eds. The terrane puzzle: new perspectives on paleontology and stratigraphy from the North American Cordillera; *Geological Society of America* Special Papaper 442, p. 39-50.

Soja, C.M., and Antoshkina, A.I., 1997. Coeval development of Silurian stromatolite reefs in Alaska and the Ural Mountains: implications for paleogeography of the Alexander terrane; *Geology*, v. 25, p. 539–542.

Stern, R.A., 2001. A new isotopic and trace-element standard for the ion microprobe: preliminary thermal ionization mass spectrometry (TIMS) U-Pb and electron-microprobe data; *Radiogenic Age and Isotopic Studies: Report 14, Geological Survey of Canada*, Current Research 2001-F1, 11 p.

Stowell, H.H., and Hooper, R.J., 1990. Structural development of the western metamorphic belt adjacent to the Coast plutonic complex, Southeastern Alaska: Evidence from Holkham Bay; *Tectonics*, v. 9, p. 391-407.

Tapponnier, P., Peltzer, G., Le Dain, A.Y., Armijo, R., and Cobbold, P., 1982. Propagating extrusion tectonics in Asia: New insights from simple experiments with plasticine; *Geology*, v. 10, p. 611-616.

Tikoff, B. and Greene, D., 1997. Stretching lineations in transpressional shear zones: an example from the Sierra Nevada Batholith, California; *Journal of Structural Geology*, v. 19, no. 1, p. 29-39.

Trettin, H.P., 1987. Pearya: A Composite Terrane with Caledonian Affinities in Northern Ellesmere Island; *Canadian Journal of Earth Sciences,* v. 24, no. 2, p. 224-245.

van der Heyden, P., 1989. U–Pb and K–Ar geochronometry of the Coast Plutonic Complex, 53° N–54° N, and implication for the Insular–Intermontane superterrane boundary, British Columbia; Ph.D. Thesis; *University of British Columbia*, 392 p.

van der Heyden, P., 1992. A Middle Jurassic to Early Tertiary Andean-Sierran arc model for the Coast Belt of British Columbia; *Tectonics*, v. 11, p. 82-97.

van Schmus, W.R., Bickford, M.E. Anderson, J.L., Bender, E.E., Anderson, R.R., Bauer, P.W., Robertson, J.M., Bowring, S.A., Condie, K.C., Denison, R.E., Gilbert, M.C., Grambling, J.A., Mawer, C.K., Shearer, C.K., Hinze, W.J., Karlstrom, K.E., Kisvarsanyi, E.B., Lidiak, E.G., Reed, J.C., Jr., Sims, P.K., Tweto, O., Silver, L.T., Treves, S.B., Williams, M.L., and Wooden, J.L., 1993. Transcontinental Proterozoic provinces. *In* Reed, J. C. Jr, Bickford, M. E., Houston, R.S., Link, P.K., Rankin, D.W., Sims, P.K., and Van Schmus, W.R., eds. Precambrian Conterminous U.S., The Geology of North America, C-2, *Geological Society of America*, Boulder, CO, p. 171–334.

Vitale, S., and Mazzoli, S., 2008. Heterogeneous shear zone evolution: the role of shear strain hardening/softening; *Journal of Structural Geology*, v. 30, p. 1383-1395.

Walker, J.D., Geissman, J.W., Bowring, S.A., and Babcock, L.E., compilers, 2012. Geologic Time scale v. 4.0: *Geological Society of America*.

Wang, W., Griffin, W.L., Chen, J., Huang, P., and Xiang, L., 2011. U and Th contents and U/Th ratios of zircon in felsic and mafic magmatic rocks: Improved zircon-melt distribution coefficients; *Acta Geologica Sinica*, v. 85, p. 164-174.

Wernicke, B., and Klepacki, D.W., 1988, Escape hypothesis for the Stikine block; *Geology*, v. 16, p. 461-465.

Wheeler, J.O., and McFeely, P., 1991. Tectonic assemblage map of the Canadian Cordillera; *Geological Survey of Canada* Map 1712A, scale 1:200000.

White, S.H., 1979. Large strain deformation: report on a tectonic studies group discussion meeting held at Imperial College, London on 14 November 1979. *Journal of Structural Geology*, v. 1, p. 333-339.

Williams, I.S., 1998. U-Pb by ion microprobe. *In* Mc-Kibben, M.A., Shanks, W.C., and Ridley, W.I., eds. Applications of microanalytical techniques to understanding mineralizing processes; Reviews in Economic Geology, v. 7, p. 1–35.

Williams, P.F., and Jiang, D., 2005. An investigation of lower crustal deformation: Evidence for channel flow and its implications for tectonics and structural studies; *Journal of Structural Geology*, v. 27, p. 1486-1504.

Williams, P.F., and Price, G.P., 1990. Origin of kinkbands and shear-band cleavage in shear zones: an experimental study. Journal of Structural Geology, v. 12, p. 145-164.

Wolf, D.E., Andronicos, C.L., Vervoort, J.D., Mansfield, M.R., and Chardon, D., 2010. Application of Lu–Hf Garnet Dating to Unravel the Relationships between Deformation, Metamorphism and Plutonism: An Example from the Prince Rupert Area, British Columbia; *Tectonophysics,* v. 485, no. 1–4, p. 62-77.

Woodsworth, G.J., Anderson, R.G., and Armstrong, R.L., 1991. Plutonic regimes. *In* Gabrielse, H., and Yorath, C.J., eds. Geology of Canada, vol. 4, Geology of the Cordilleran Orogen in Canada; *Geological Survey of Canada*, Ottawa, p. 491-531.

Xu, X., Ma, T., Sun, L., and Cai, X.P., 2003. Characteristics and dynamic origin of the large-scale Jiaoluotage ductile compressional zone in the eastern Tianshan Mountains, China; *Journal of Structural Geology*, v. 25, p. 1901-1915.

Yin, A., Taylor, M.H., 2011, Mechanics of V-shaped conjugate strike-slip faults and the corresponding continuum mode of continental deformation; *Geological Society of America* Bulletin, v. 123, p. 1798–1821

Yorath, C.J., Sutherland Brown, A. and Massey, N.W.D., 1999. LITHOPROBE, southern Vancouver Island, British Columbia: geology; *Geological Survey of Canada*, Bulletin 498, 145 p.

Zheng, Y.D., Wang, T., Ma, M., and Davis, G.A., 2004. Maximum effective moment criterion and the origin of low-angle normal faults; *Journal of Structural Geology*, v. 26, p. 271-285.

Zheng, Y., Zhang, J., and Wang, T., 2011. Puzzles and the maximum-effective-moment (MEM) criterion in structural geology; *Journal of Structural Geology*, v. 33, p. 1394-1405.